DESIGN AND CONSTRUCTION OF A FIXTURE TO EXAMINE THE EXPLOSIVE EFFECTS OF Al/I_2O_5

by

Joshua L. Smith

Submitted in Partial Fulfillment
of the Requirements for the Degree of
Master of Science in Mechanical Engineering
with Specialization in Fluid and Thermal Sciences

New Mexico Institute of Mining and Technology
Socorro, New Mexico
May, 2016

ABSTRACT

A fixture is designed and built to enable flow measurementS on Al/I_2O_5 thermite products to identify the explosive effects including shock wave propagation speed, product gas expansion, and explosive impulse. The explosions are contained in this purpose-built fixture to produce a near-one-dimensional explosion process and allow optical access. Initial laboratory tests are performed with the Al/I_2O_5 to measure explosive sensitivity, including BAM friction, modified type 12 impact, and spark sensitivity. The material is characterized by the response to these tests and studied for sensitivity changes over a one-month aging period. The hygroscopic nature of the material makes this study important to determine effects of ambient humidity present. The custom fixture has pressure ports to track the shock wave and viewing windows in order to view the explosive events with high speed cameras and an imaging spectrometer. Schlieren imaging, an optical technique that visualizes gradients in the refractive index of fluids, shows the various interactions between the shockwave, product gas, and ambient air environment. The imaging spectrometer uses a high-speed camera as a detector that captures the absorbance spectrum; this allows identification of product species in the explosion products, with iodine being of particular interest.

Keywords: Al/I_2O_5 thermite; aluminum iodine pentoxide thermite; aging; small-scale sensitivity; schlieren; imaging spectroscopy

ACKNOWLEDGMENTS

I would like to thank my adviser Dr. Michael J. Hargather for the tremendous amount of support and encouragement throughout my college career: From Heat & Mass Transfer in my undergraduate degree, to being encouraged to explore a graduate degree, to becoming a member of the Shock and Gas Dynamics Lab, to concluding my Master's degree, it has been a genuine pleasure. My entire tenure as a graduate student was intensely informative and yet he always ensured it was enjoyable. It has been a great honor to work together and learn from him.

The numerous people around campus that helped me throughout this project deserve a special thanks: Doreen, the Mechanical Engineering Secretary, has been a consistent help and never fails to live up to her "Duchess of Awesome" nickname. Ryan, the Mechanical Engineering Machinist, has always been willing to enable work at any time and nothing is ever an inconvenience. Brad and Tim, from Ordnance at EMRTC, are always prepared for the next test, offer great suggestions, and help with scheduling even on short notice.

My fellow Shock and Gas Dynamics labmates are a constant source of inspiration and help. Every one of you have made constructive suggestions and comments that have improved my approach to engineering problems. I am thankful for the freely-offered long days of setup and testing, the commentary that made even the dullest days intriguing, the numerous celebrations for all of our accomplishments, and mostly the friendship. James, Austin, Kyle, Stewart, Jeff, Rudy: Thank you all.

My friends have been beyond supportive. Marci, thank you for always being the great individual you are and for being my other half; you mean so much to me. Trey and Isabella, thank you for being the best roommates I could possibly imagine. Syngen, John, Jared, and Jarrett, thank you each for understanding the long periods of silence and being the best friends imaginable when we finally got the chance to catch up. I feel incredibly lucky to have such an outstanding group of friends.

My family has provided a constant reminder of their support in my endeavors. My parents, Don and Deborah, and my sister, Hannah, are always available to push me to better myself and convey their support. My grandpa, Earnest, for his constant reminders that I will persevere and be happy to have put in my best effort. My entire family has been supportive of my love for math, science, and engineering throughout my life and deserve a lot of the credit for what I have accomplished. Thank you, I love you all.

Thank you to DTRA for sponsoring this research (HDTRA1-14-1-0070).

This thesis was typeset with LaTeX[1] by the author.

[1]The LaTeX document preparation system was developed by Leslie Lamport as a special version of Donald Knuth's TeX program for computer typesetting. TeX is a trademark of the American Mathematical Society. The LaTeX macro package for the New Mexico Institute of Mining and Technology thesis format was written for the Tech Computer Center by John W. Shipman.

CONTENTS

LIST OF TABLES

LIST OF FIGURES

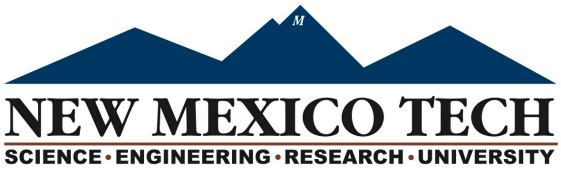

This thesis is accepted on behalf of the faculty
of the Institute by the following committee:

Dr. Michael J. Hargather

_____

Academic Advisor

Dr. Michael J. Hargather

_____

Research Advisor

Dr. Larry DeChant

_____

Committee Member

Dr. Tie Wei

_____

Committee Member

I release this document to New Mexico Institute of Mining and Technology

Joshua L. Smith 4/28/2016

_____

Student Signature Date

CHAPTER 1

INTRODUCTION

1.1 Research Motivation

The Geneva Protocol of 1925 prohibited the use of biological weapons [1]. The threat is ongoing nearly a hundred years later, however, due to conflicts throughout the world involving entities that do not comply with such treaties. Within the last decade, biological threats such as anthrax have been pushed to the forefront of public consciousness [2]. A practical large-scale defense against biological weapons currently does not exist. The Defense Threat Reduction Agency (DTRA), the United States' agency solely dedicated to the defense against weapons of mass destruction [3], has demonstrated increasing interest in researching and developing technologies for biocide defense efforts. The possibility of biological warfare on any scale makes the research of defeat mechanisms imperative and potentially life-saving.

Mechanically, the delivery and dispersion of the chosen biocidal is a major obstacle. Explosives are one of the easiest forms by which a chemical can be rapidly distributed over a large area, while allowing storage for long periods of time with eventual initiation in a controlled and consistent way. The large pressure differential created causes turbulent flow which leads to complex interactions between gases and is the ideal mixing environment. For maximum effectiveness against biological threats, it must be ensured that the biocidal defeat agent present be fully initiated prior to dispersal.

After initiation, the ability to quantify the effectiveness of the mixing is important. Currently, there does not exist any research directly focused on the interactions between an ambient environment and the product gases from an explosively-initiated material. One computational study was conducted on turbulent mixing, but only used point pressure gages [4]. Simulations have also been performed on turbulent combustion and the characterization of an explosive charge's mixing layer, but physical tests must be conducted to verify the results [5, 6]. Brouillette and Schwaederle have focused on shock wave interactions with a boundary between fluids (Richtmyer-Meshkov instability), but not the mixing of the gas that follows at a later time [7, 8]. Frost and Zhang focus on the dispersal of solid particles, but once again not on the gas that arrives at some time after the solid particles have been propelled into the environment [9, 10]. The closest research found was performed by Hank and focused on mixing of

the products, but at a macro level around geographical features and throughout a city [11].

To allow this mixing to be studied, a method must be developed to identify the appropriate chemical species. If the improper species is located, then the data obtained becomes meaningless. A setup that allows the proper gas front to be identified will enable future turbulent mixing quantification and the improvement of current simulations.

1.2 Literature Review

1.2.1 Aluminum Iodine Pentoxide

Literature shows that both iodine and silver have biocidal properties [12, 13]. Ag_2O (silver oxide), $AgIO_3$ (silver iodate), and I_2O_5 (iodine pentoxide) have all been studied as potential biocidal oxidizers with aluminum as the fuel. Ag_2O was found to be a poor oxidizer and required the addition of other oxides to achieve an acceptable reaction [14]. $AgIO_3$ was deemed a better oxidizer than CuO and $Fe_2)_3$, but combines both biocidal elements [15]. I_2O_5 was shown to kill *Bacillus subtilis* (an analog to *Bacillus anthracis*, anthrax) as an effect of the iodine exposure rather than from temperature or other cause [16]. Iodine will be used as the biocide to be studied.

To produce iodine, the oxidizer I_2O_5 will be combined with aluminum to form a biocidal thermite [17, 18]. Thermites are comprised of two metals or a metal and an oxidizer that are self-propagating exothermic reactions [19, 20]. Al/I_2O_5 has been the focus of numerous material properties focused studies. Jian showed that the reaction is limited by the decomposition of the oxidizer [21]. Ivanov found that the iodation with aluminum occurs at 300-660°C [22]. The propagation of the thermite directly depends on the particle size of the fuel and oxidizer; the smaller the particles the faster the reaction occurs [23]. Al/I_2O_5 has also been the focus of some experiment-backed simulations. Martirosyan has simulated pressure output from micro- and nano- versions of the thermite and found the pressure waves from the reactions [24, 25].

The use of I_2O_5 is not without concern. The I_2O_5 compound is extremely hygroscopic, so storage and use can be difficult [26]. Health concerns for humans exist and the material must be handled appropriately [27].

1.2.2 Small-scale Sensitivity Tests

Small-scale sensitivity tests such as the Modified Type 12 Impact Tool, BAM Friction Tester, and Spark Gap Tester allow a comparative sensitivity to be derived for various stimuli. Once a safe level has been determined, new materials can be compared by the values obtained from these tests to determine the

relative safety. The Modified Type 12 Impact Tool and the BAM Friction Tester are used by the United Nations to determine the safety of transportation of explosive materials [28]. The United States' Department of Defense (DOD) has their own standard for these tests [29], but references the United Nations' transport specification heavily. The United States' Lawrence Livermore National Laboratory (LLNL) published papers on these methods as well as the Spark Gap Tester [30–32]. The procedure from the LLNL paper on the Spark Gap Tester is followed and the UN Transport of Dangerous Goods is used for Modified Type 12 Impact Tool and BAM Friction Tester procedures. These methods are utilized in this research to determine any specific sensitivities the material possesses in order to implement the appropriate precautions and to explore the effect of hydration of the hygroscopic oxidizer used. No research was found that focused on the sensitivity of the thermite as it was exposed to the atmosphere compared to an inert environment. Some work has been done exploring the ignition of the thermite by an electric spark, impact, and thermally, but not by using any of the testing procedures covered here. [33, 34]

1.2.3 Schlieren Method

Tracking the thermite products requires a visualization method. The schlieren optical method can be used to image phenomena in transparent media [35]. This method enables the distinction between fluids of differing densities to be visualized, and will be utilized to visualize the flow from the explosion and make certain measurements such as the time of arrival for the gas products.

The schlieren method is used in various explosive applications. Shockwave and combustion observations are a wide use [36]. Schlieren is also a major method for shock tube measurements (a similar application to what will be implemented in this research). The method was highlighted in Houas's review of shock tube diagnostics [37]. Wagner used the method to study interactions of shock waves with particle fields having volume fractions residing between the dilute and granular regimes within a shock tube [38]. Hargather has used the schlieren optical method to track particles and shockwaves [39, 40]. The ability to distinguish between particles at a high resolution is directly related to the success of tracking a specific chemical species through a flow and comparing the data to spatially-resolved absorption spectra.

1.2.4 Imaging Spectroscopy

The schlieren method allows the distinction between fluids, but does not give information as to what species are being visualized. Figure 1.2 depicts the output images from another optical technique: imaging spectroscopy. The three dimensions consist of wavelength (x-axis), spatial (y-axis), and intensity (z-axis)

information. The spatial dimension (determined by the entrance slit on the imaging spectrometer) is placed along the direction in which the fluid will be flowing during testing to maximize information obtained. The study of molecular spectra was first compiled in 1950 by Herzberg [41]. Joens improved upon this work and focused on theoretical comparisons to experimentally-found spectra [42].

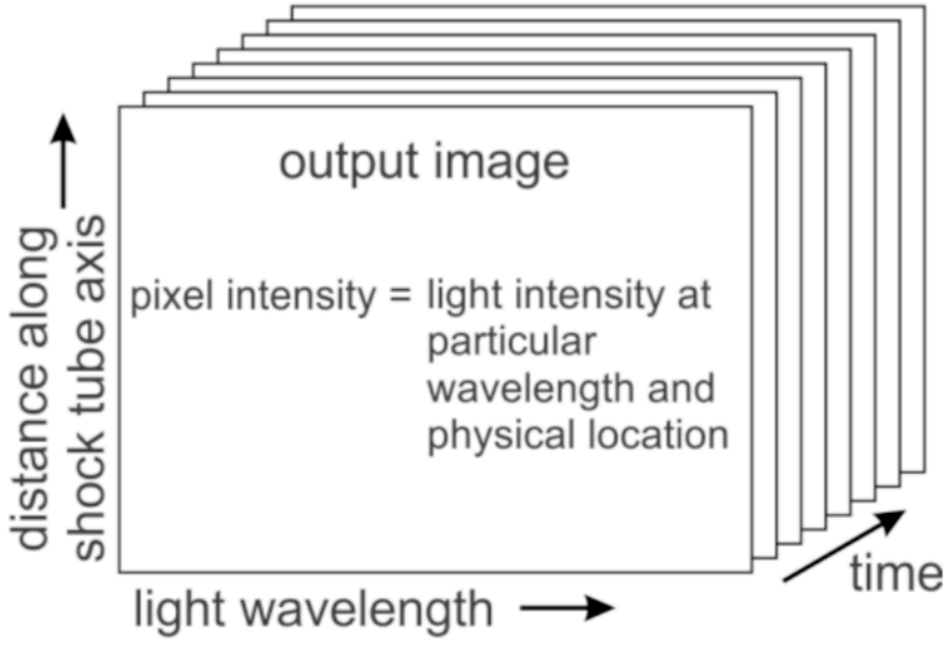

Figure 1.1: Output from an imaging spectrometer

More recent work from Saiz-Lopez and Mainuddin has found a high-resolution experimentally-determined iodine absorption profile and a way to locate iodine in flow measurements [43, 44]. Absorption spectroscopy measures the intensity of the original signal that the gas currently in the test section is absorbing. Various iodine-containing molecules have been compared for their spectra response [45]. Peuker uses the spectra response from AlO as a diagnostic in explosives materials testing and Glumac has made spectroscopy measurements in explosive environments and identified specific species [46–48].

1.3 Objectives of the Present Research

This research seeks to identify the iodine front within the product gas flow of Al/I_2O_5 thermite and atmosphere. The material will be studied for aging effects in order to more fully understand the hygroscopic nature of the thermite. A fixture will be designed and built to study the propagation of the product gases

with schlieren and imaging spectrometer techniques. This setup will enable the investigation of the mixing regime based on changes in mass of thermite.

CHAPTER 2

MATERIAL CHARACTERIZATION

2.1 Material Formulation

For the aluminum iodine pentoxide thermite, 325-mesh aluminum (Alpha-Aesar part #11067) and Sigma-Aldrich 278890 iodine pentoxide were used. The chemical formula for the aluminum and iodine pentoxide reaction was calculated with a stoichiometric balance of pure materials:

$$10Al + 3I_2O_5 \rightarrow 5Al_2O_3 + 3I_2 \tag{2.1}$$

By using the molecular weights and the molar ratio from the stoichiometric formula, the thermite contains 78.77% of I_2O_5 and 21.23% Al by weight.

The material obtained from the supplier was expected to have reacted with water in the atmosphere [26], so the possibility of having ta completely hydrated material as a worst-case scenario was explored. The I_2O_5 hydrates to form HI_3O_8 and result in equation 2.2 when combusted with aluminum.

$$10Al + 2HI_3O_8 \rightarrow 5Al_2O_3 + 3I_2 + H_2O \tag{2.2}$$

The appropriate mass ratio for this reaction is 79.03% HI_3O_8 and 20.93% Al by weight. The small difference between the stoichiometric unhydrated and hydrated weight percentages yielded the determination that it was unnecessary to account for the hydration when forming the mixture.

The differences in products of the reactions were also of concern between the hydrated and unhydrated cases. The adiabatic flame temperature of aluminum in the unhydrated reaction reaches at least 3253K [49]. Farley showed through differential scanning calorimetry tests that an elevated temperature causes the hydrogen in the HI_3O_8 to reform water at 479.85K. The decomposition of I_2O_5 into O_2 and I_2 occurs at 660.75K [50]. The iodine gas will thus be produced whether the oxidizer has been exposed to humidity and allowed to hydrate or not. The unhydrated reaction is used throughout this research.

The density of the mixture was calculated to find the percent theoretical maximum density (TMD) used throughout the testing. Aluminum iodine pentoxide has a TMD of 4.119 g/cm^3 [49]. A simple volumetric and mass measurement was made and the loose powder's density was found to be 2.04 g/cm^3. The loose powder had a packing of 49.9% TMD.

2.2 Sensitivity Testing

The sensitivity of an explosive material is important for safety. To characterize a material, the Department of Defense's "Test Method Standard for Safety and Performance Tests for the Qualification of Explosives (High Explosives, Propellants, and Pyrotechnics)" was used [29]. In this document, the general UN standards for "Transport of Dangerous Goods" were referenced and provided a wide array of testing standards and procedures for characterizing a new material [28]. Lawrence Livermore produced papers on each of these three tests as well which provided a thorough explanation of each [30–32]. Rather than follow the complete procedure for the classification of the Al/I_2O_5 thermite, some individual tests were used to understand its sensitivity to initiation, thus allowing safe handling. The tests performed were: The small-scale BAM Friction Sensitivity, Static-Spark Sensitivity, and Modified Type 12 Impact Tool Tests. This trio of small-scale sensitivity tests covers the general methods of accidental initiation and determines what safety precautions should be used before handling a material.

An initial test suite was conducted using internal New Mexico Tech (NMT) procedures, but differences were found between the UN, LLNL, and internal NMT documentation. The initial data presented provided a general expectation of material response, but all available procedures were evaluated before continuing with more thorough testing. The procedures involved variances such as NMT's recommended 40 milligrams of sample for the Modified Type 12 Impact Tool compared to the UN's recommended 30 milligrams. In these instances, the UN procedure took precedence followed by the LLNL papers. The NMT documentation was only used for the static-spark sensitivity material holders since this information was not explicitly stated elsewhere.

The BAM Friction Test (Figure 2.1) was developed to test the friction sensitivity of an explosive. Lawrence Livermore's 1996 report was used as background and the UN's "Transport of Dangerous Goods": Test 3(b)(i) was followed for the detailed procedure[28, 31]. The friction machine consists of a porcelain pin that slides across a porcelain plate. The explosive being tested is placed in a line along the pin's path.

Approximately 10 mm^3 is used per test which is 20.4 milligrams of Al/I_2O_5 thermite. This is a binary test with a Go considered an event and a No-Go considered a non-event. The determination between a Go/No-Go is largely qualitative and based on sparks, sounds, and remnants on the porcelain plate (Figure 2.2 shows the remnants from a Go above the result from a No-Go). One of nine weights is hung from one of six notches in order to apply a load of 0.5 kg to 36 kg. The initial weight is chosen from experience and the weight denoted for the test is decided by systematically finding the lowest weight at which six samples in a row prove to be No-Go's.

The UN does not state a specific calibration material, but PETN is used as a standard calibration material for the BAM Friction Test at NMT with historical data to ensure the machine does not change responses over time. Table 2.1 shows

the initial data for the calibration of PETN and Table 2.2 shows the data for the Al/I_2O_5 thermite using NMT internal procedures. These tests were stopped at 5 no-go's due to a discrepancy between procedures. The UN considers any material that with a value of 8.0 kg or higher on the BAM Friction Test to be considered friction-safe.

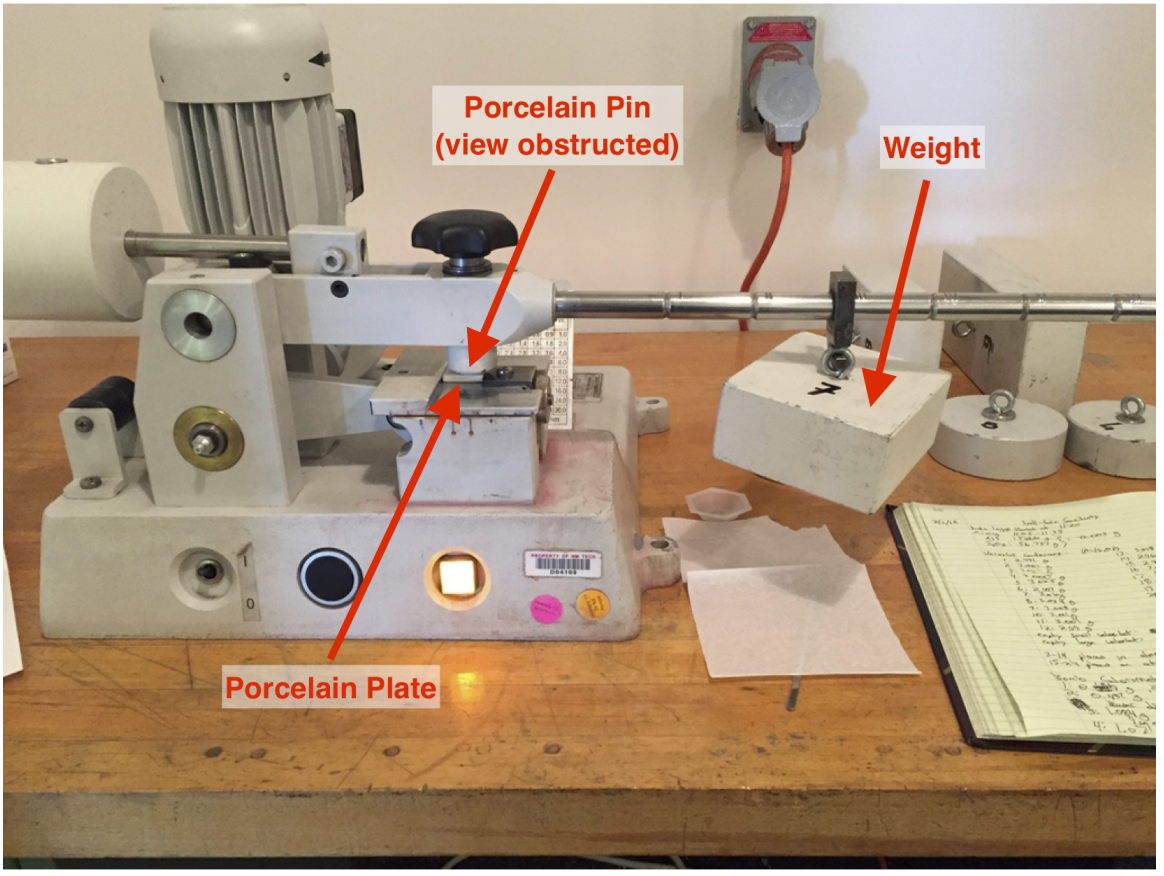

Figure 2.1: BAM Friction Sensitivity Apparatus

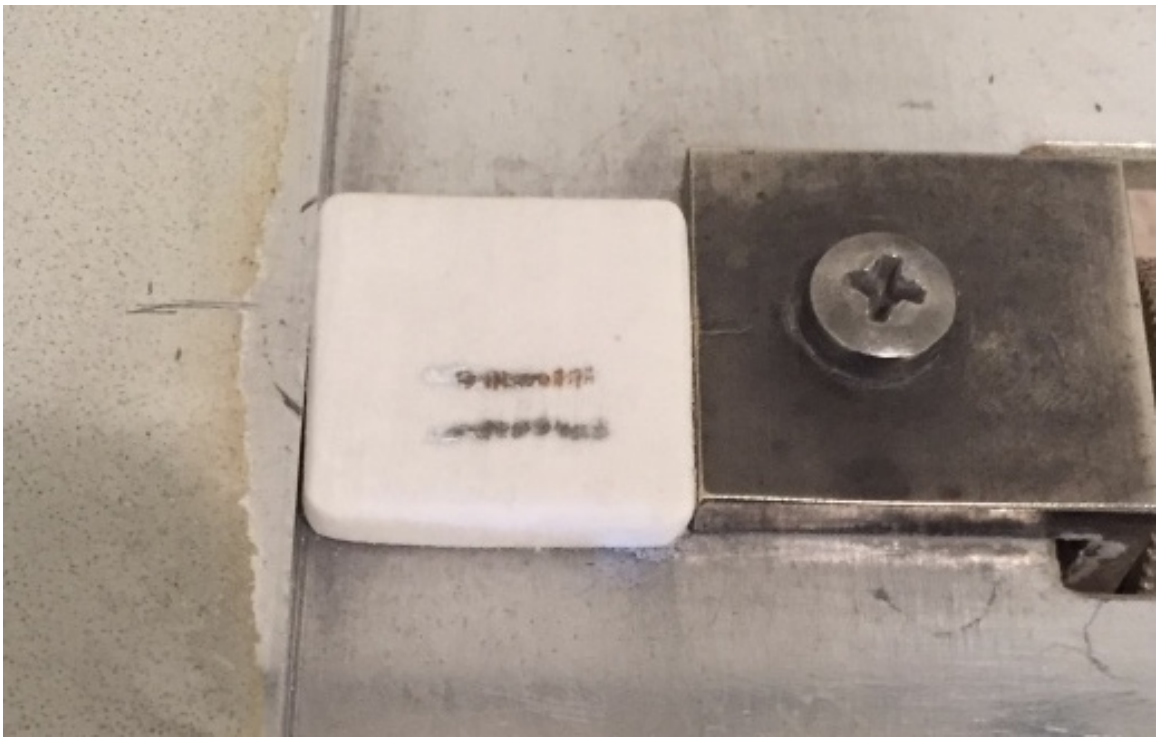

Figure 2.2: BAM Friction Sensitivity Apparatus setup and indication of a go vs. a no-go (determined by the purple remnants on the plate on the top test)

Table 2.1: Initial PETN BAM Friction Apparatus Data

PETN Calibration: 5.4 kg			
Run	Weight (kg)	Go/No Go	Comments
1	8	Go	Snap
2	6	Go	Snap
3	5.4	No Go	
4	5.4	No Go	
5	5.4	No Go	
6	5.4	No Go	
7	5.4	No Go	

Table 2.2: Initial Al/I_2O_5 BAM Friction Apparatus Data

Al/I2O5: 9.6 kg			
Run	Weight (kg)	Go/No Go	Comments
1	16	Go	Snap, spark
2	14.4	Go	Snap, spark
3	12.8	No Go	
4	12.8	Go	Snap, spark
5	11.2	No Go	
6	11.2	No Go	
7	11.2	No Go	
8	11.2	Go	Snap
9	9.6	No Go	
10	9.6	No Go	
11	9.6	No Go	
12	9.6	No Go	
13	9.6	No Go	

The Static-Spark Sensitivity Test (Figure 2.3) was developed to test the spark sensitivity of an explosive to understand the possibility of initiation by electro-static discharge. Lawrence Livermore's 1999 report was used as background and for the detailed procedure [32]. The static-spark machine has a charging system, a voltage meter, and a discharge mechanism. Test samples (Figure 2.4) are prepared using a punch to make small metal circles to which a plastic washer is attached. This creates a consistent volume of the explosive (approximately 0.21 cm^3, 0.0013 in^3) and a pathway for the electrons to travel.

A metal pin is placed in the machine's plunger and then the test sample is secured in position with tape. The safety shield door is closed and the desired voltage is set. The machine is set to discharge a specified voltage and is discharged by the contact the plunger makes to the test sample. This is a binary test with a Go considered an event and a No-Go considered a non-event. The determination between a Go/No-Go is largely qualitative based on any destruction to the sample holder or tape. The initial voltage is chosen from experience. The reported voltage denoted for the test is the lowest voltage at which at most one in ten sequential samples is a Go. Figure 2.5 shows a test in progress at the moment the capacitor is discharged through the material. The iodine in the oxidizer of the Al/I_2O_5 thermite has a melting point of 113.7°C and was observed to melt and leave trace amounts of purple iodine on the tape, but no thermite initiation was seen and due to the lack of damage to the tape these tests were No-Go's.

RDX is used as a standard calibration material for the Static-Spark Sensitivity Test at NMT with historical data to ensure the machine does not change responses over time. Table 2.3 shows the data for the calibration of RDX and Table 2.4 shows the data for the Al/I_2O_5 thermite. By not initiating at 3.5 kV

(the highest possible value for the machine used), the thermite is deemed to be completely insensitive to a static spark stimuli.

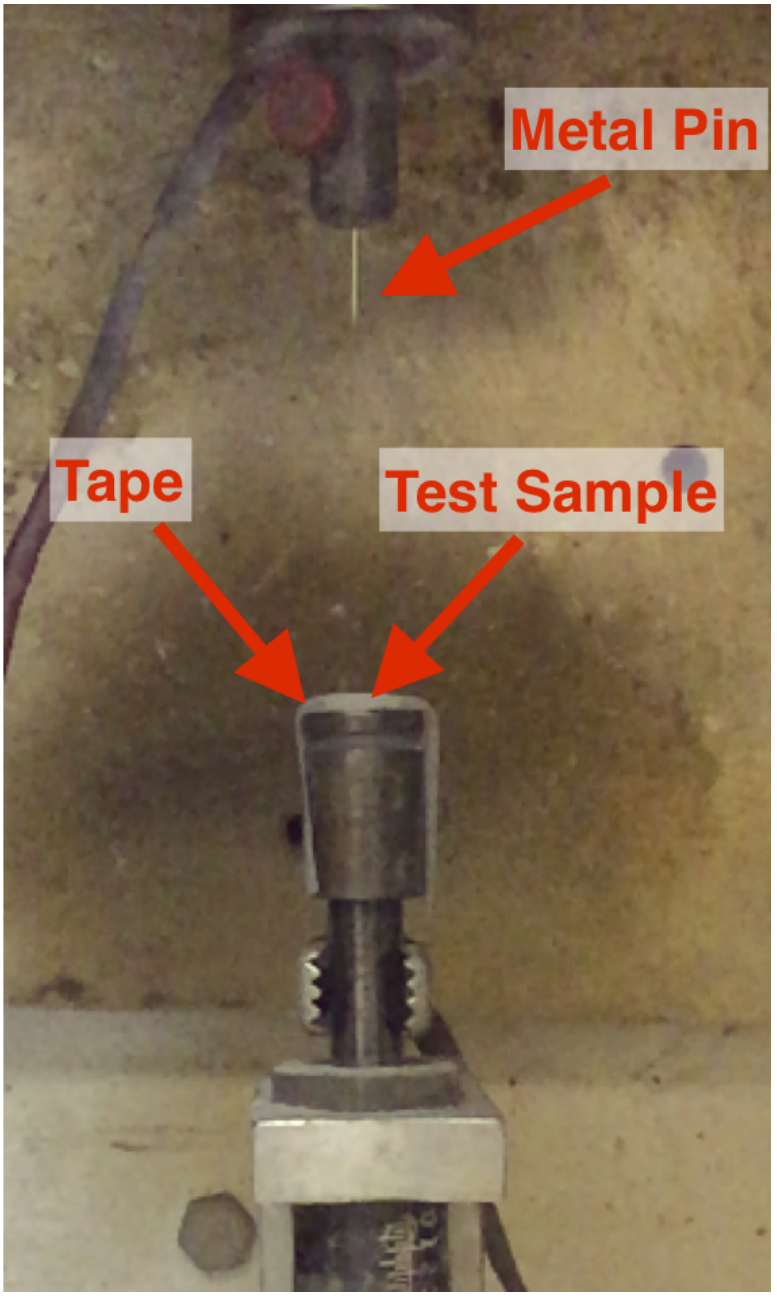

Figure 2.3: Static-Spark Sensitivity Test

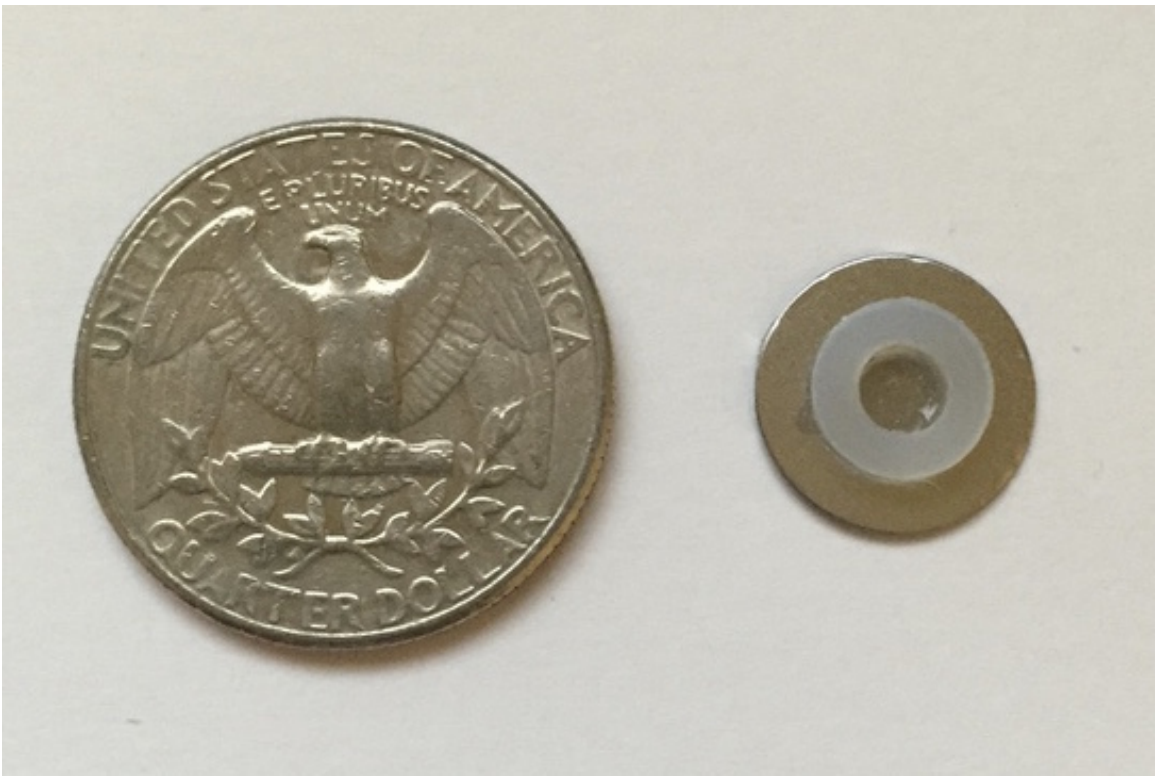

Figure 2.4: Static-Spark Sensitivity test cup - The explosive being tested is placed in the inside of the plastic washer, with enough material to fill the entire cylindrical volume

Figure 2.5: Static-Apark Sensitivity 3.5 kV test in progress

Table 2.3: Initial RDX Static-Spark Sensitivity Data

RDX Calibration: 1.73 kV			
Run	Voltage (kV)	Go/No Go	Comments
1	1.73	No Go	
2	2	No Go	
3	2.24	No Go	
4	2.45	Go	Material Consumed
5	2.24	Go	Material Consumed
6	2	No Go	
7	2	Go	Material Consumed
8	1.73	No Go	
9	1.73	No Go	
10	1.73	No Go	
11	1.73	No Go	
12	1.73	No Go	
13	1.73	No Go	
14	1.73	No Go	
15	1.73	No Go	
16	1.73	No Go	
17	1.73	No Go	

Table 2.4: Initial Al/I_2O_5 Static-Spark Sensitivity Data

Al/I2O5: 3.46 kV			
Run	Voltage (kV)	Go/No Go	Comments
1	3.0	No Go	
2	3.0	No Go	
3	3.0	No Go	
4	3.0	No Go	
5	3.0	No Go	

The Modified Type 12 Impact Tool (Figure 2.6) was developed to test the impact sensitivity of an explosive. Lawrence Livermore's 1995 report was used as background and the UN's "Transport of Dangerous Goods" Test 3(a)(v) was followed for the detailed procedure [28, 30]. The Modified Type 12 Impact Tool has a drop mass, a 2.5 kg intermediate mass, and an anvil on which the sample sits. Each sample is measured to be 30 +/- 5 mg. The sample is placed on the anvil and the intermediate weight is gently placed on top of the sample (Figure 2.7). The drop mass is then raised to a specified height and dropped. This is a binary

test with a Go considered an event and a No-Go considered a non-event. The determination between a Go/No-Go is largely qualitative and based on sparks, sounds, and the appearance of residue or smoke.

The initial height is chosen from experience. The height of each test is systematically varied from the initial test: If a Go was recorded, then the height is lowered and if a No-Go was recorded then the height is raised. Once twenty-five tests are completed and the height is determined from a Bruceton analysis of the data, a comparison with a known explosive (generally used for calibrating the machine the same day) is used to decide how dangerous the tested material is for handling. The Bruceton analysis estimates the height at which 50% of the tests are a Go [30]. The heights at which the mass is placed are determined by a log scale and are 6.5, 8, 10, 12, 15, 19, 24, 29, 36, 45, 55, 69, 85, 105, 131, 162 and 200 cm [28].

RDX is used as a standard calibration material for the Static-Spark Sensitivity Test at NMT with historical data to ensure the machine does not change responses over time. Table 2.5 shows the data for the calibration of RDX and Table 2.6 shows the data for the Al/I_2O_5 thermite. The UN considers any material with a value higher than RDX on the BAM Friction Test to be considered impact-safe.

Figure 2.6: Modified Type 12 Impact sensitivity test

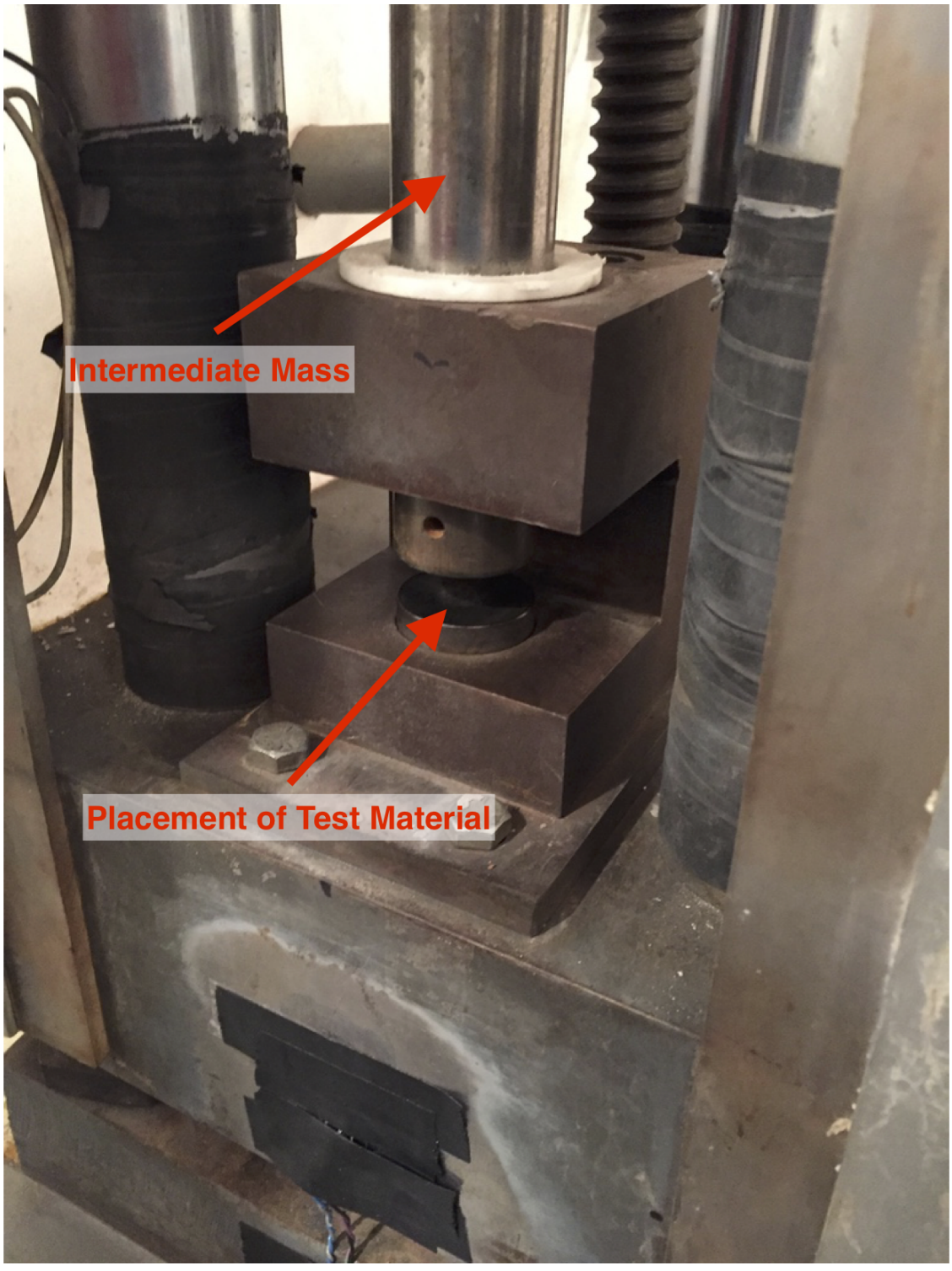

Figure 2.7: Modified Type 12 Impact Tool intermediate mass under which the test material is placed

Table 2.5: Initial RDX Modified Type 12 Impact Tool Sensitivity Data

Run	Height (cm)	Go/No Go	Comments
1	36	Go	
2	29	Go	smell
3	24	No Go	
4	29	Go	
5	24	No Go	
6	29	Go	black residue, smoke
7	24	Go	
8	19	No Go	
9	24	No Go	
10	29	Go	smoke
11	24	Go	
12	19	No Go	
13	24	No Go	
14	29	Go	smoke
15	24	Go	smoke,
16	19	No Go	
17	24	No Go	
18	29	Go	
19	24	Go	smoke
20	19	No Go	
21	24	Go	
22	19	No Go	
23	24	Go	smoke
24	19	No Go	
25	24	Go	black residue
Bruceton Analysis:	21.82		

Table 2.6: Initial Al/I_2O_5 Modified Type 12 Impact Tool Sensitivity Data

Run	Height (cm)	Go/No Go	Sound	Comments
1	36	Go		Flash
2	29	No Go		
3	36	No Go		
4	45	No Go		
5	55	No Go		
6	69	No Go		
7	85	Go	Pop	Flash, smell, purple residue
8	69	Go		Flash, purple residue
9	55	Go		Flash, purple residue
10	45	No Go		
11	55	No Go		
12	69	No Go		
13	85	Go	Pop	Flash, smell, residue
14	69	Go	Pop	Flash, smell, residue
15	55	Go	Pop	Flash, smell, residue
16	45	Go	Pop	Flash, residue
17	36	Go	Pop	Flash, residue
18	29	No Go		
19	36	No Go		
20	45	Go	Pop	Flash, smell, residue
21	36	No Go		
22	45	No Go		
23	55	Go		Barely any residue
24	45	Go	Pop	Flash, smell, residue
25	36	No Go		
Bruceton analysis:	47.93			

After sensitivity tests were performed, initial burn tests were conducted in a fume hood. The thermite powder was piled onto a consumable paper, placed on a ring stand, and initiated with cannon fuse which contains black powder (Skylighter part #GN2010). Figure 2.8 was captured with a color Photron Mini. The purple gas is indicative of iodine [51].

Figure 2.8: Initial test of 2.5 grams Al/I_2O_5 thermite

2.2.1 Aging Study

The thermite used is extremely hygroscopic and can react with the water in the atmosphere under normal storage conditions. The possibility of changes in sensitivity or properties important to this research needed to be explored. The I_2O_5 was expected to have reacted fully with the atmosphere through the packaging and shipping process, thus effectively already having been "aged" significantly, but this needed to be verified. To achieve this, a four week aging study was planned and executed.

The Al and /I_2O_5 powders were mixed together to form the Al/I_2O_5 thermite on day 0 and was then tested on days 0, 1, 3, 7, 14, and 28. In order to compare any changes to the material exposed to the atmosphere, half of the Al/I_2O_5 thermite was stored in an Atmosbag (Sigma-Aldrich Part #: Z564397) under dry nitrogen gas (Figure 2.9). The material exposed to the atmosphere was placed next to the Atmosbag. The Atmosbag and thermite exposed to the atmosphere were contained within an unsealed traditional glovebox for secondary containment.

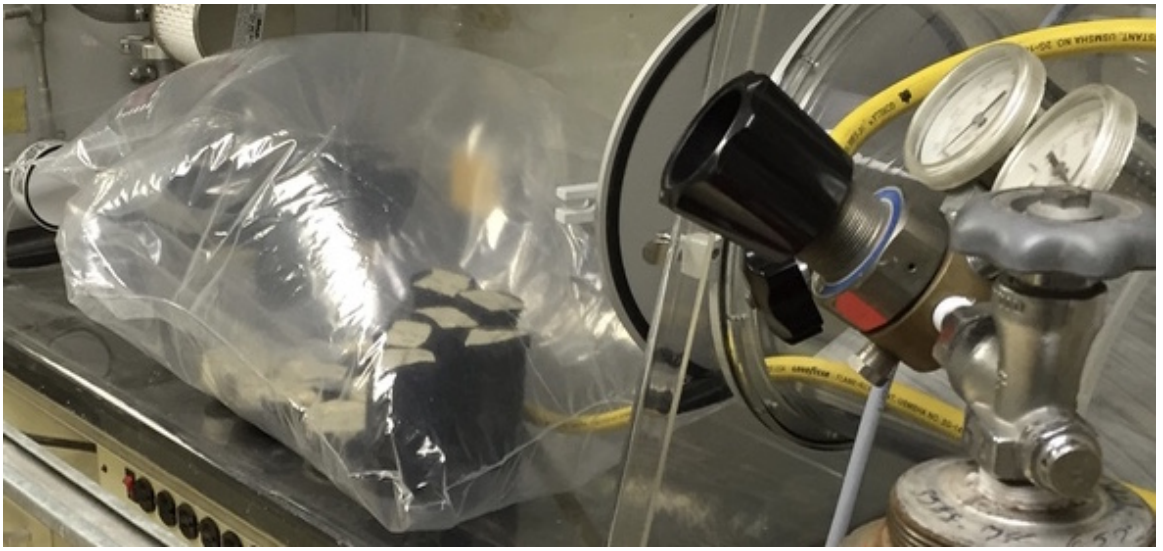

Figure 2.9: Storage of Al/I_2O_5 thermite under nitrogen for aging study

The temperature, pressure, and relative humidity present in the room that the material was stored in were recorded using an ExTech Model SD700 Datalogger at intervals of 10 minutes for the entire 4 week study (Figures 2.10-2.12). The temperature from 19.2 to 25.2 degrees Celsius, the pressure ranged from 24.53 to 25.19 inches of mercury, and the relative humidity ranged from 4.9 to 20.4 percent.

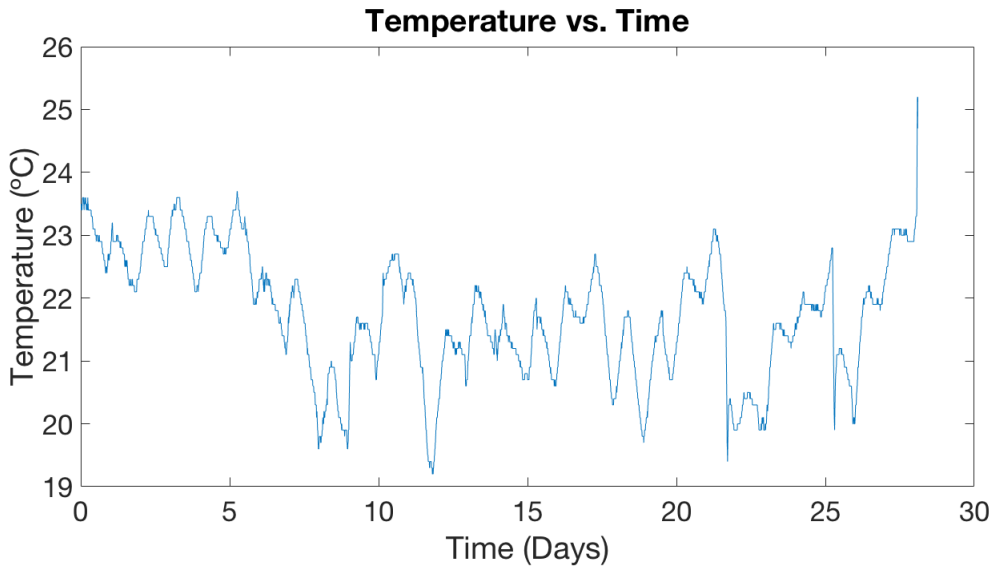

Figure 2.10: Atmospheric temperature (°C) throughout aging study

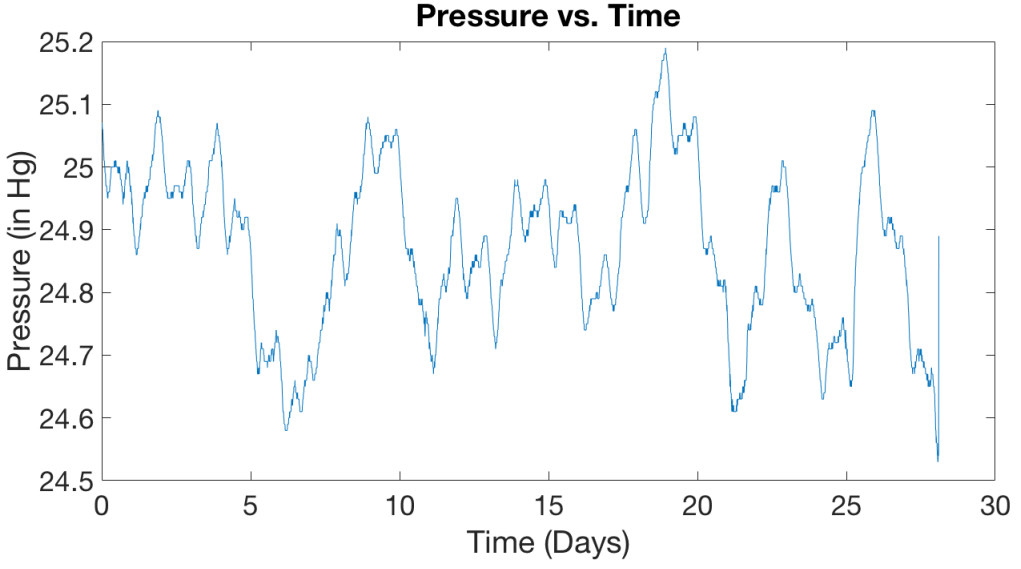

Figure 2.11: Atmospheric pressure (in Hg) throughout aging study

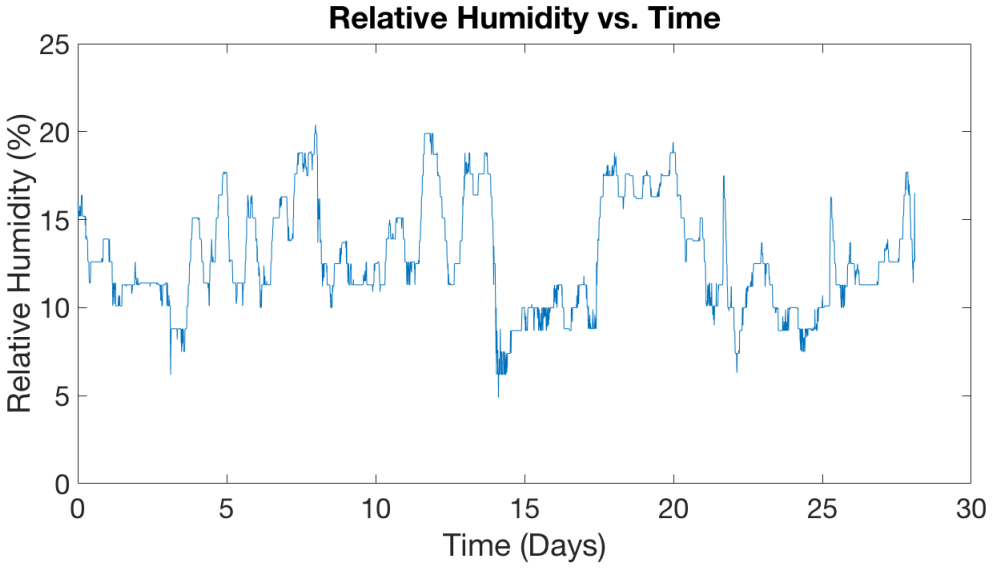

Figure 2.12: Atmospheric relative humidity throughout aging study

The static spark test was not shown to have any "Go's" at 3.5 kV throughout the month with material stored under either atmospheric or nitrogen environments. The final results from the aging study for the Type 12 Impact Tool and BAM Friction Apparatus are shown in Figures 2.13-2.14. The Type 12 Impact Tool results show that the nitrogen-stored thermite was less sensitive than the material exposed to the atmosphere. The BAM Friction Apparatus results show no trends.

The Al/I_2O_5 thermite stored under nitrogen was noticed to have qualitatively similar particle size to the initial mixture, and the Al/I_2O_5 thermite that was not stored under nitrogen seemed to form slightly larger structures. This seemed to happen within the first day of storage and was due to the extended exposure to humidity. This effect did not seem to translate into any major sensitivity differences between the materials, but could have had an effect on the Type 12 Impact Tool trend between the storage methods. The thermite initiation is caused by the shearing of the particles and would lead to more sensitivity when larger particles are present. While this trend exists, the effect is limited as evidenced by the nitrogen-stored material being more sensitive on some days than the atmosphere-stored material on other days. The BAM Friction aging study results do not show any trends between the storage conditions or over time.

The results from the aging study confirmed the hypothesis that the material was sufficiently hydrated previous to receipt from the supplier and would not show any clear differences when exposed to a low level of relative humidity. This was expected due to the rapid hydration rates shown in [26]. The hydration of the material prior to delivery proven by the aging study and the guaranteed removal of the water present during the material's reaction led to all further research being done with the assumption that the material was Al/I_2O_5.

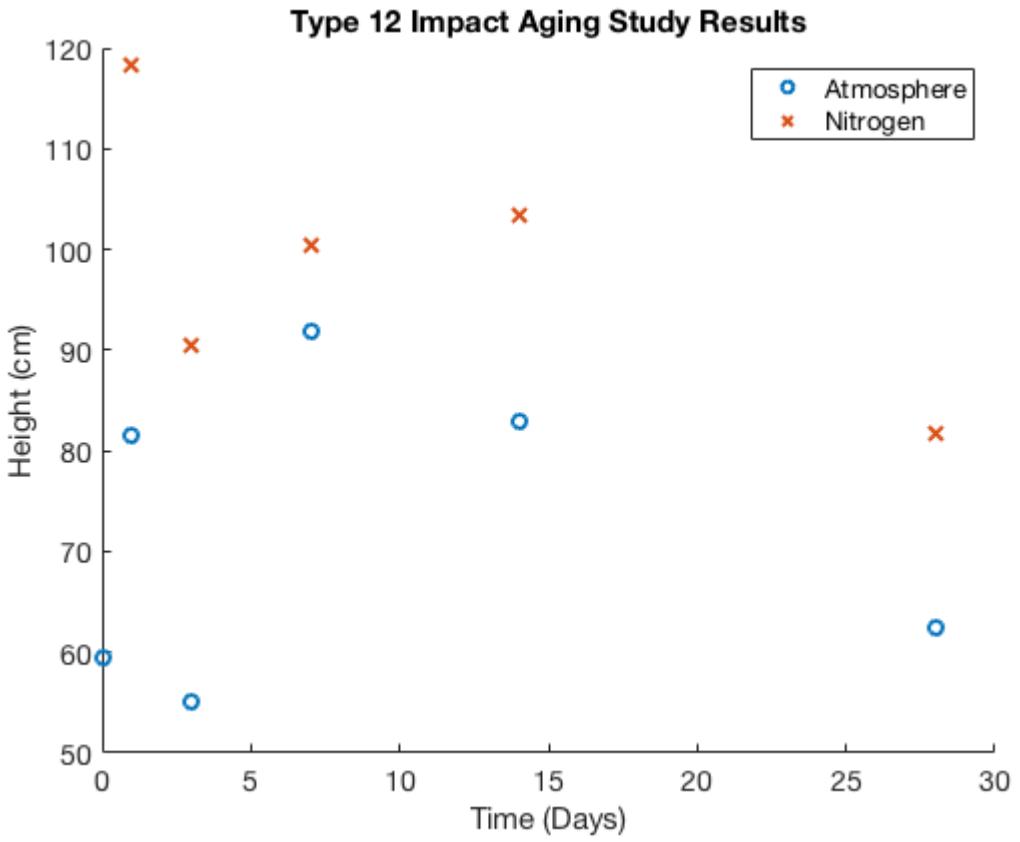

Figure 2.13: Aging study results from Type 12 Impact Tool

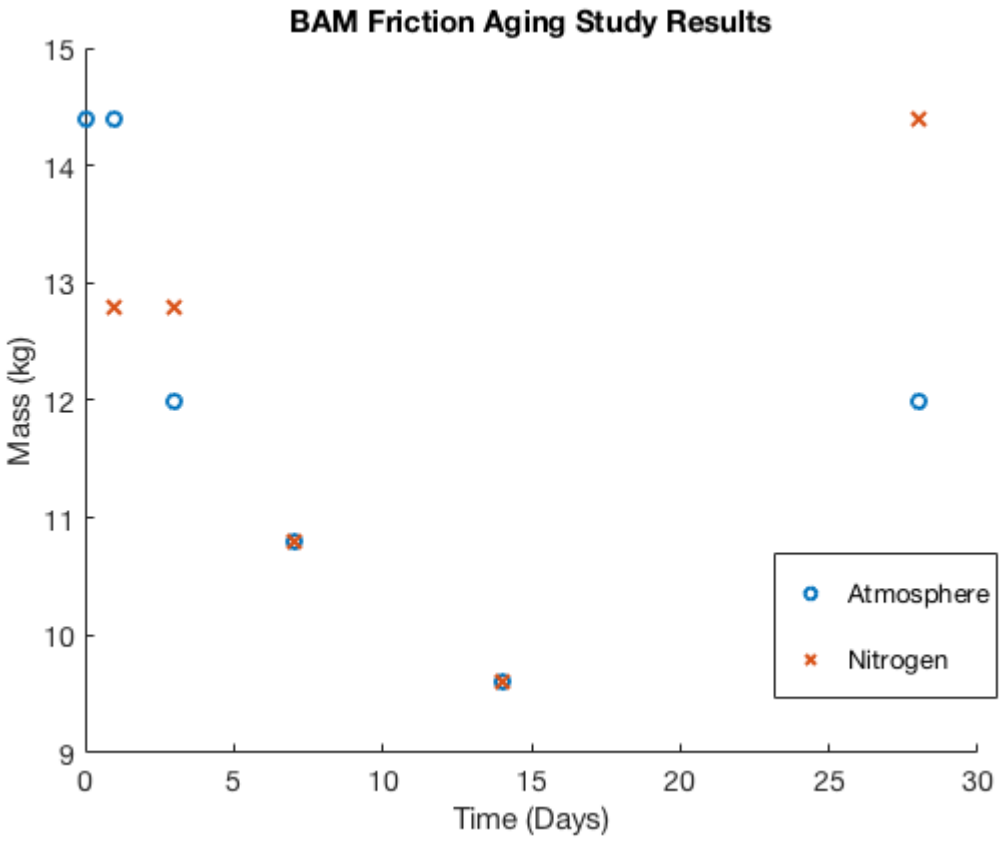

Figure 2.14: Aging study results from BAM Friction Apparatus

CHAPTER 3

INSTRUMENTATION METHODS

3.1 Schlieren

The schlieren optical technique visualizes refractive index gradients in transparent materials [35]. In a gas these refractive index gradients are a function of the gas density, temperature, pressure, and gas species. A dual-lens setup, such as the one used during this research, is shown in Figure 3.1.

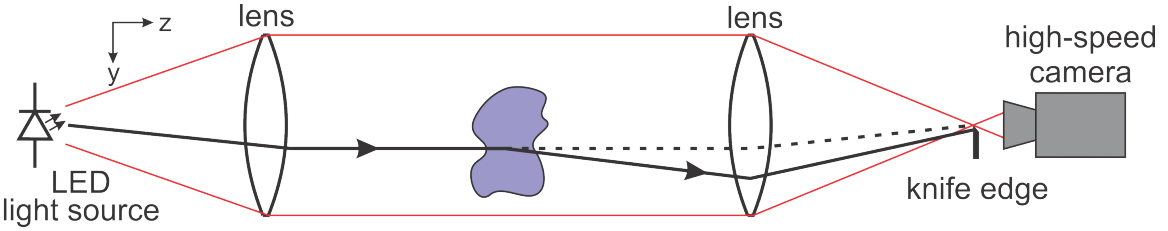

Figure 3.1: Diagram of a dual-lens schlieren setup

An LED is used as a point light source and is located at the focal point of the left lens in Figure 3.1. This light is incident on the first of the matching lenses and the light is collimated. This parallel light between the two lenses creates the test section in which the object of interest is placed. A knife edge is located at the focal point of the second lens. The knife edge placement is of the utmost importance as it creates the schlieren image by blocking the light rays that have been refracted by the object of interest within the test section. Proper placement of the knife edge provides an overall gray image with lighter areas showing light rays that were bent away from the knife edge and darker areas depict where light rays were bent into the knife edge. Following the knife edge, a high-speed camera is placed in order to record the schlieren event [35]. If the knife edge is removed from the light path a shadowgraph image is achieved. Shadowgraphy visualizes the second derivative of the refractive index field, and is useful for visualizing strong gradients.

The schlieren optical method is also used to make quantitative measurements in addition to being a visualization method. A system calibration after

setup can be completed with a long-focal length lens that allows the pixel intensity to be quantified in terms of refraction angle. Once this calibration is complete, various schlieren setups, including the parallel-light schlieren used, have been shown to provide quantitative density measurements within 2-3% when compared to theory [52]. Quantitative measurements will not be made in this research, but the repeatability of the method is important and enables the direct comparison between tests.

For this research, schlieren is used to track the shock wave from the explosive event and the product gases from the Al/I_2O_5 thermite. The shock speed can be determined optically by creating a pixel to distance calibration. This is done by taking an image of an object with a known dimension and then relating this to the number of pixels in the image that the object spans. The time between each image based on the frames per second that the sensor captures data in addition with the calibration length combine to give a velocity at which any trackable object (such as a shockwave) is traveling.

A shadowgraph image of a thermite and detonator test can be seen in Figure 3.2.

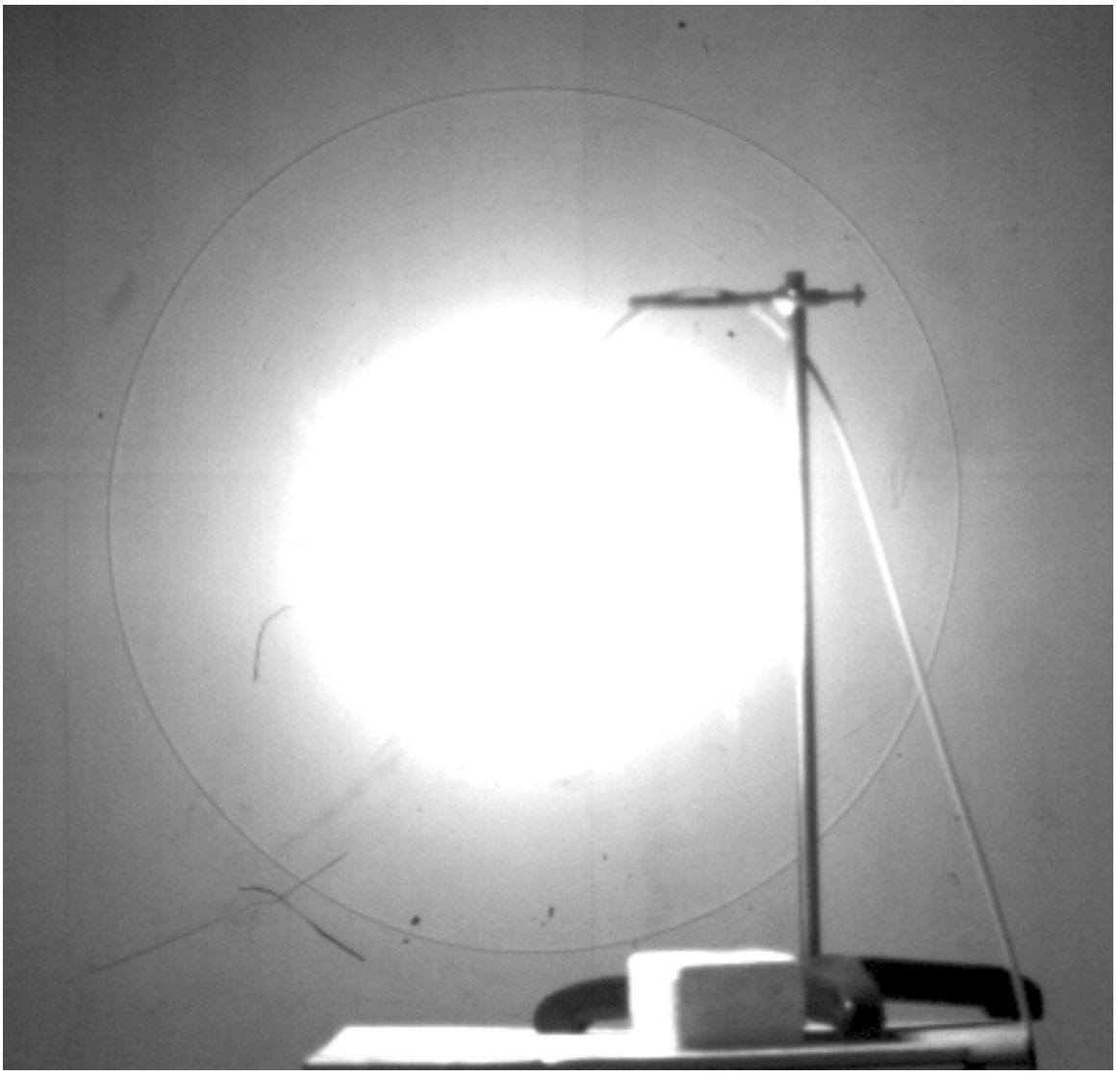

Figure 3.2: Shadowgraph image of an RP-2 Detonator with 5 grams of Al/I_2O_5 thermite

3.2 Spectroscopy

Spectra contain wavelength and intensity information. In a spectrometer, light enters the entrance slit and is refracted onto a diffraction grating that resolves the light's wavelengths. The light is spatially amalgamated by wavelength and sent out the exit slit onto the detector, thus creating a higher intensity for the more ubiquitous wavelengths present. Spectrometers are instruments that group these operations into a single instrument that allows the user to provide a light input at the entrance slit and a detector at the exit slit to collect a spectral response.

Basic spectrometers are used to capture a snapshot of the light that enters the slit and produce the spectrum of light present. These instruments have the ability to yield information over large sections of the spectrum at a single point in time, but do not give any spatial information. They are also limited as to the scan rate time between spectra.

Imaging spectrometers differ from traditional spectrometers in their ability to add a third dimension of information. The source image is reimaged onto the exit slit without changing the spatial orientation of the light. This allows not only the wavelengths and intensities to be found, but also locate the spectrum for every pixel of the CCD detector along the length of the entrance slit. A high-speed camera can be used as the detector to find changes in spectrum in high-speed events, thus providing a fourth dimension of information. Flows can thus be analyzed to distinguish between various chemical species present in a flow and to pinpoint the pixel at which they appear. A figure of the Horiba microHR used in this research is depicted in Figure 3.3 [53].

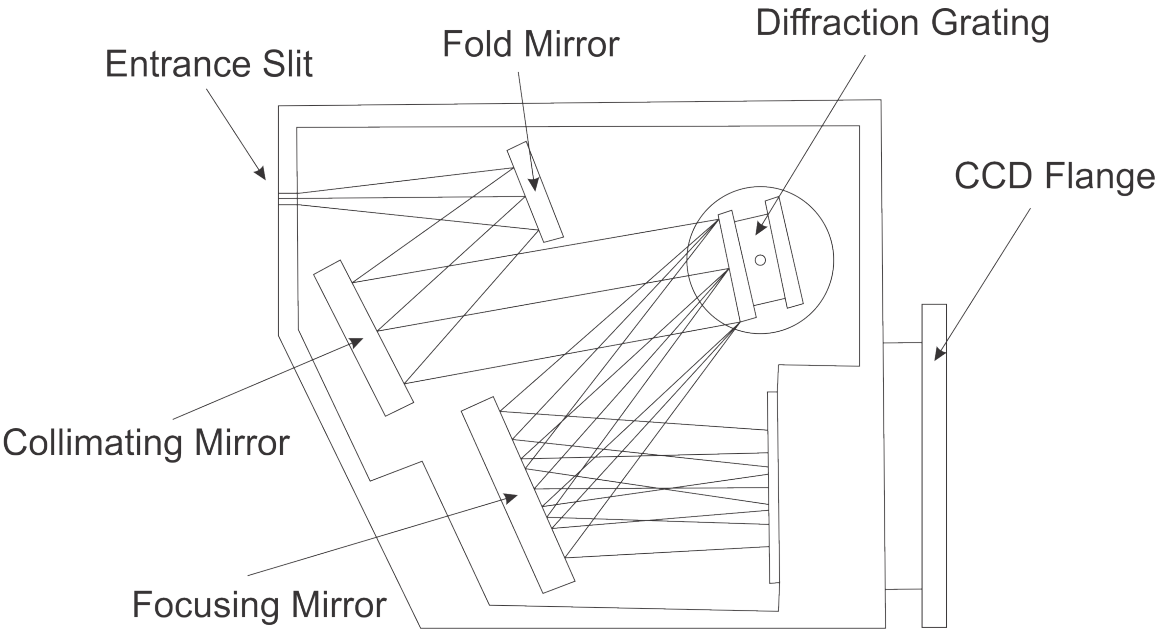

Figure 3.3: Diagram of the internal components of the Horiba microHR imaging spectrometer [53]

Absorption spectroscopy is a method that measures the response of a source light through a fluid. The spectrum with the flow present is compared to the spectrum of the source light and a calibration image of stray light (sources unrelated to the system) as formulated in equation 3.1 [54]. The spectra of the sample is compared to the base signal input from the light source with a correction for any systemic additions from the environment. This leads to values around 1 when there is no absorption and lower values when absorption exists. To graphically

present this in a more logical way the natural log of the data is taken. This results in values of 0 when no absorption exists.

$$\frac{Spectra_{\text{sample}} - Spectra_{\text{LED off}}}{Spectra_{\text{LED}} - Spectra_{\text{LED off}}} \tag{3.1}$$

Various fluids, such as iodine gas, create a known profile of absorption at specific wavelengths that can be viewed in order to locate the chemical species within the image created from the imaging spectrometer. The setup used in this research was developed based on literature on absorption spectroscopy [55, 56] and through discussions with Professor Glumac from UIUC [54]. The setup is depicted in Figure 3.4. An LED acts as a point light source and the first lens creates collimated light through the test section. A green LED is chosen due to iodine's absorption profile from 450-650 nm and the green LED's output focused on 532 nm [43]. This allows the light to pass through any chemical species present and get absorbed or pass through if only air is present. Once the light column reaches the second lens, it is focused back down to the length of the spectrometer entrance slit in order to capture as much information spatially as possible. The imaging spectrometer (Horiba MicroHR) then produces an image that is sent to the detector, a high-speed camera (Photron SA-X2). The use of a high-speed camera allows the spectra obtained to be compared to schlieren images and ensure that the flow can be time-resolved sufficiently for analysis.

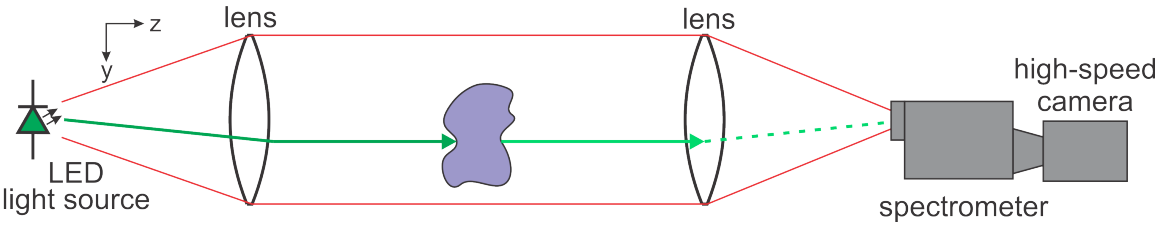

Figure 3.4: Diagram of a dual-lens imaging spectrometer setup

3.2.1 Verification of Iodine Identification

To characterize the imaging spectrometer and high-speed camera setup, a mercury/argon fiber source (Ocean Optics Part #HG-1) was used to calibrate the wavelengths viewed. Figure 3.5 depicts the image obtained from the spectrometer (image processed to enhance pixel intensities and produce a visually-understandable image) and Figure 3.6 shows the plotted emission profile. These peaks, provided by the calibrator's manufacture, determined the specific properties of the system. The grating present in the Horiba microHR (Holographic Plane grating 520 19, spectral range of 450-850) led to a 44 nanometer wavelength range viewed at the sensor and centered on the wavelength entered into the spectrometer's control software.

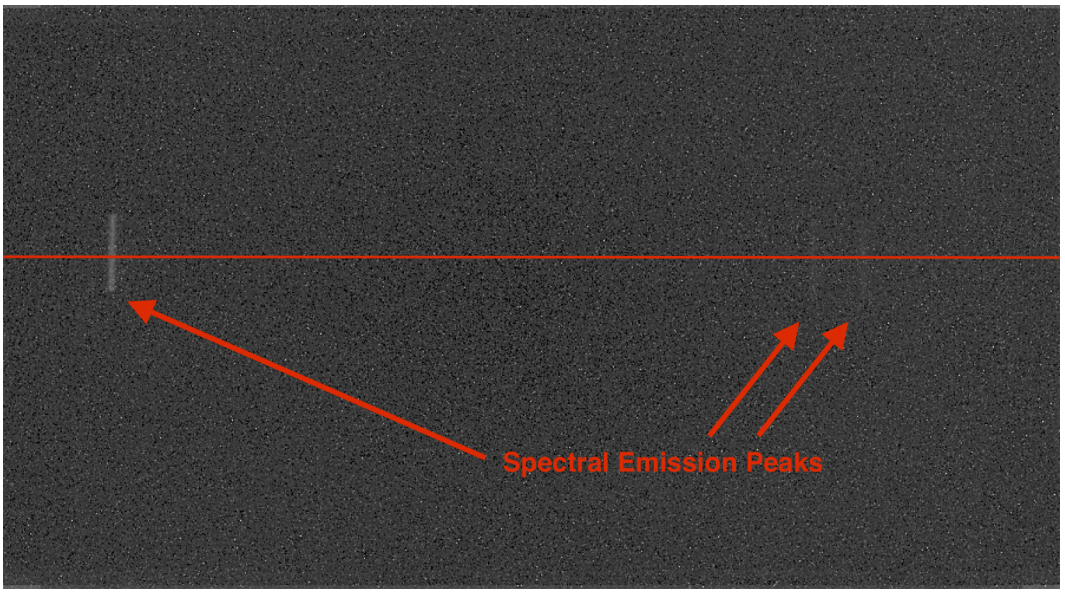

Figure 3.5: Image produced using spectrometer calibrator. Image processed to enhance pixel intensities and produce a visually-understandable image.

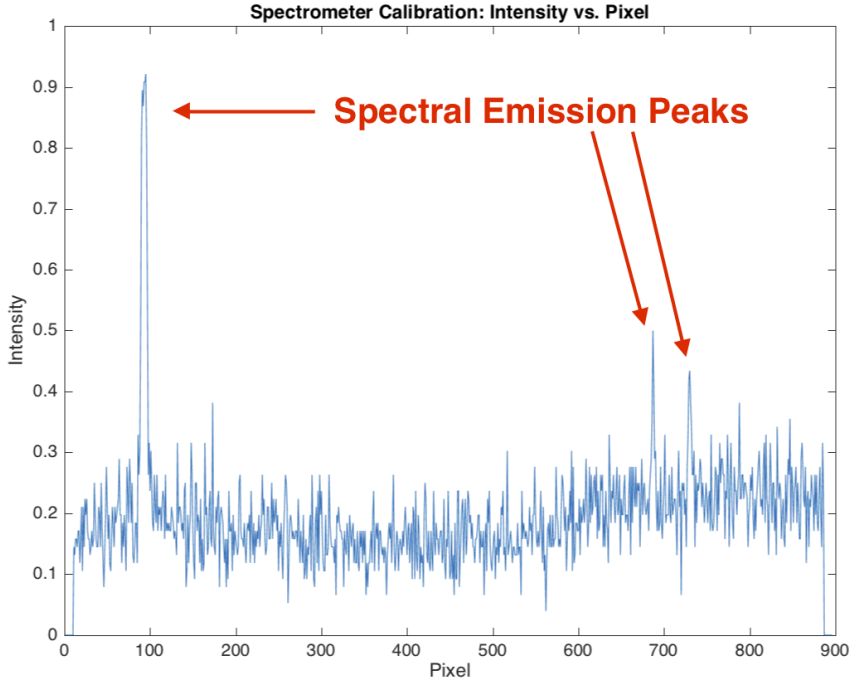

Figure 3.6: Plot of intensity vs. wavelength used to determine system properties.

Iodine is the only gas that has an absorption profile in the visible spectrum

[54]. This profile was roughly determined by Tellinghuisen in 1973 and more recently detailed in higher resolution by Saiz-Lopez [43, 57]. Figure 3.7 depicts the wide absorption spectrum captured by Saiz-Lopez and Figure 3.8 shows a view of the absorption spectrum of iodine gas in the visible range with an included comparison to previous lower resolution work. The units are arbitrary (a.u.) since a slight change in the amount of light provided would change the value that the sensor detects which makes comparisons to other setups difficult.

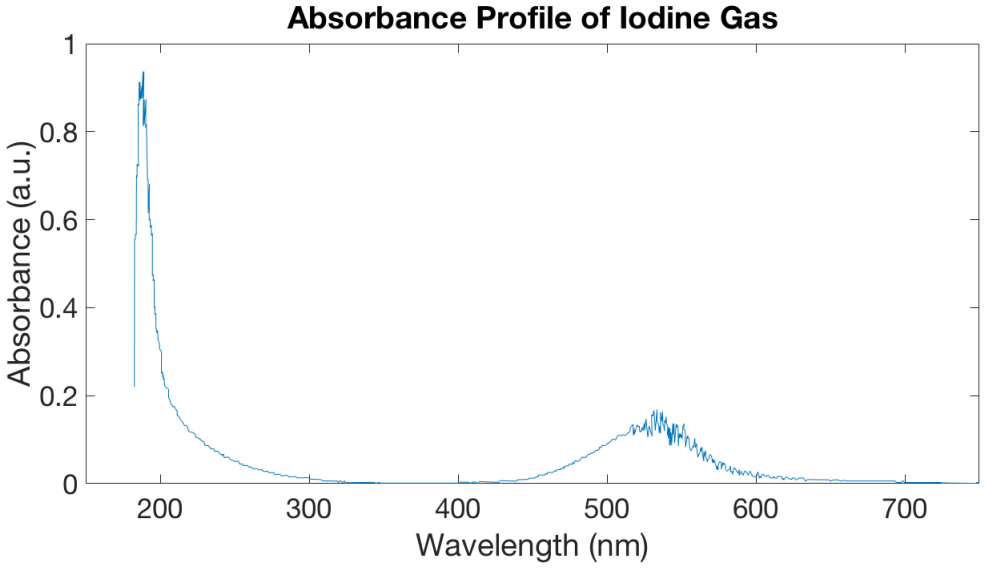

Figure 3.7: Full absorption spectrum of iodine gas digitally reproduced from [43]

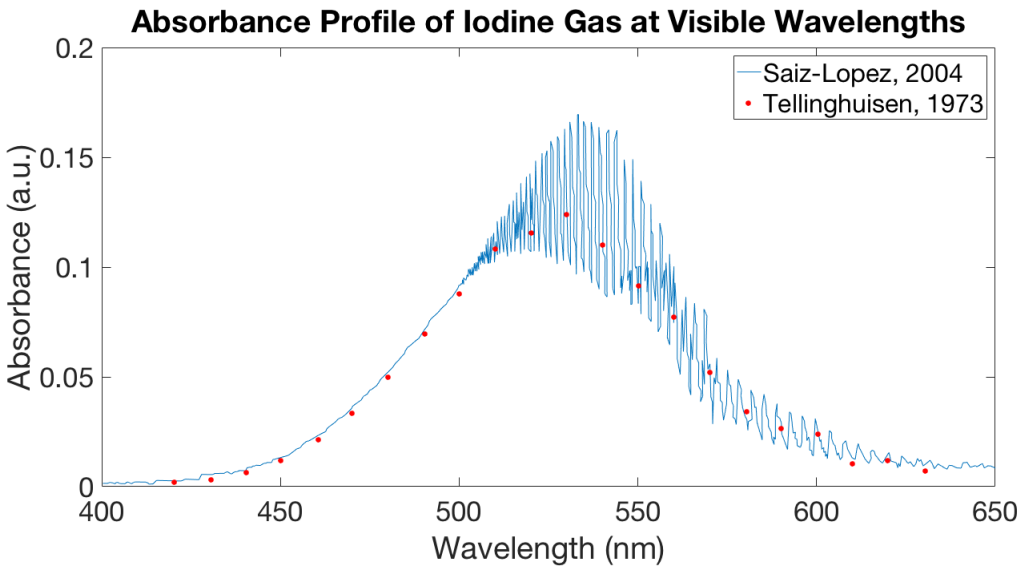

Figure 3.8: Comparison of absorption profiles from literature digitally reproduced from [43]

This work focuses on the visible portion of the spectrum due to the presence of an iodine absorption profile to observe and with knowledge of the lack of interference from other species in this range. To validate the imaging spectrometer setup, an iodine cell from Thorlabs (Part # GC19100-I) was purchased and used to measure the spectral response of iodine gas with the present imaging spectrometer setup. Upon heating the cell, it was shown that iodine is present based on the profile of the response compared to literature. Figure 3.9 shows the setup of the iodine cell being heated and Figure 3.10 shows the light incident on the spectrometer slit in which the iodine cell (circular shadow) can be seen as well as the mount used.

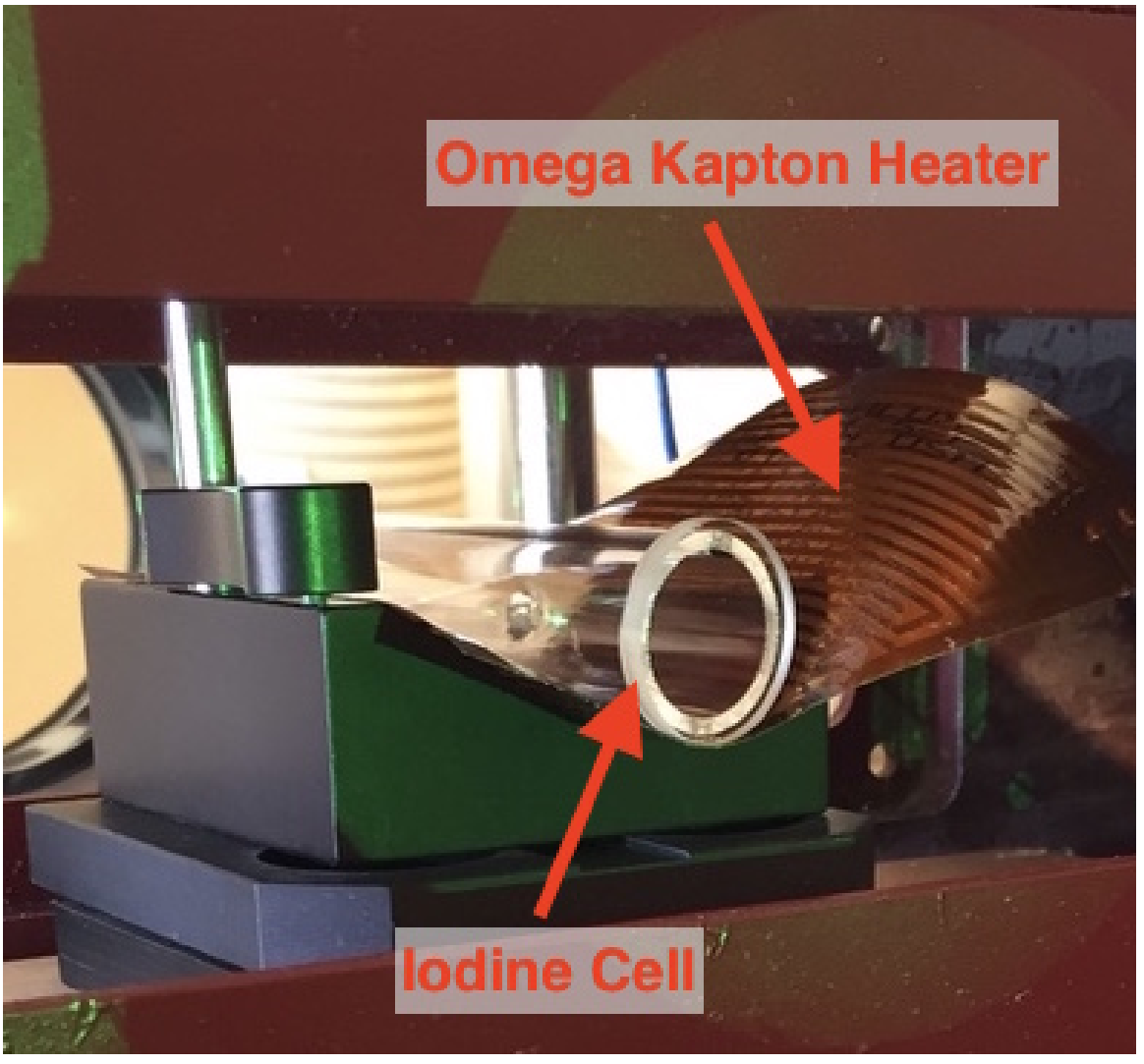

Figure 3.9: Setup of the iodine cell within the test section of the spectrometer

Figure 3.10: Light incident on spectrometer entrance slit. The circular shadow in the center is the iodine cell.

To ensure accurate data was taken, an arc lamp with wider spectrum output was used in the lab to capture a wide absorption profile for comparison to literature. Only 44 nanometers can be captured at any one time, so multiple tests were conducted to complete the desired spectrum and placed side-by-side. Figure 3.11 shows this data which compares well to the absorption of iodine from literature (Figure 3.8). A profile of the expected data from future tests was taken and is shown in Figure 3.12. This contains the wavelengths from Figure 3.11 in which iodine's absorption profile has reached it's maximum and is now declining.

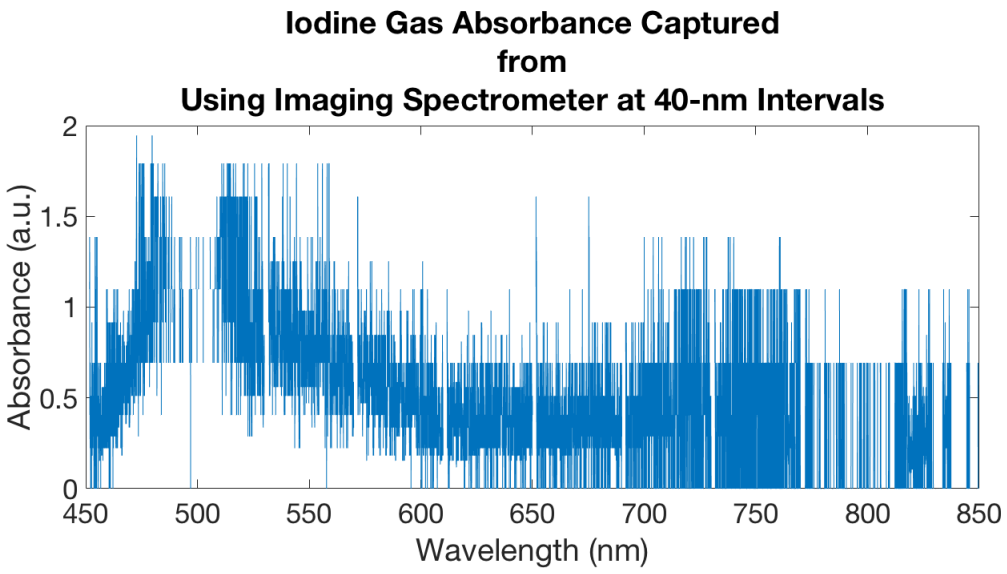

Figure 3.11: Absorbance from iodine calibration using imaging spectrometer

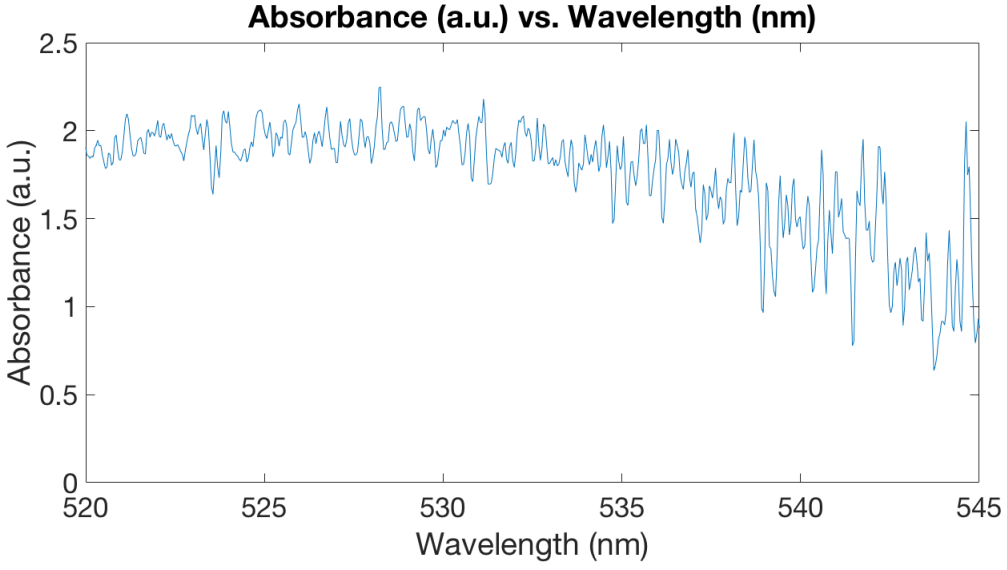

Figure 3.12: Typical iodine response in wavelength range of field setup

This process made it easy to verify the absorption profile of iodine and to ensure identification of the correct species due to the stationary gas and ability to know where in the image the profile should be observed.

The limits of this setup are determined by the light source and the imaging spectrometer grating used. The imaging spectrometer is limited in the overall band of the spectrum that can be captured due to the grating used and the ability to reflect the appropriate wavelengths. It can provide data from 450-850 nm as

shown in Figure 3.11. The green LED output used in field tests is centered around 532 nm and is a narrow band of wavelengths. The output falls drastically moving away from 532 nm. The light source used to capture the wide spectrum of iodine gas shown in Figure 3.11 was not used in field tests due to test setup ease with the green LED and the ability to only capture 40 nm during tests.

3.3 Pressure Transducers

PCB Piezotronics' pressure transducers are used as an additional method to track the shockwaves. A typical shockwave's pressure profile can be seen in Figure 3.11. the initial rising edge is extremely sharp due to the large pressure differential that the shockwave creates. The peak pressure is not used, but the time of arrival with respect to one another and the physical separation of the sensors allows the speed of the shockwave to be calculated.

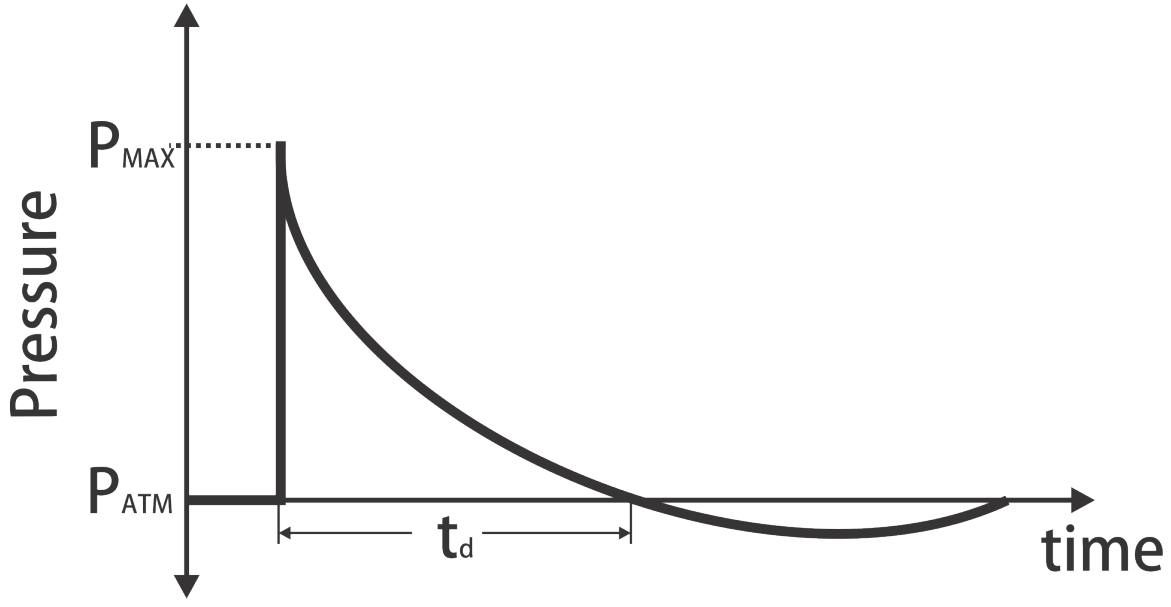

Figure 3.13: Typical pressure profile of a shockwave

CHAPTER 4

TUNNEL FOR HIGH-SPEED OPTICAL RESEARCH (THOR)

The Tunnel for High-speed Optical Research, THOR, was custom- designed and built for this research. The fixture required that an explosive charge could be initiated, creating an explosion that would propagate through a contained chamber which could be approximated as nearly one-dimensional. The fixture required that simultaneous schlieren and imaging spectrometer optical techniques could be applied as well as traditional piezoelectric pressure data be recorded. In addition, a modular design for future expansion to higher masses of explosives and other research applications was also taken into consideration.

4.1 Design

The chosen design was a three-piece fixture with individual sections for the explosion location, diagnostics, and an exhaust section. A square cross-section was utilized to simplify the optical diagnostics, allowing windows to be placed on each of the four walls, yielding transverse diagnostic paths. Two pressure ports were included to track the shock wave from the event for comparison to the shock speed to be calculated from the schlieren images and to measure time-resolved pressure throughout the events. A cross-section of 10.16 centimeters by 10.16 (4 inches by 4 inches) centimeters was determined to allow a sufficient view-window (5.08 centimeters, or 2 inches, in height) and minimize the metal thickness due to the incident pressure from the explosive event. The lengths of the three sections of the fixture were then decided: 20.32 centimeters (8 inches) for the explosive driver section, 35.56 centimeters (14 inches) for the diagnostic section, and 35.56 centimeters (14 inches) for the exit section for a total of 91.44 centimeters (36 inches) of length. An initial schematic of the fixture can be seen in Figure 4.1.

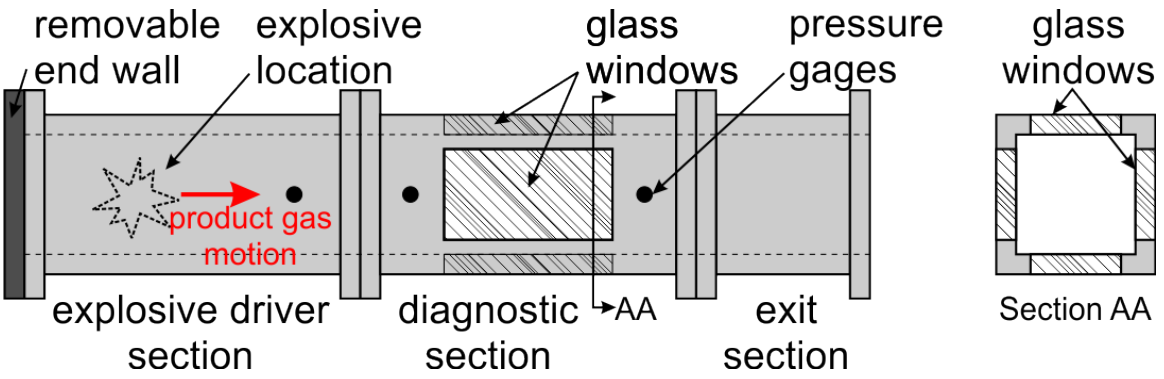

Figure 4.1: Schematic of the modular design concept for THOR

In addition to these specifications, a maximum explosive amount of 5 grams was chosen. Small-scale experiments were planned in order to limit the amount of gas produced and ease the visualization by not creating an impenetrable flow. To allow for future expansion of research with the fixture, a large TNT equivalence of 3 was also applied to account for various possible explosives [58]. This resulted in a maximum 15 gram TNT equivalence mass for the fixture to withstand. The peak overpressure ratio versus scaled distance from [59] and [60] were used to find the estimated pressure on the interior fixture wall. The scaled distance is found using equation 4.1.

$$Z = \frac{R}{(\frac{WT_a}{P_a})^{1/3}} \tag{4.1}$$

This equation results in a factor of the peak overpressure as a function of distance. R is the radius from the event, W is the mass of explosive in kg, T_a is the ambient temperature in K, and P_a is the ambient pressure in bar. The average ambient pressure and temperature throughout 2015 in Socorro, NM was found to be 101880 Pascals (1.0188 bar) and 288.65 K [61]. Figure 4.2 shows the graphical depiction of the scaled distance and overpressure factor relationship. An expected peak overpressure of 200 P_{atm} was determined based on average atmospheric conditions and the expected interior dimensions of THOR.

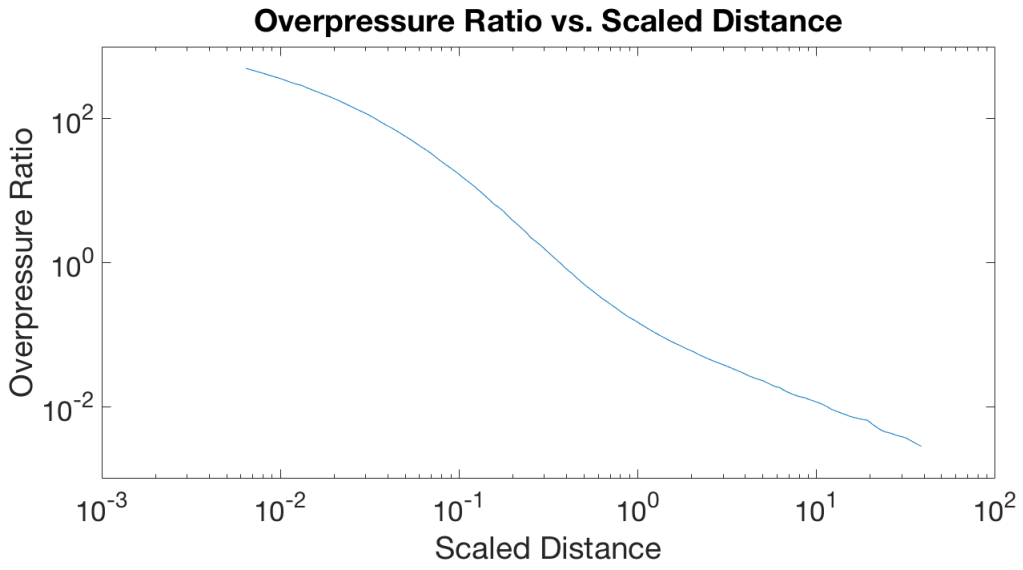

Figure 4.2: Peak overpressure ratio versus scaled distance [59]

The material selection was the final determining factor of the necessary wall thicknesses: A hardened steel (Rockwell C26), 4140/4142 steel alloy, was chosen to minimize the material thickness and resist fracturing during repeated stress loading [62]. Roark and Young's Formulas for Stress and Strain experimentally found equation 4.2 to determine the stress on a rectangular plate that has fixed edges and a uniform pressure load [63]. q is the pressure applied to the plate (peak overpressure used), b is the dimension of the shortest side of the plate, and t is the thickness of the plate.

$$\sigma_{\max} = \frac{\beta_1 q b^2}{t^2} \tag{4.2}$$

Equation 4.2 was used to calculate the resultant maximum stress and then compared to the steel's yield stress until an acceptable safety factor was found. For the explosive section, a thickness of 1.905 centimeters (0.75 inches) results in a safety factor of 2.6. The same calculations were completed for each of the sections based on the decrease of peak pressure with distance. The diagnostic section was constructed with a 1.27 centimeters (0.5 inches) thickness and the exit section was constructed with a 0.635 centimeter (0.25 inches) thickness. This saved money, machining time, and weight. To increase modularity beyond the three sections, four walls were machined independently and then bolted to one another to achieve the square cross-section. Flanges were designed that slid onto the two ends of each of the three sections and bolted into place. These flanges are then bolted to one another to create the fixture. With this high degree of modularity, a single wall of one of the sections can be replaced if necessary.

To direct the flow through THOR in a single direction, a 1.905 centimeter (0.75 inch)-thick end plate is bolted to the end of the explosive section to direct the

flow through the other side. For the windows, optically-clear acrylic was used in order to ensure they survive repeated tests and enable the optical methods. They are bolted from the inside out with a countersunk head in order to keep a smooth sidewall to prevent the introduction of any turbulence. The complete 3D model can be seen in Figure 4.2.

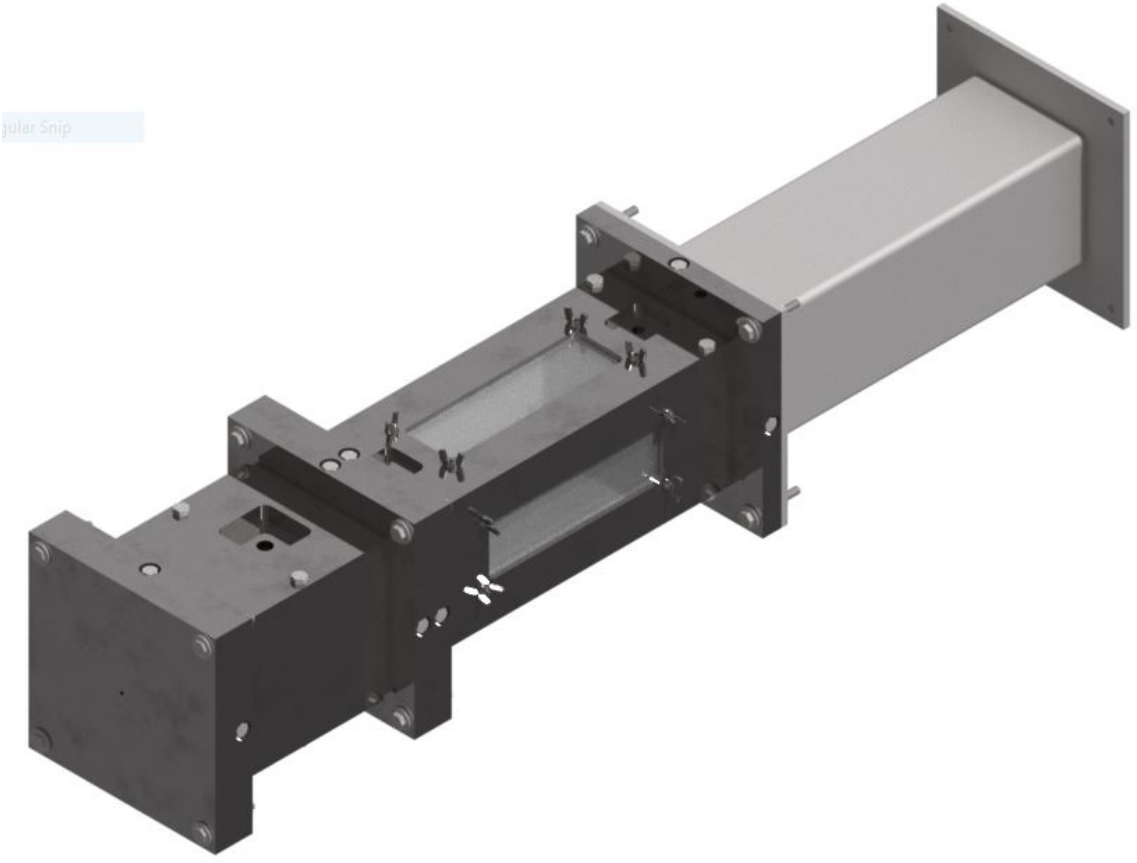

Figure 4.3: Complete 3D model of THOR

4.2 Build

The build process of THOR involved cutting the raw stock to size and then end-milling the interior geometries. Figure 4.3 shows the machining being performed for one of THOR's windows. Figure 4.4 shows the author performing the machining. Once the parts were prepared, the numerous through-holes were drilled and the threaded holes tapped. The modularity of the fixture results in a total of 40 bolts/screws. The exit section could not be bolted due to the material thickness being too thin. A square tube was purchased to allow this thickness

and the flanges were welded to the exit section. After machining was completed, THOR was primed and painted to prevent any oxidation.

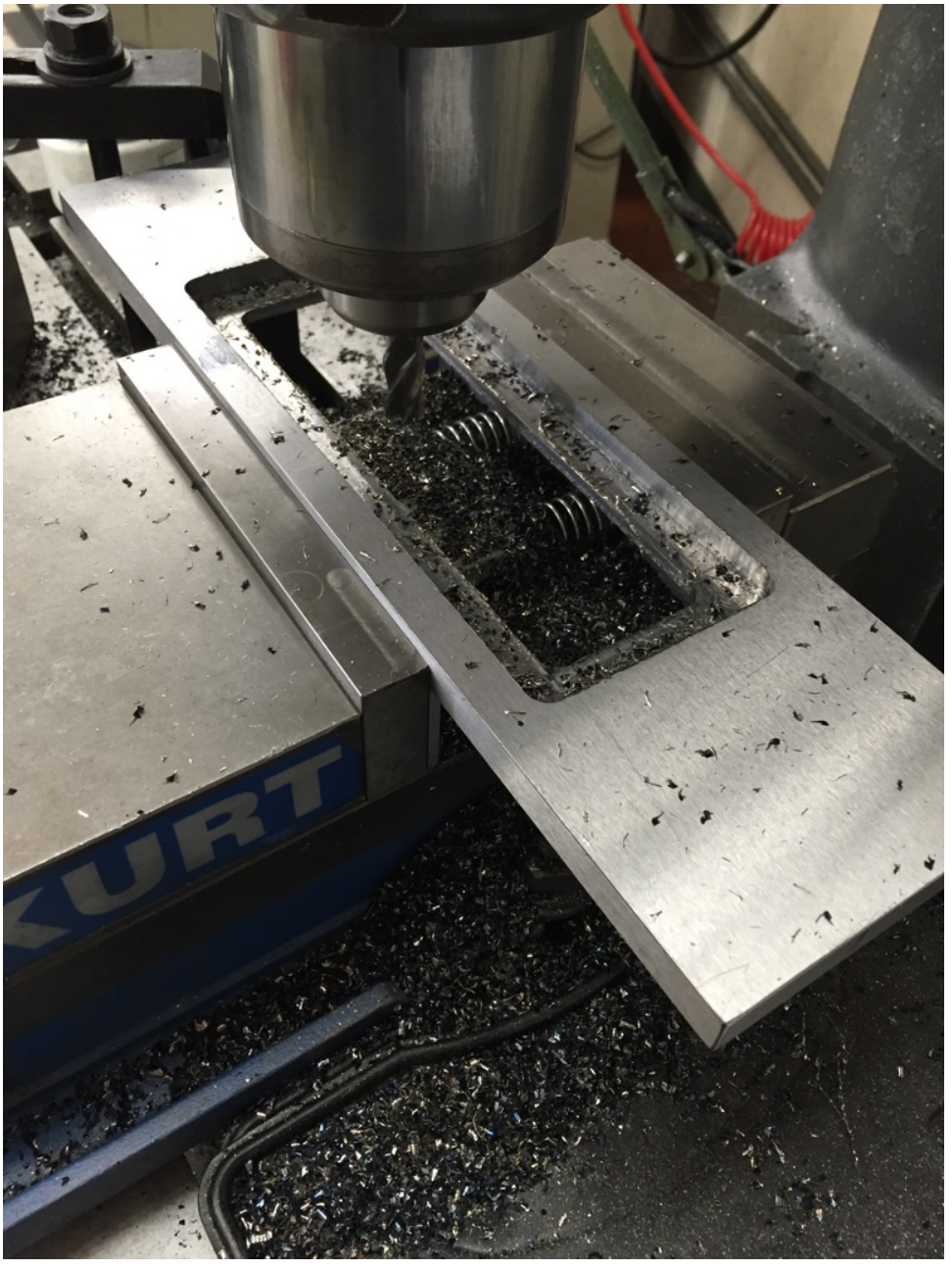

Figure 4.4: End-mill machining of THOR window

Figure 4.5: Machining of THOR by Author

For quick and precise construction of the windows, a laser cutter was used. The outline of the window with the curved corners and preparation holes for the bolts can be made much faster when compared to traditional machining techniques. A sheet of acrylic could be cut into windows within 30 minutes. The countersink for the bolt head was the only step left after laser cutting.

4.3 Modifications

For the first test of THOR, loose thermite powder was contained within a water balloon with an inserted Teledyne RISI RP-2 detonator to test the fixture. A large amount of thermite (12 grams) was used to show that THOR would indeed contain the event and act as expected. An image from this successful test can be seen in Figure 4.5. These initial tests were conducted to determine if any modifications were necessary, and it was found that the length of the exit section was insufficient. The exit section exists to remove the interference that is caused due to compressible flow features, but the 35.56 centimeter (14 inch) length of the exit section did not provide sufficient time. The shock wave created by the detonator

leaves the exit section and an expansion wave is sent back into the fixture due to the pressure differential. This expansion wave travels through the fixture and bounces off of the closed end, leaves the fixture, and creates a shock wave that is sent back into the fixture due to the change in pressure. With the 91.44 centimeter (36 inch) exit section, this second shock wave is incident on the gas front as it reaches the diagnostic section windows, as seen in Figure 4.6. The shock reaches the diagnostic windows at the same time as the gas front, so the turbulence could not be appropriately measured. Figure 4.7 details the compressible flow features that are evidenced with THOR and Figure 4.8 shows a streak image for comparison to an actual test with the original exit section. A 2.44 meter (8 feet) exit section was machined to prevent this from happening in future tests.

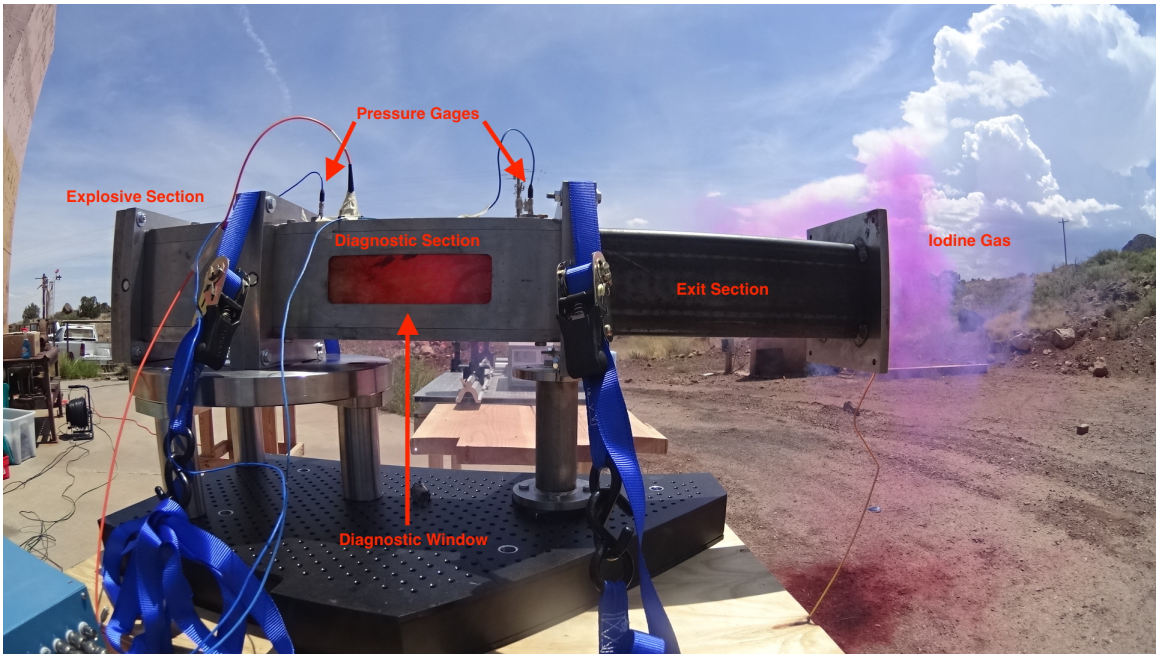

Figure 4.6: Test of THOR with 12g of thermite and a RP-2 detonator used for initiation. The purple gas is indicative of iodine gas.

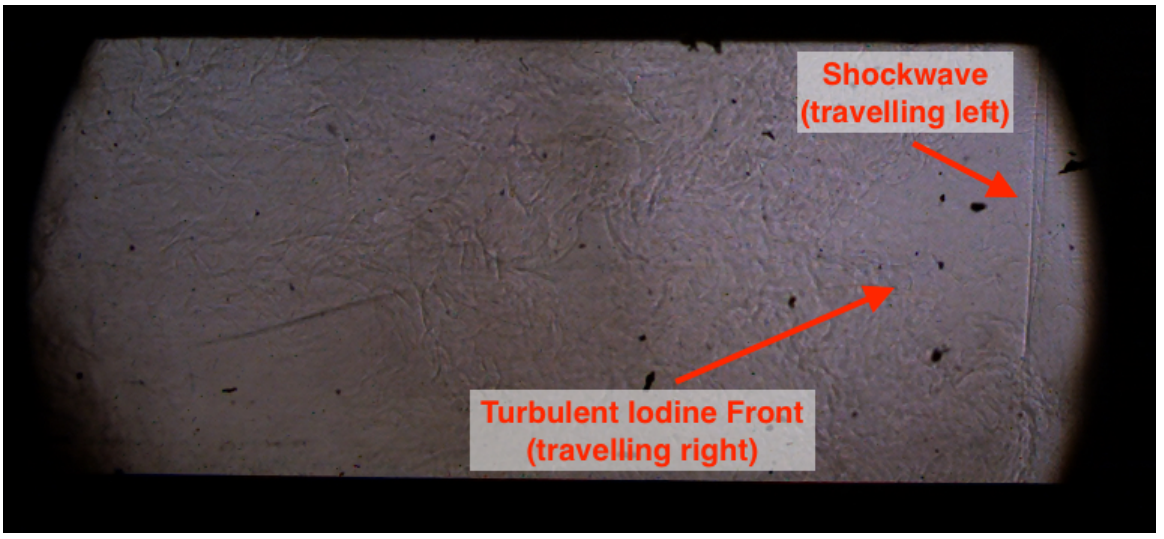

Figure 4.7: Interaction between shock and iodine gas front. The gas front has reached the windows, but has been disrupted by compressible flow features.

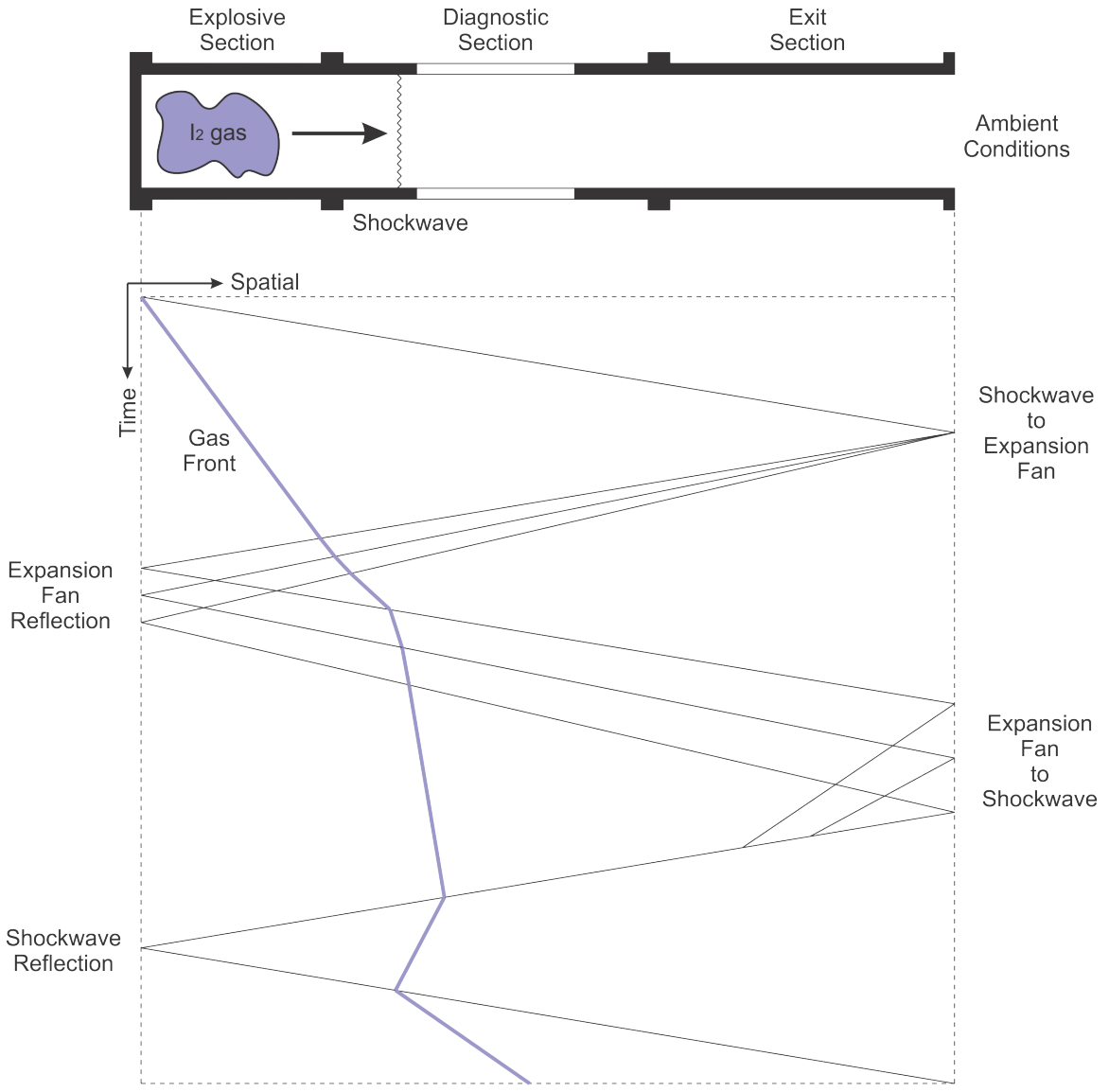

Figure 4.8: THOR's shock and gas front interactions with the original 35.56 centimeter (14 inch) exit section: The shockwave leaves THOR, sends an expansion wave back into THOR, and then creates a shockwave that interacts with the gas front in the diagnostic section upon traveling back into THOR.

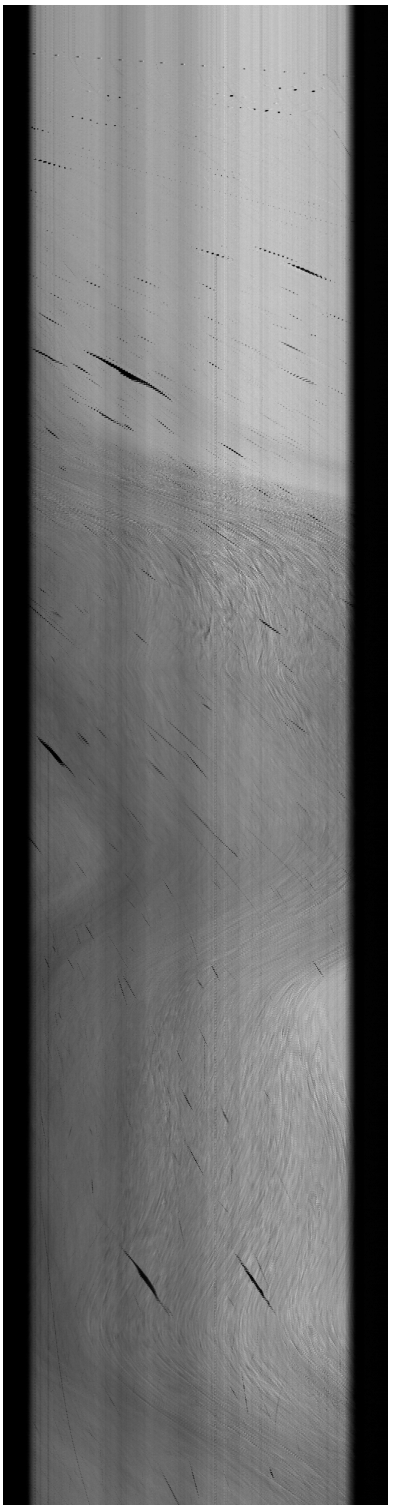

Figure 4.9: Streak image of thermite test with original exit section for comparison to wave diagram

Following the initial loose-powder tests, pellets were pressed in order to achieve a consistent setup. Nitrocellulose was used as a binder and expected to increase the rate of propagation [64]. Upon initiation with a bridgewire, the pellets became projectiles with the thermite in immediate contact with the bridgewire fracturing away and slowly initiating (Figure 4.9) rather than the fast propagation throughout the entire pellet as was planned. The pellets were found almost fully intact after the test (Figure 4.10).

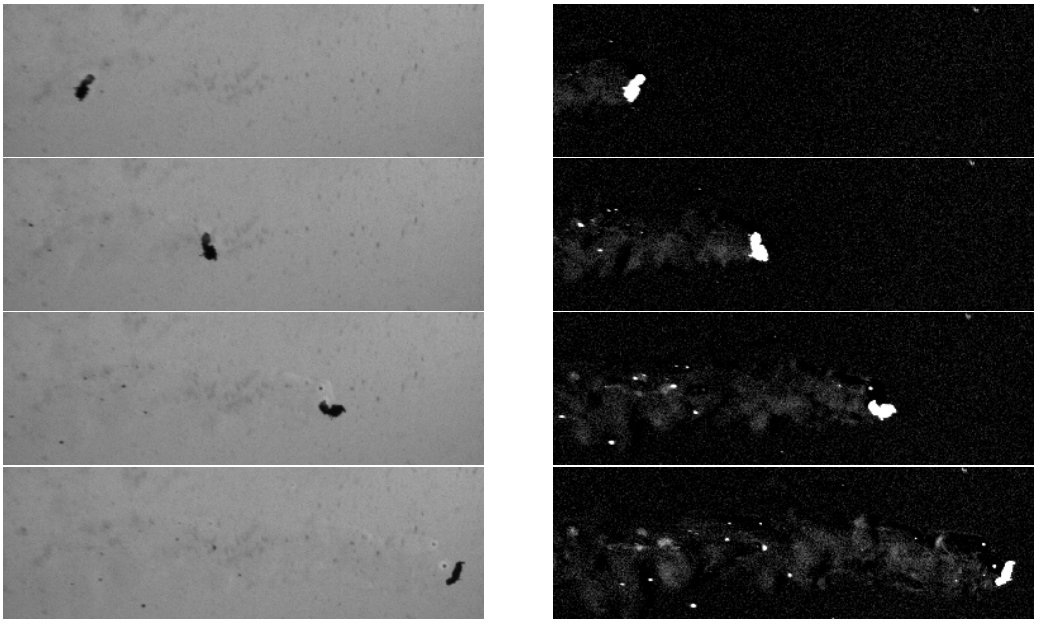

Figure 4.10: Raw images (left) and processed images (right) of Al/I_2O_5 thermite reacting as pellet travels down THOR as projectiles

Figure 4.11: Al/I_2O_5 thermite pellet after test, found mostly intact

To correct this issue, a powder containment vessel was developed (Figure 4.11). It consists of a Swagelok tube fitting to clamp onto the detonator shell that houses the RP-2 detonator, a cone that contains the exact volume of the loose powder of thermite for the planned mass, and a plastic transparency to encapsulate the Al/I_2O_5 thermite. This containment method was used for all subsequent testing.

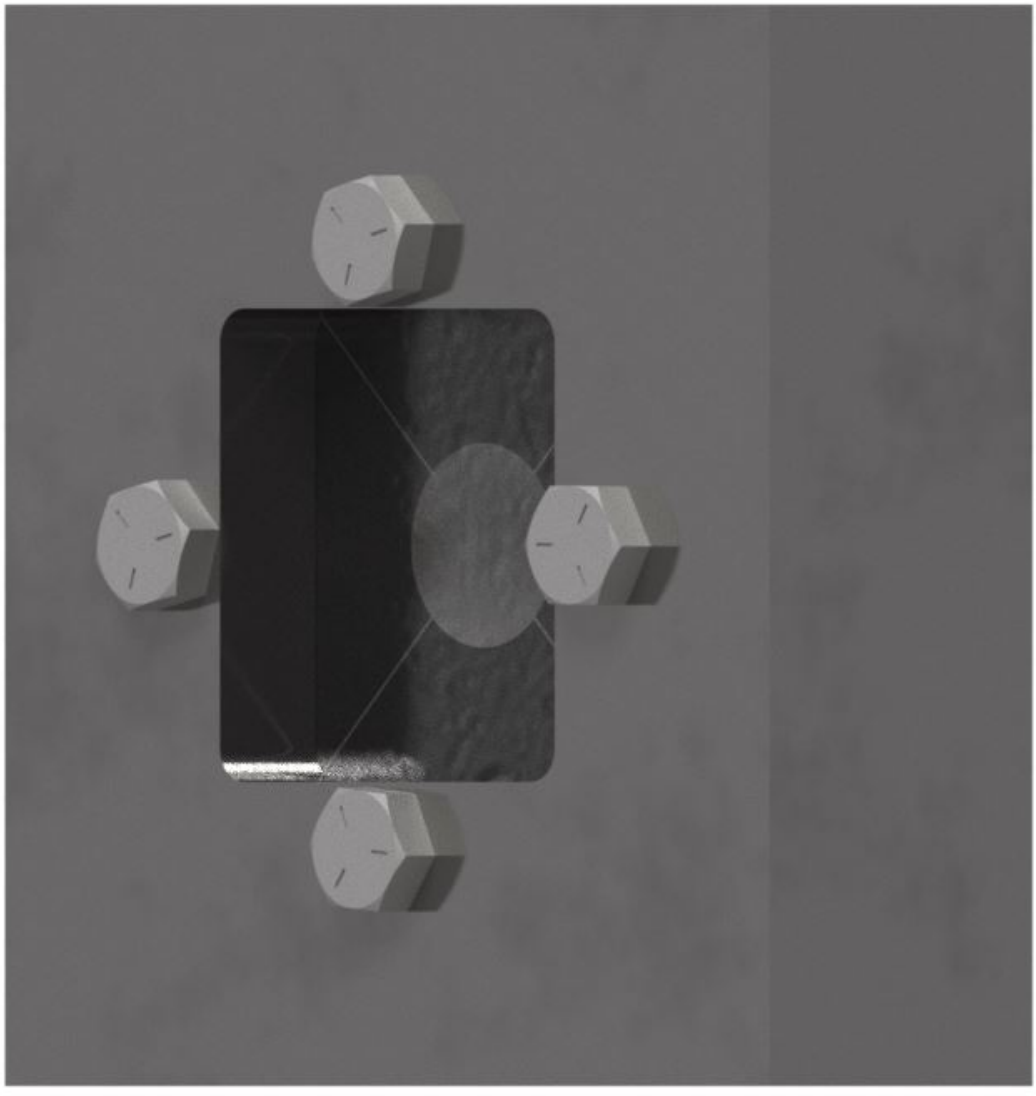

Figure 4.12: Powder containment vessel

Final THOR drawings can be found in appendix A.

CHAPTER 5

IODINE IDENTIFICATION IN AL/I_2O_5 PRODUCT FLOW AND SHOCK SPEED VERSUS THERMITE MASS

5.1 Setup

The setup of THOR, the optical systems, and the pressure transducers can be seen in Figures 5.1-5.4. THOR is positioned on an optical table for easier alignment. The exit section's end is placed outside of the room in order to safely exhaust the iodine gas created. Looking into the room, the spectrometer system is seen from right to left and the schlieren setup is sent into the room and reflected through THOR optical diagnostic section vertically via mirrors. The green LED passes through the first lens, then the collimated light travels through the diagnostic windows, the light is incident onto the second lens that then demagnifies it onto the spectrometer's entrance slit. The schlieren setup is situated so that mirrors are used to direct the light through the diagnostic section. The LED is positioned underneath THOR and pointed towards the explosive section. The first mirror is placed underneath THOR at the diagnostic section's location and the light is sent vertically through the first schlieren lens, through THOR, and then onto the second schlieren lens. From there, another mirror directs the light to the knife-edge and Phantom v711 high-speed camera that is located on a platform above the spectrometer and Photron SA-X2 high-speed camera. On top of THOR, on either side of the diagnostic windows, the PCB Piezotronics pressure transducers can be seen. They are flush mounted into the interior volume.

Figure 5.1: The overall setup of THOR

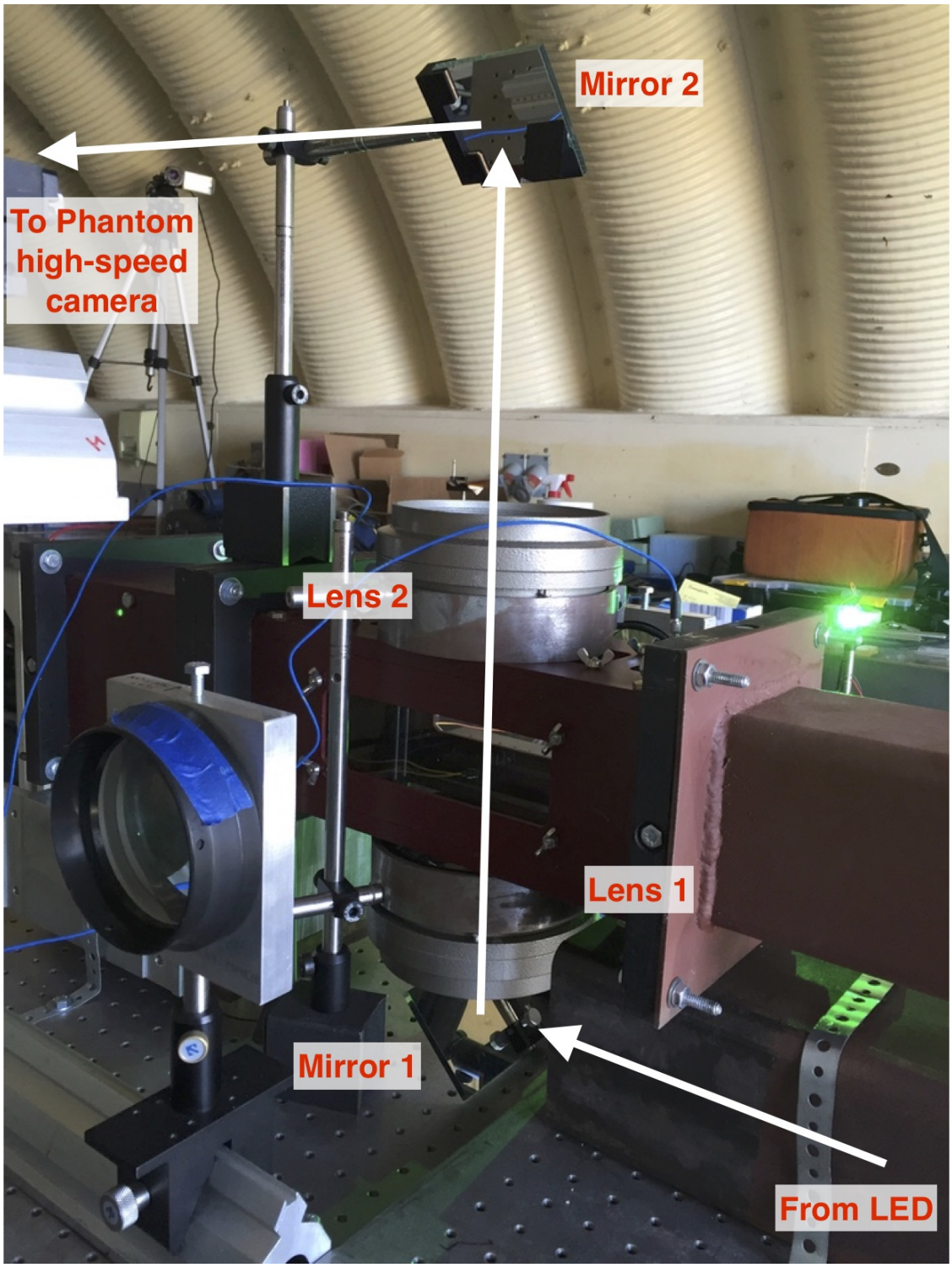

Figure 5.2: The schlieren setup through THOR

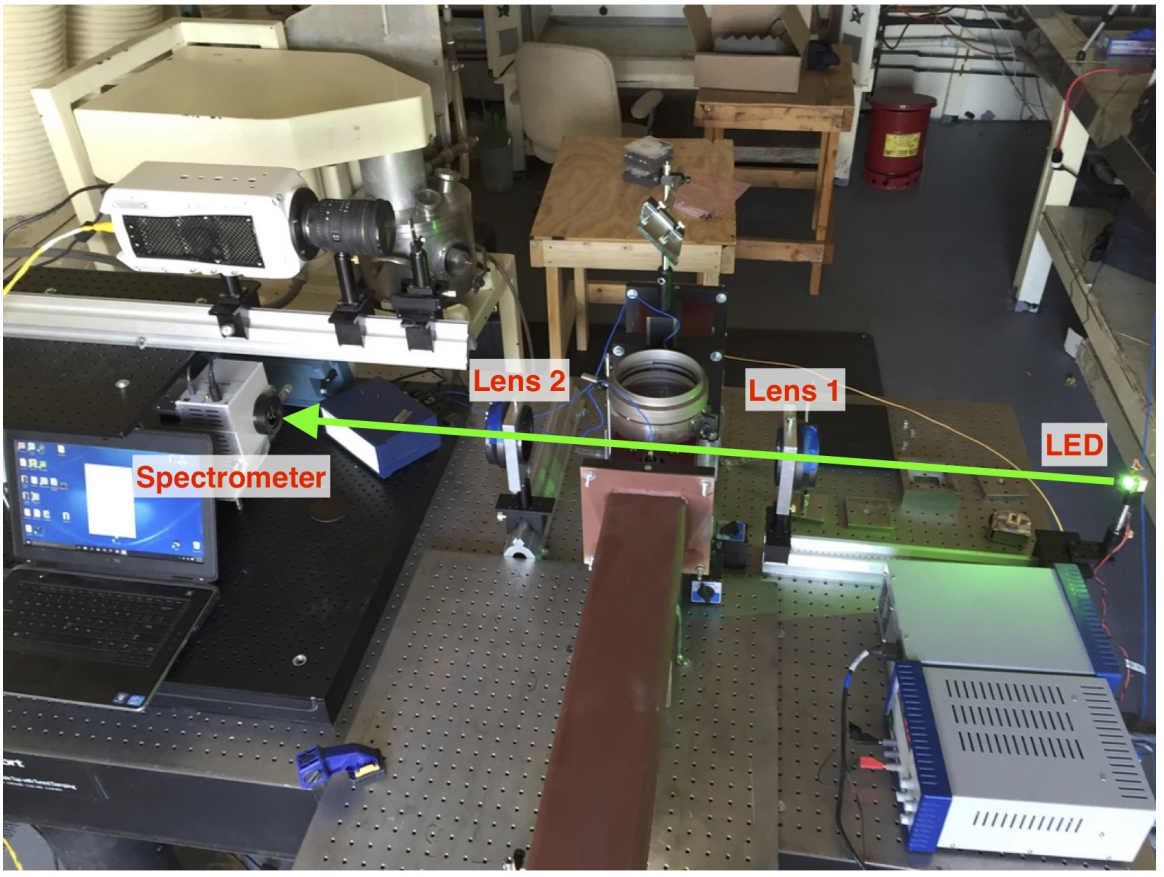

Figure 5.3: The spectrometer setup through THOR

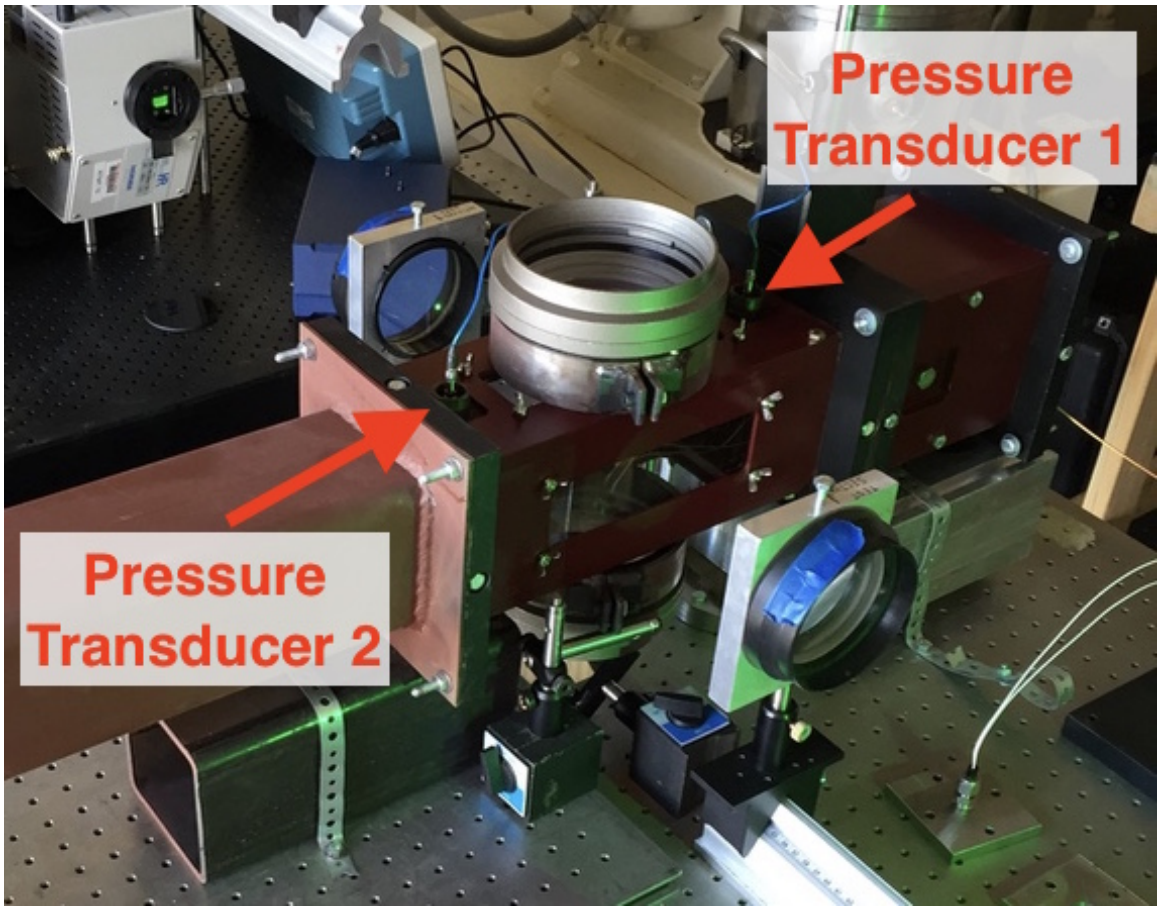

Figure 5.4: The pressure transducers located on the top-side of THOR

5.2 Shock Speed Versus Thermite Mass Present

The speed of the shock wave created by the initial reaction of the detonator was found to change dependent on the amount of Al/I_2O_5 thermite present. The more thermite present, the higher the speed of the shock. Throughout this work, two basic setups for the ignition of the thermite were used: A small plastic bag with the detonator inserted that was hung inside of THOR (Figure 5.5) and a metal fixture that enabled the detonator to be centered and directed straight down THOR (Figures 5.16-5.17).

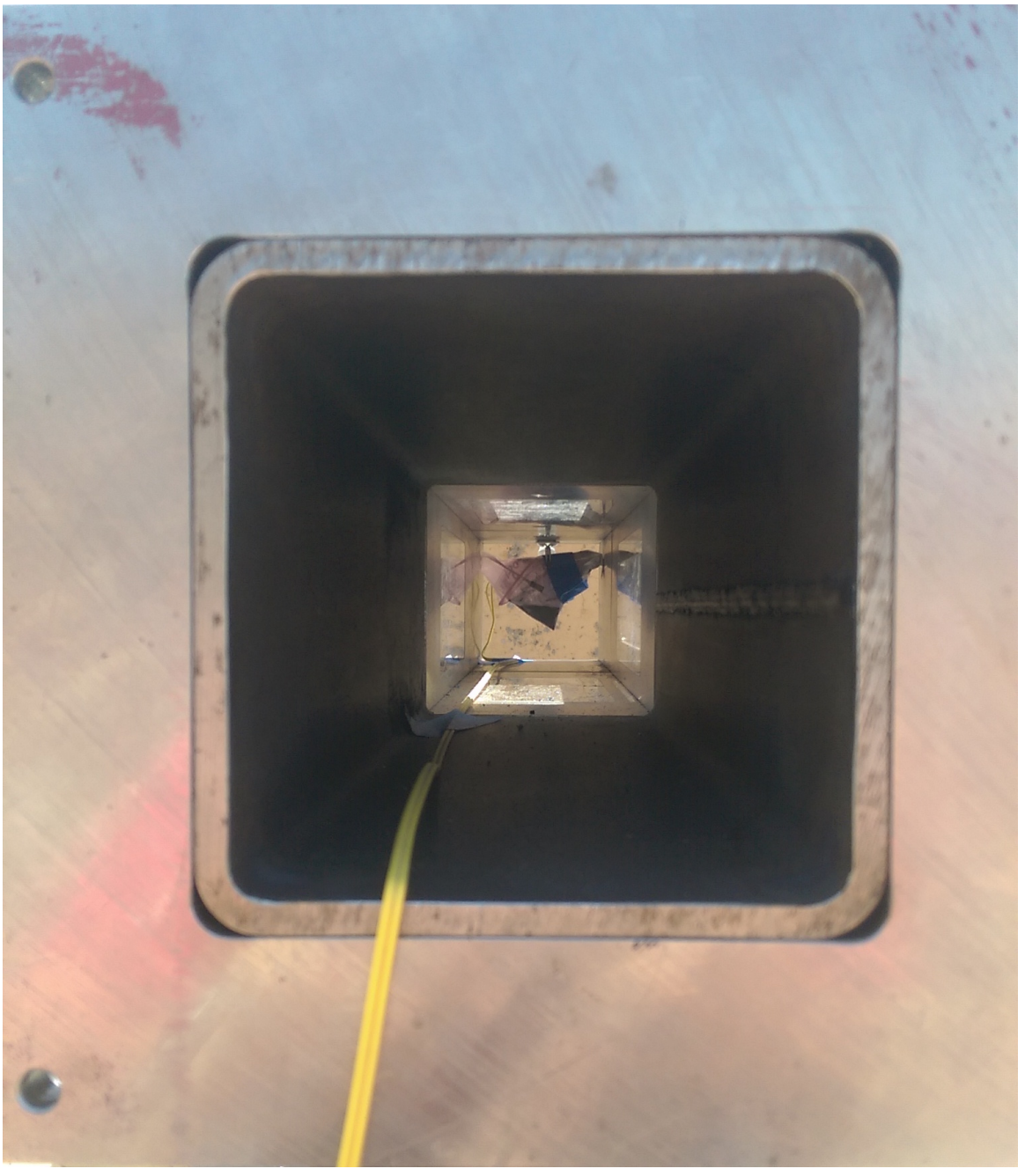

Figure 5.5: Setup for initial THOR tests: A bag of Al/I_2O_5 thermite hung in the explosive section.

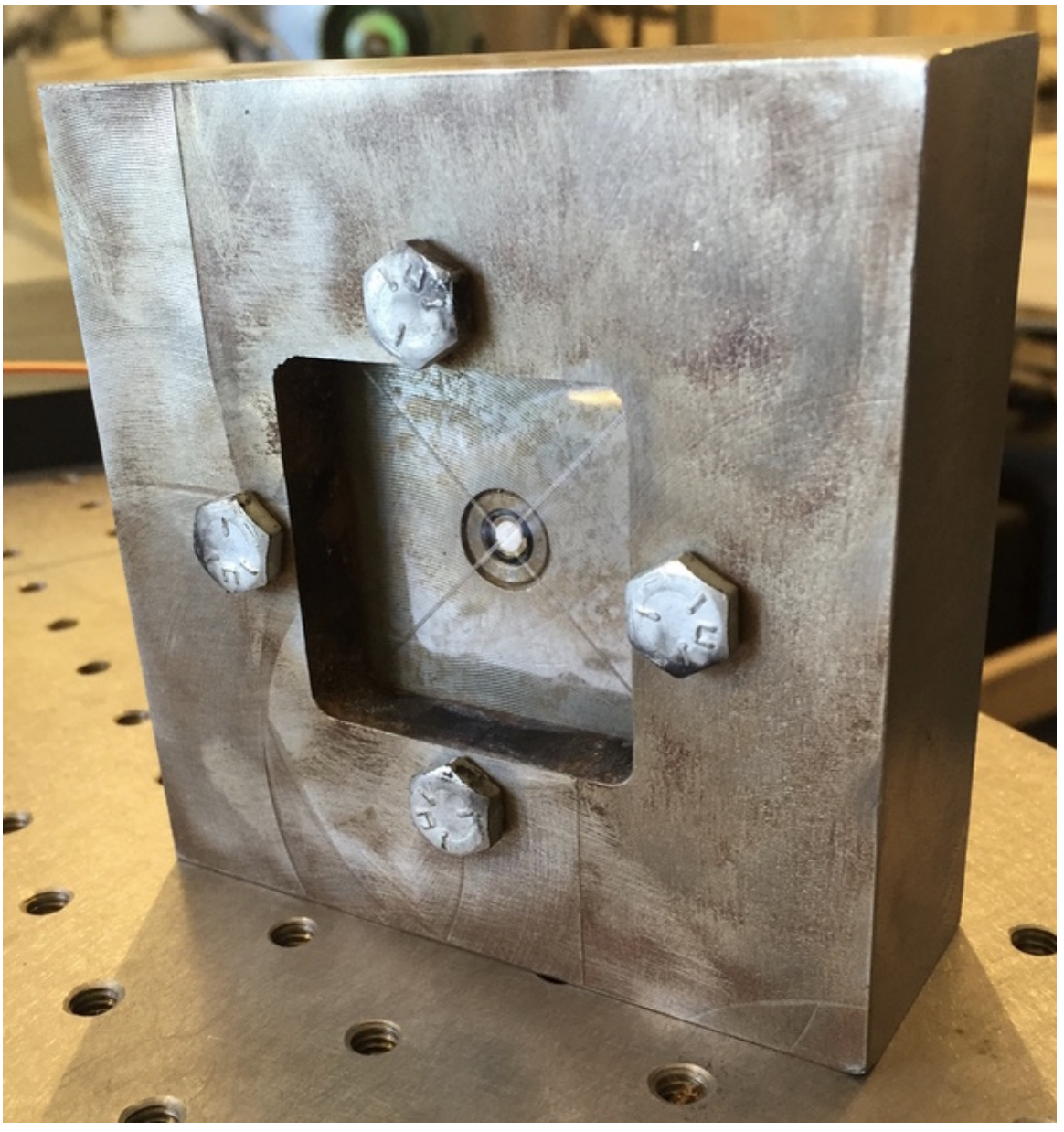

Figure 5.6: Setup of THOR tests with powder containment fixture

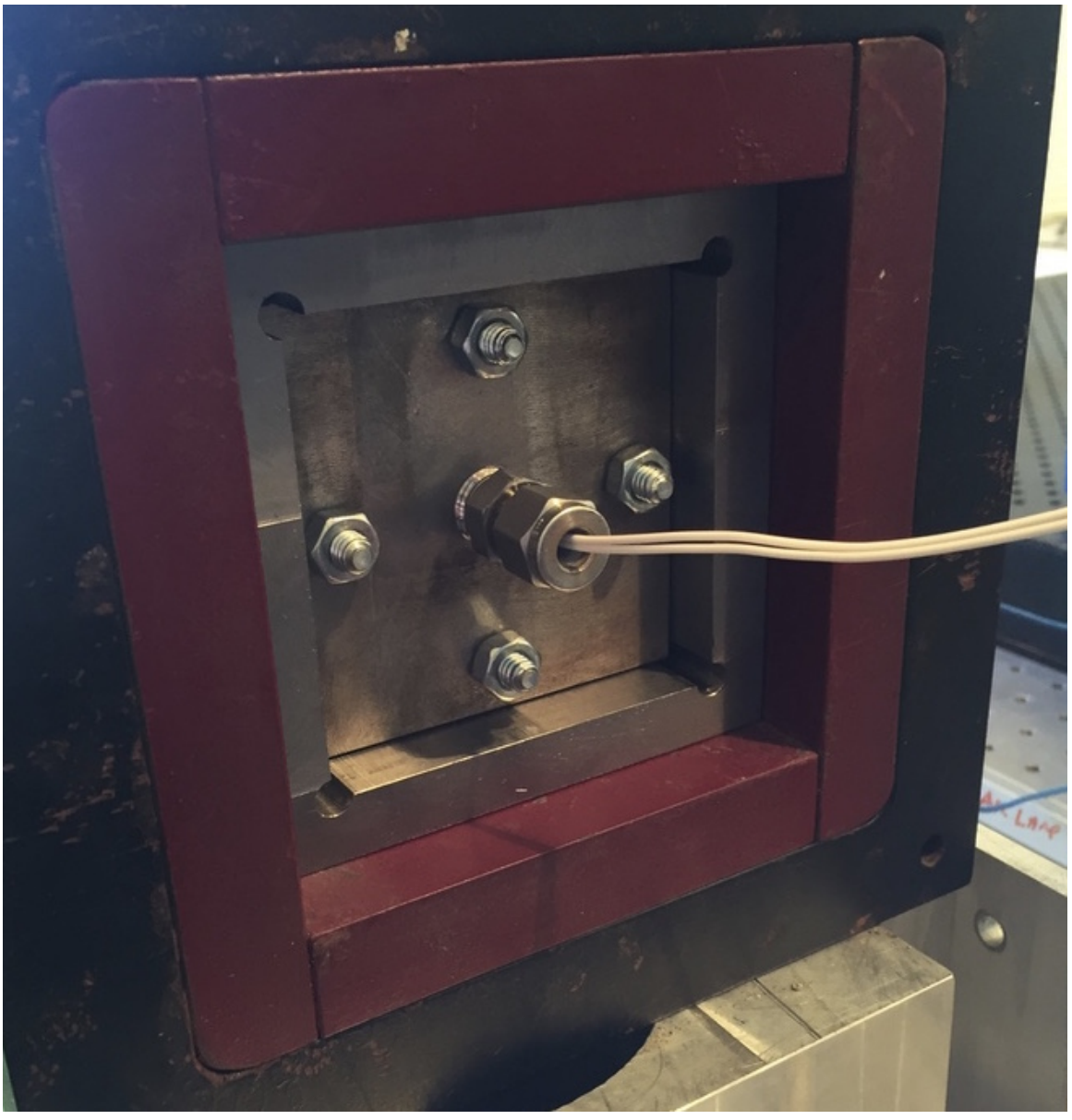

Figure 5.7: Powder containment fixture inserted into THOR

A clear comparison between the methods used in this research to contain the thermite can be seen in Figure 5.8. The loose powder tests (left) had a packing density of approximately 49.9% TMD. The thermite containment fixture (right) had material that was packed at a higher density of approximately 60% TMD. The clear gap of air between the detonator and thermite powder in the bag setup was a clear difference as the thermite fixture ensured close contact with the high-explosive contained within the detonator. This contact was ensured due to the Swagelok tube fitting on one side holding the detonator in place and the transparency on the opposite. The bag setup also did not have a consistent detonator

direction as the orientation differed for each test.

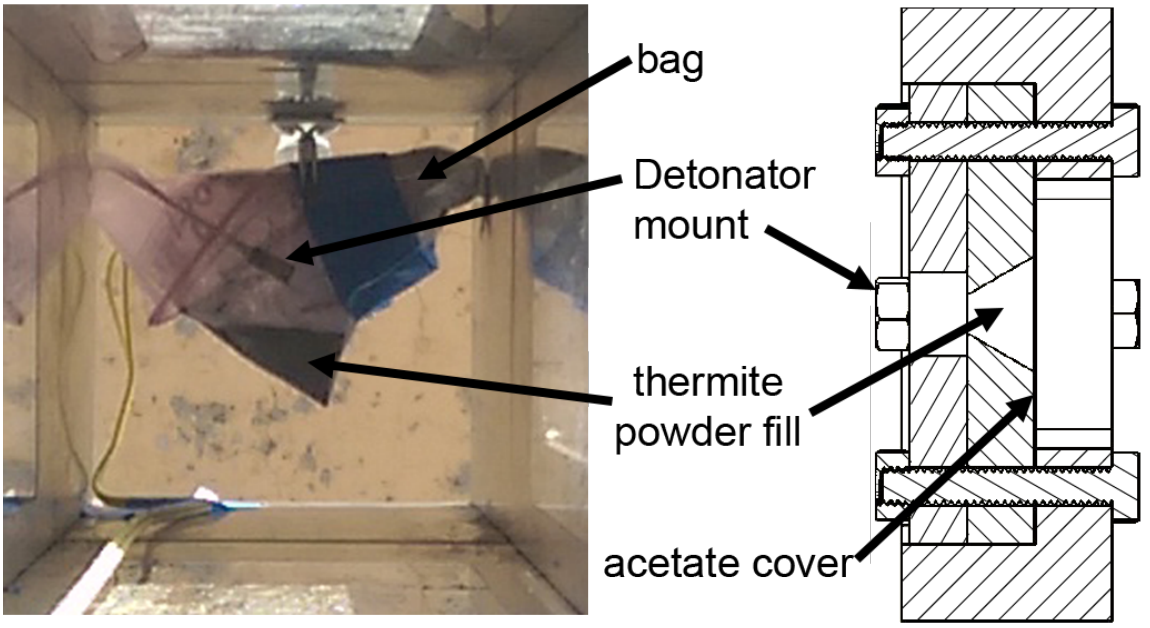

Figure 5.8: Comparison between powder containment methods

A series of images from the schlieren optical system that are used to determine the speed of the shock can be view in Figure 5.9. These images were taken at 70,000 frames per second. Two images were left out in between each pair of images shown here in order to display the shock's movement over time. The time between each of these images is 0.043 milliseconds. For a fiducial, the height of the viewable window is 5.08 centimeters (2 inches) tall.

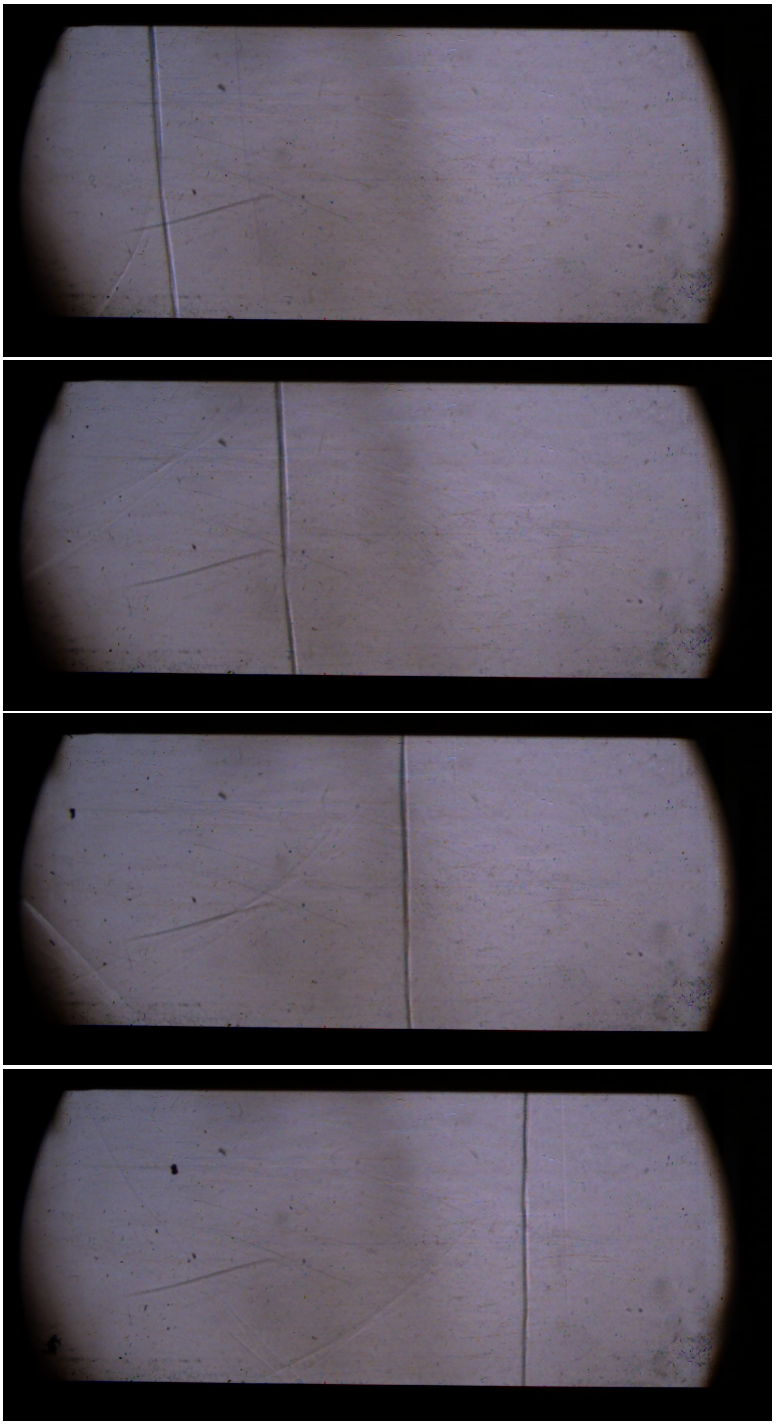

Figure 5.9: Series of images depicting the shockwave traveling through the diagnostic section that are used to optically calculate the speed of the shock

A typical pressure profile from this work is seen in Figure 5.10. The profile after the sharp rising edge is due to thermal and stress/strain effects dissipat-

ing since the piezoelectric sensor reacts to any mechanical forces incident on the sensor.

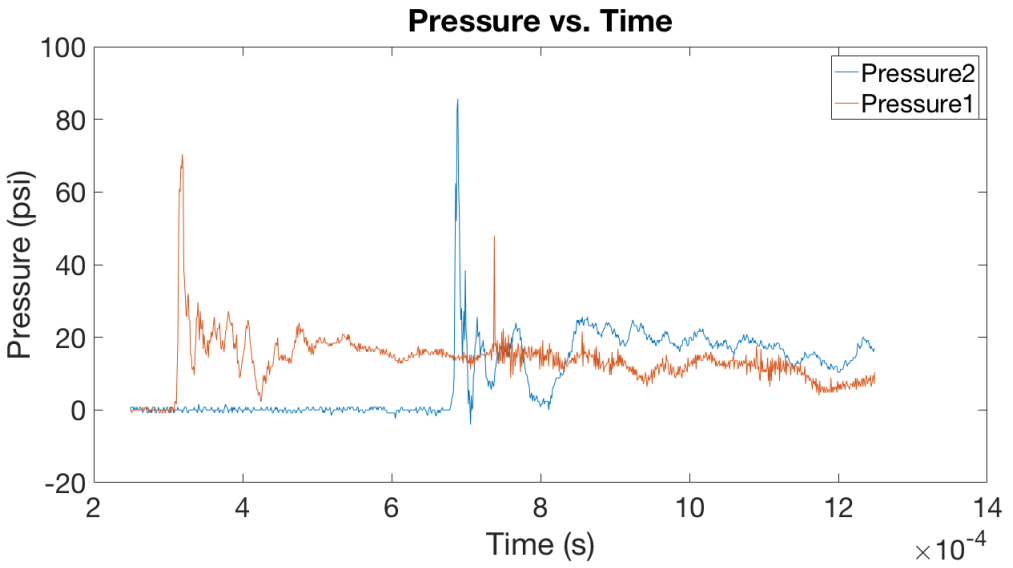

Figure 5.10: Pressure profile from a test of an RP-2 detonator and 2 grams of Al/I_2O_5 thermite

The compilation of this data can be seen in Figure 5.11. A clear relationship exists between the additional Al/I_2O_5 thermite and the speed of the shock wave produced. The data distinguishes itself between the bag and fixture setup methods. Linear fits are added between the two setups to illustrate this relationship more clearly. This difference in shock speeds is due to the interactions between the detonator reaction and the thermite present.

The first method of using a bag with the RP-2 detonator inserted inside did not guarantee that the explosive train present in the RP-2 would have immediate contact with the Al/I_2O_5 thermite when propagating outwards. The fixture setup, however, ensured that no air pocket is present between the explosive train of the detonator and the Al/I_2O_5 thermite. This allowed a path for the reaction to travel along and ensure that the material is placed such that a maximum amount of the material will be consumed and the energy will be directed in a one-dimensional approximation through THOR. The centered placement and direction of the detonator also led to fewer shock reflections which could be attributing to the amount of energy that gets represented via the speed of the leading shockwave.

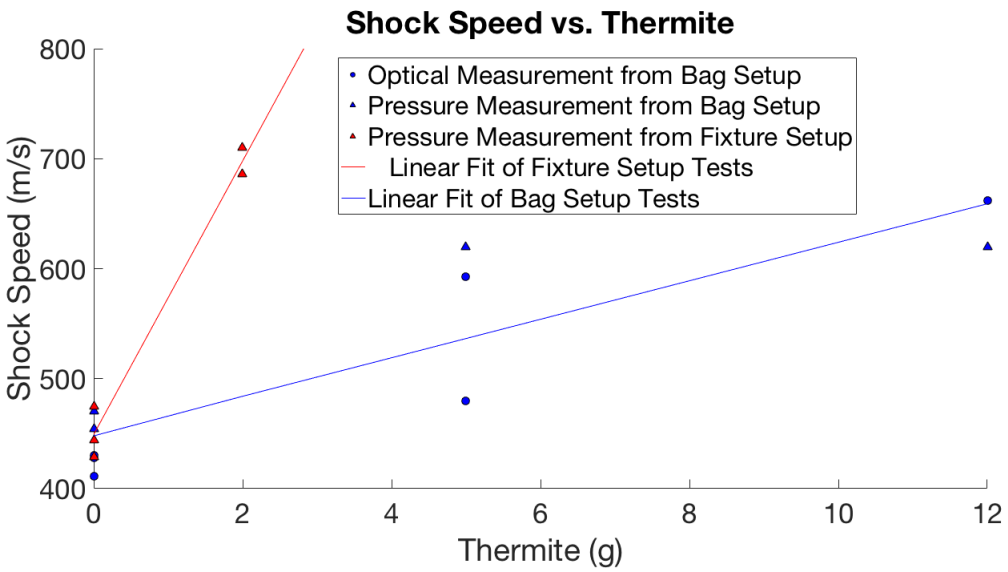

Figure 5.11: Speed of shockwave (m/s) vs. thermite present (g)

5.3 Identifying Iodine Gas Front

The process discussed in chapter 3 was utilized on test data to identify the time at which iodine was present in the diagnostic section of THOR. Examples of the absorbance responses when determining whether or not iodine is present are shown in Figures 5.12 and 5.13. The absorption profile in Figure 5.13 reflects the expected outcome compared to literature and the imaging spectrometer calibration.

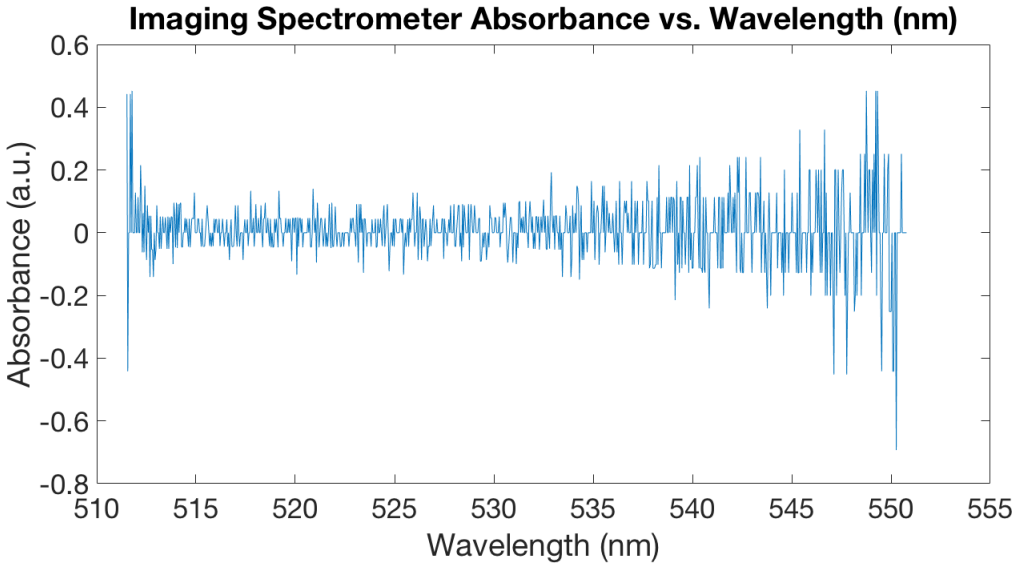

Figure 5.12: Absorption spectra of an RP-2 detonator

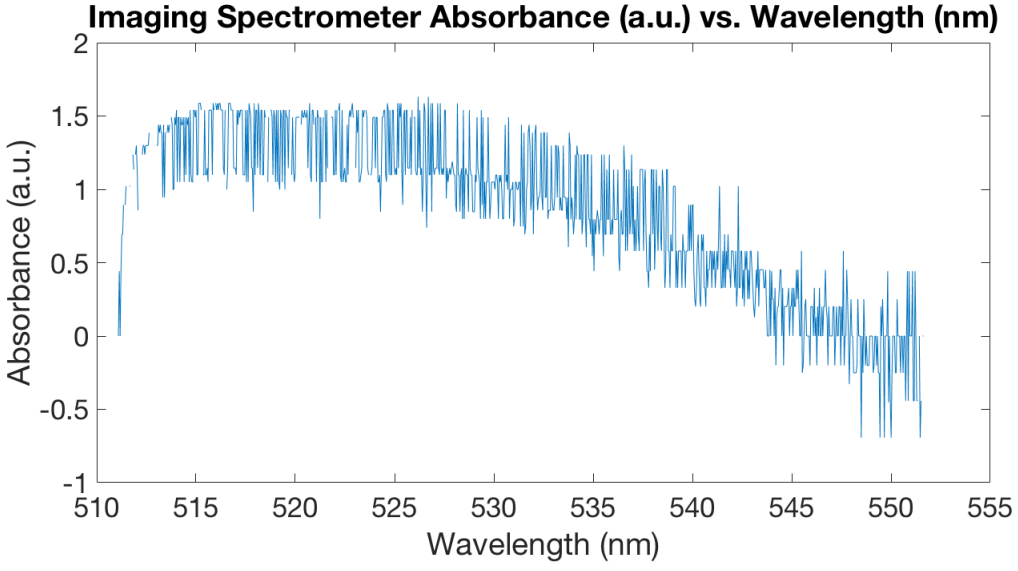

Figure 5.13: Absorption spectra of an RP-2 detonator with 2 grams of Al/I_2O_5 thermite

In order to determine the time of arrival for the gas, the absorbance spectra were evaluated over time. Streak images were employed in order to do this effectively and efficiently. Every image's pixel intensity values from a test were divided by the calibration image's pixel intensity values which created an image where each spatial pixel line's intensities corresponded to the values for the absorption spectra at that physical location. The streak images for a test with

an RP-2 (Figure 5.14) and an RP-2 with 2 grams of Al/I_2O_5 thermite (Figures 5.15 and 5.16) can be seen below. Three pixels were taken from each image for the first 250 images of the dataset and stacked on top of each other to form the resultant image.

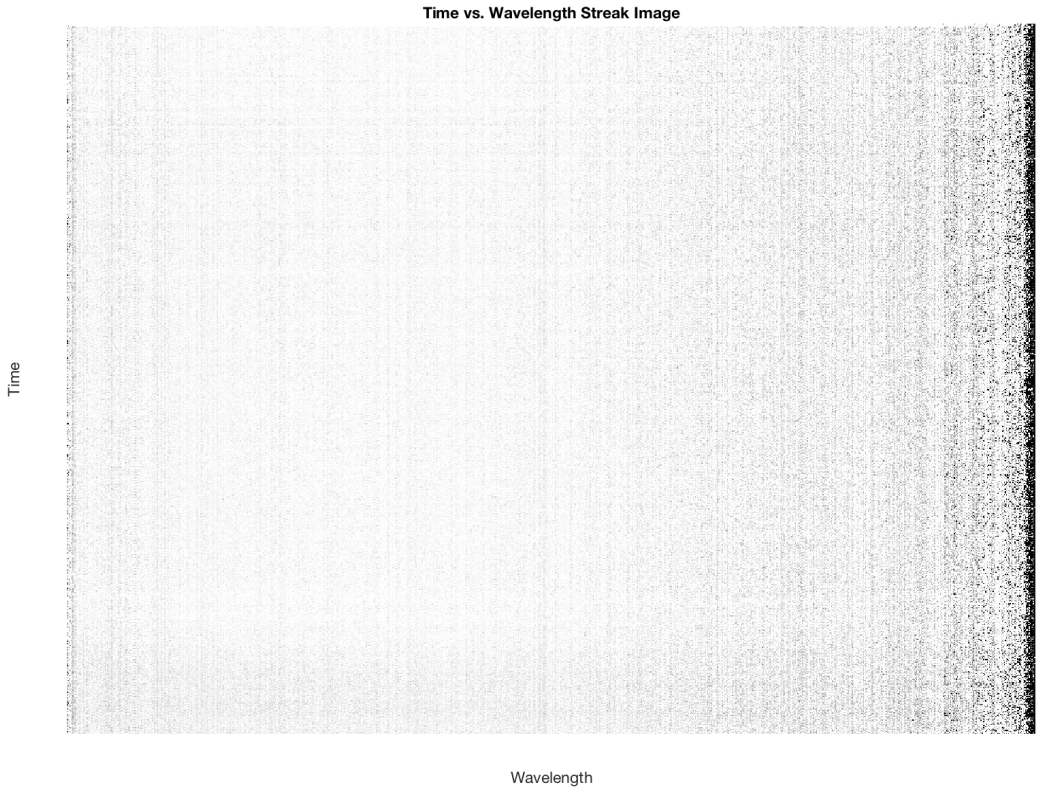

Figure 5.14: Time vs. wavelength streak image of an RP-2 detonator

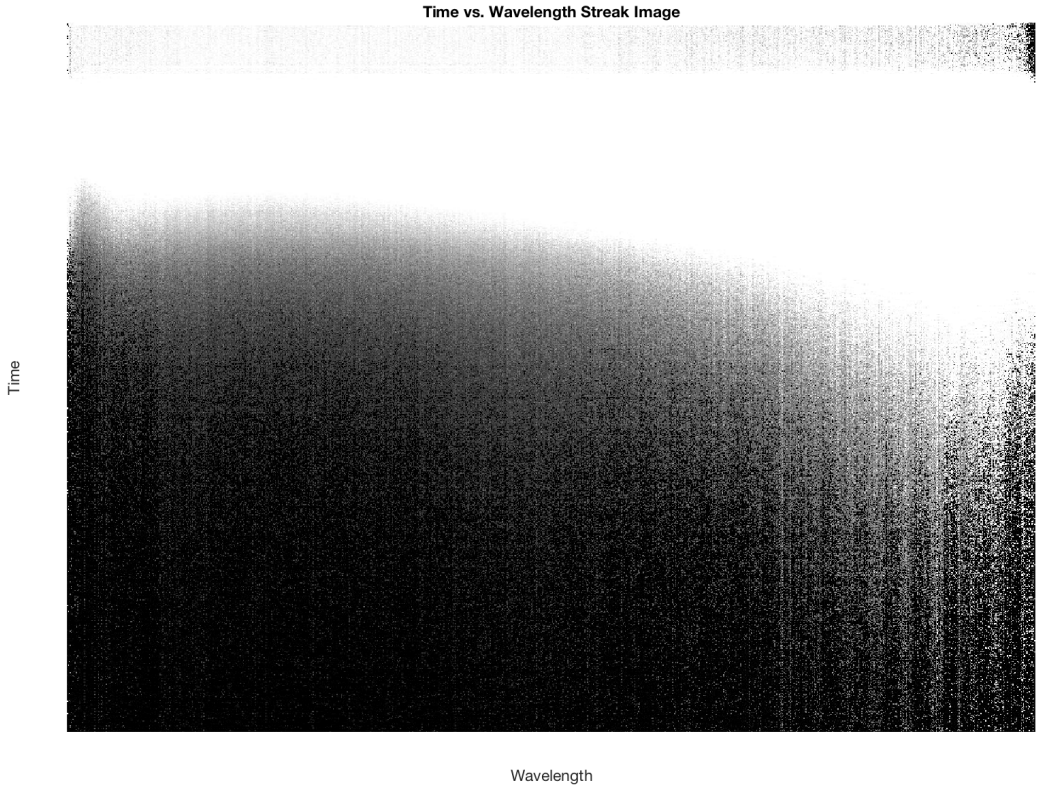

Figure 5.15: Time vs. wavelength streak image 1 of an RP-2 Detonator with 2 grams of Al/I_2O_5 thermite

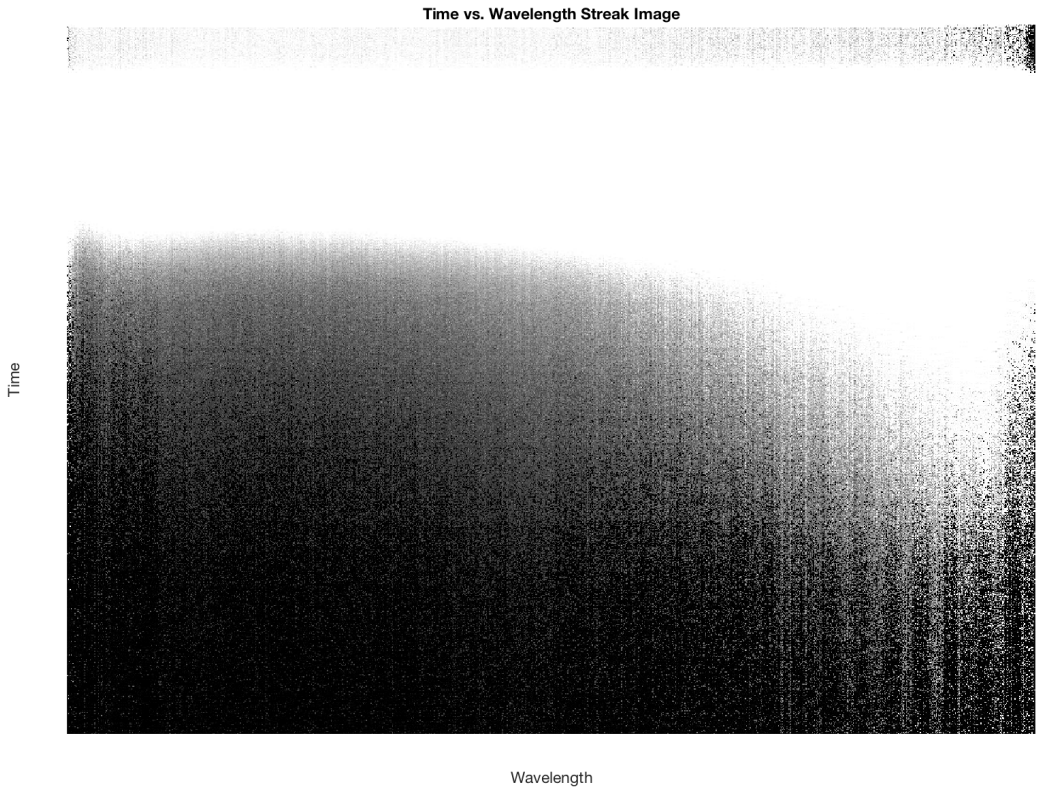

Figure 5.16: Time vs. wavelength streak image 2 of an RP-2 Detonator with 2 grams of Al/I_2O_5 thermite

These streak images make the determination of the time of arrival of the gas much easier. This can be seen visually by examining the streak images and comparing between those with the iodine gas and those without. The only difference between the two tests is the addition of the iodine gas product from the Al/I_2O_5 thermite reaction. This logic leads to a simple concentration calculation being made based on the intensity values of the pixels of the streak image over time. The center pixel of the images was chosen to determine the concentration of iodine gas present. Concentration plots for the two tests of 2 grams of Al/I_2O_5 thermite above were made and are shown in Figures 5.17 and 5.18. A negative iodine concentration is depicted by the polynomial fit due to the discontinuity that exists from the initial flash from the thermite reaction. The time of arrival of a gas concentration can then be determined. By tracking a concentration of 20% iodine gas, the discontinuity in data is avoided. These times were determined by finding the image that the appropriate spectra came from and relating to time based on the 20,000 frame per second capture rate. The time of arrivals were 3.98 ms (Figure 5.17) and 4.35 ms (Figure 5.18) for the two 2 gram Al/I_2O_5 thermite tests shown here.

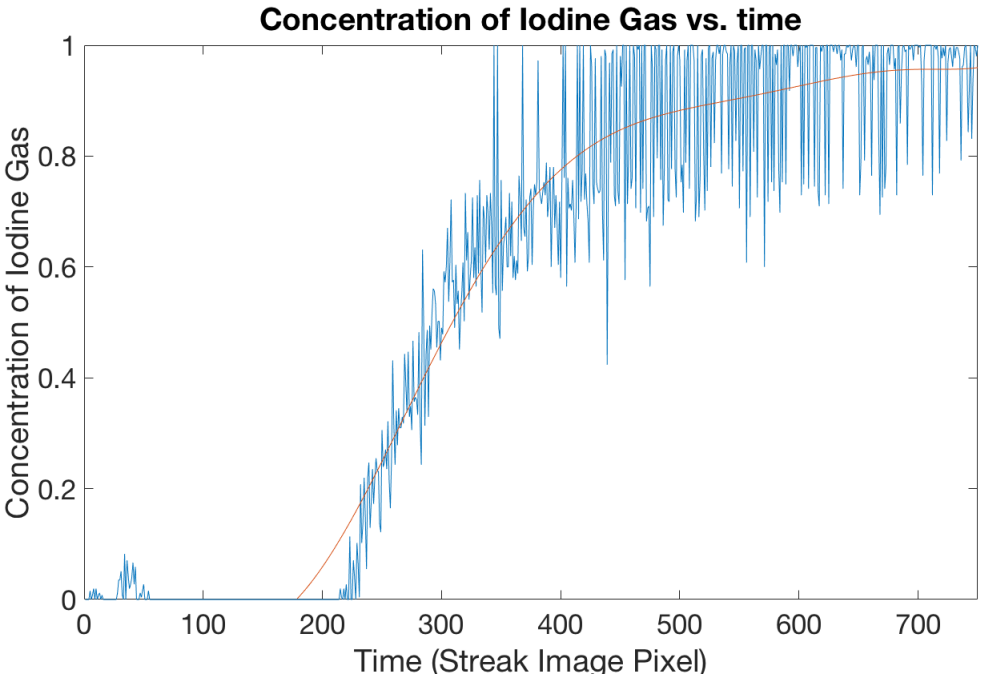

Figure 5.17: Estimated concentration of iodine present over time for streak image 1

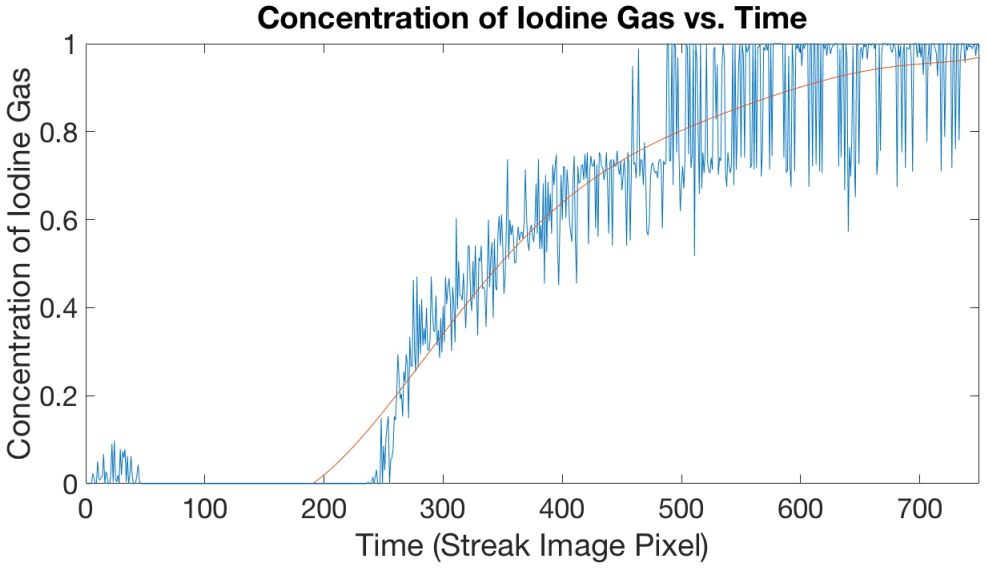

Figure 5.18: Estimated concentration of iodine present over time for streak image 2

CHAPTER 6

CONCLUSIONS AND FUTURE RESEARCH RECOMMENDATIONS

6.1 Conclusions

Al/I_2O_5 thermite was characterized by studying the sensitivity of the material to impact, friction, and electrical stimuli and also determining the effect of hydration. The material was found to be relatively insensitive in each test. The material, as hypothesized, was received from the supplier already hydrated due to the rapid reaction with any present in the atmosphere and further aging did not change the sensitivity or performance results.

THOR was built to house simultaneous schlieren and imaging spectrometer optical techniques as well as pressure measurements. It was designed to contain up to 15 grams TNT equivalence and withstood the detonators and thermite initiated within, but was not tested near the designed limit. Some modifications were made to limit compressible flow effects throughout the diagnostic section, but it enabled the desired data acquisition.

Iodine gas in a flow was located spatially, a time of arrival of the gas was determined, and a concentration gradient was hypothesized. The location of iodine was determined via an imaging spectrometer and comparison of the absorption profile to literature. The time of arrival of the gas was calculated based on the speed at which the high speed camera sensor was capturing images. The creation of a streak image for the spectroscopic measurements included the ability to see the absorption response at a single spatial pixel over time and determine an estimate for the concentration of iodine gas present throughout the early time of the test.

A shock speed relation to the amount of thermite present in addition to the RP-2 detonator was found. Two setups were compiled to form a basis for a relation between the addition of thermite and the increase in speed of the shockwave. Pressure and optical techniques were used to determine the shock wave speeds.

6.2 Future Research Recommendations

6.2.1 Further THOR Tests

THOR has been built to allow simultaneous schlieren, spectroscopy, and pressure measurements. It can be used to test any explosive material up to 15 grams TNT equivalence. By using the same setup and testing various materials, a characterizing database could be made. Data from these tests would lead to a thorough understanding of the reaction properties of each material.

The spectroscopic aspects of the fixture would enable each material's emission and absorption spectrum to be catalogued. This is important in spectroscopic applications when attempting to identify materials present. This research focused on iodine which is the only gas to have an absorption spectrum in the visible range, but other wavelength ranges become convoluted due to different materials' emission and absorption properties. By compiling data over a wide wavelength range and knowing the components of each material tested, spectroscopic species identification would be made much easier.

6.2.2 Quantifying Turbulence

The quantification of turbulence follows naturally from this research. The identification of iodine has been completed, so further studies on the interactions between the products of Al/I_2O_5 and the surrounding atmosphere can be made. Using this procedure to identify the iodine gas front, the accompanying schlieren images could be used to obtain quantitative information concerning the amount of interactions present. This can lead to studies to improve mixing and eventually achieve the ability to thoroughly clear an area of any biological hazards.

6.2.3 Transition to Field Scale Tests

For a clear understanding of the interactions between the explosive and the environment, larger outdoor testing must be done. Field scale tests would come with various obstacles to overcome: the use of new imaging techniques that enable easy visualization of large targets but retain high resolution detail, a method to obtain spectroscopic measurements at a larger scale, and the implementation of three-dimensional analysis. These field scale tests would result in a more thorough understanding of turbulent mixing quantification and enable simulations to be created that accurately depict reality.

APPENDIX A

THOR DRAWINGS

A.1 THOR

A.1.1 Removable End

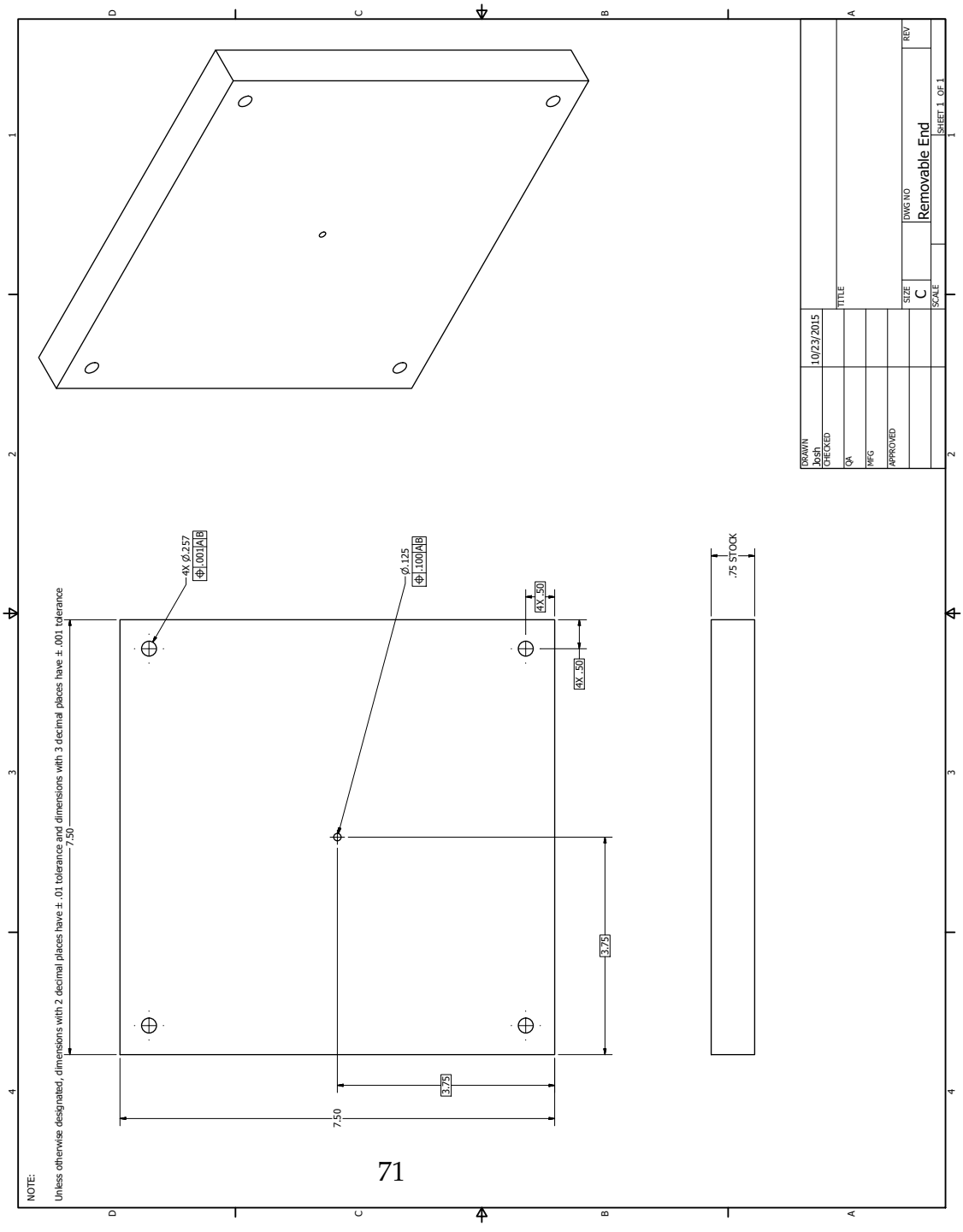

A.1.2 Explosive Section Wall 1

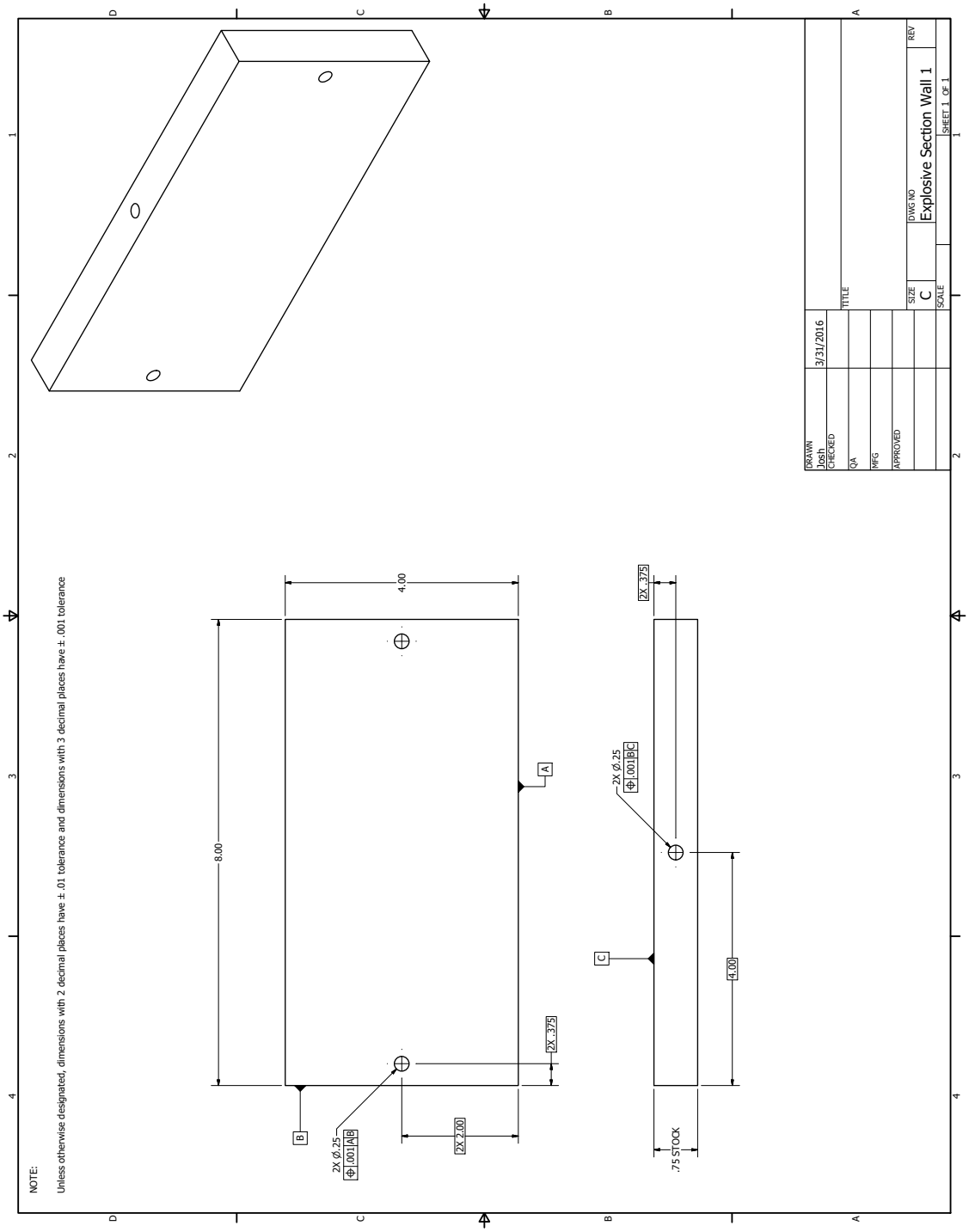

A.1.3 Explosive Section Wall 2

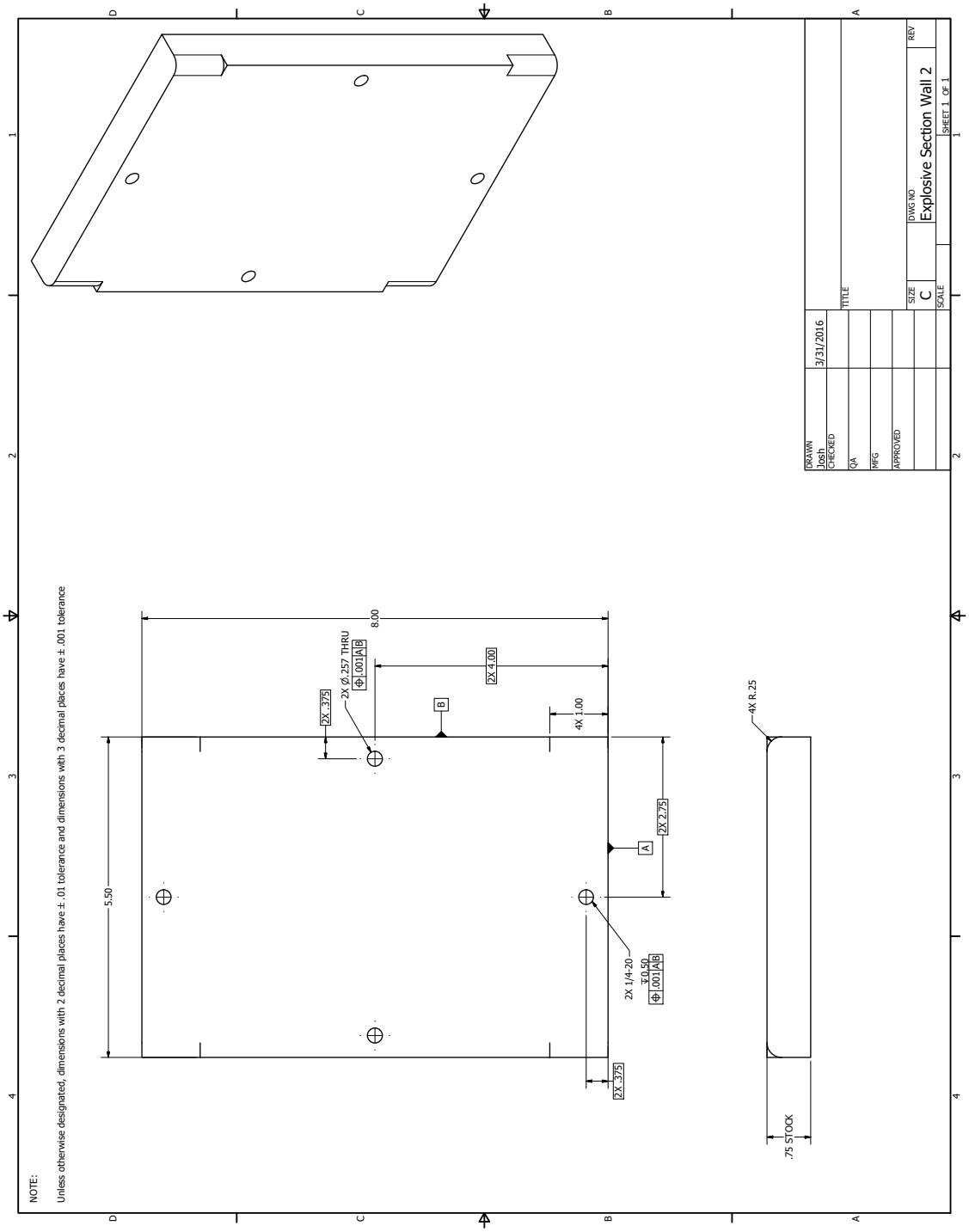

A.1.4 Explosive Section Wall 3

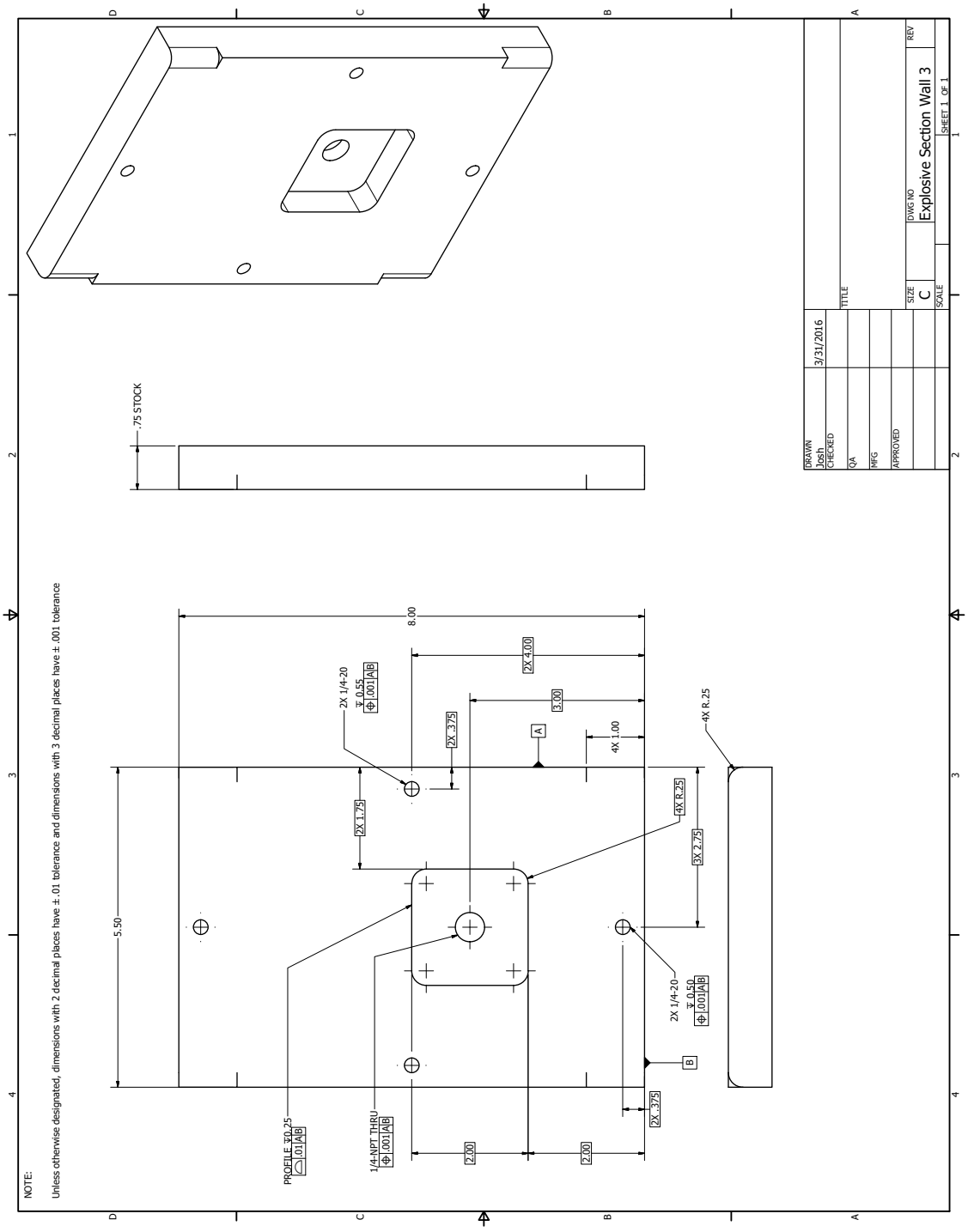

A.1.5 Explosive Section Flange

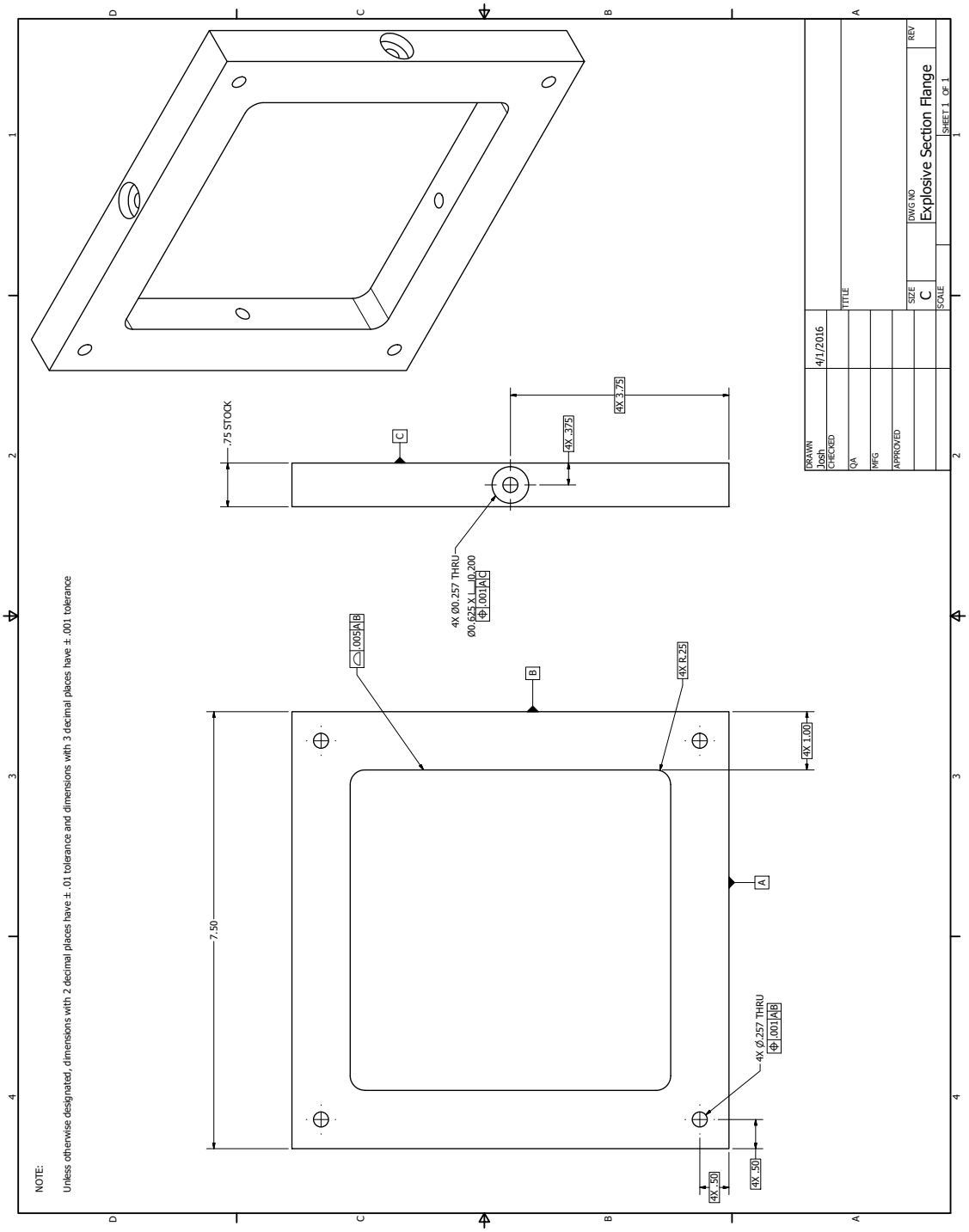

A.1.6 Explosive Section

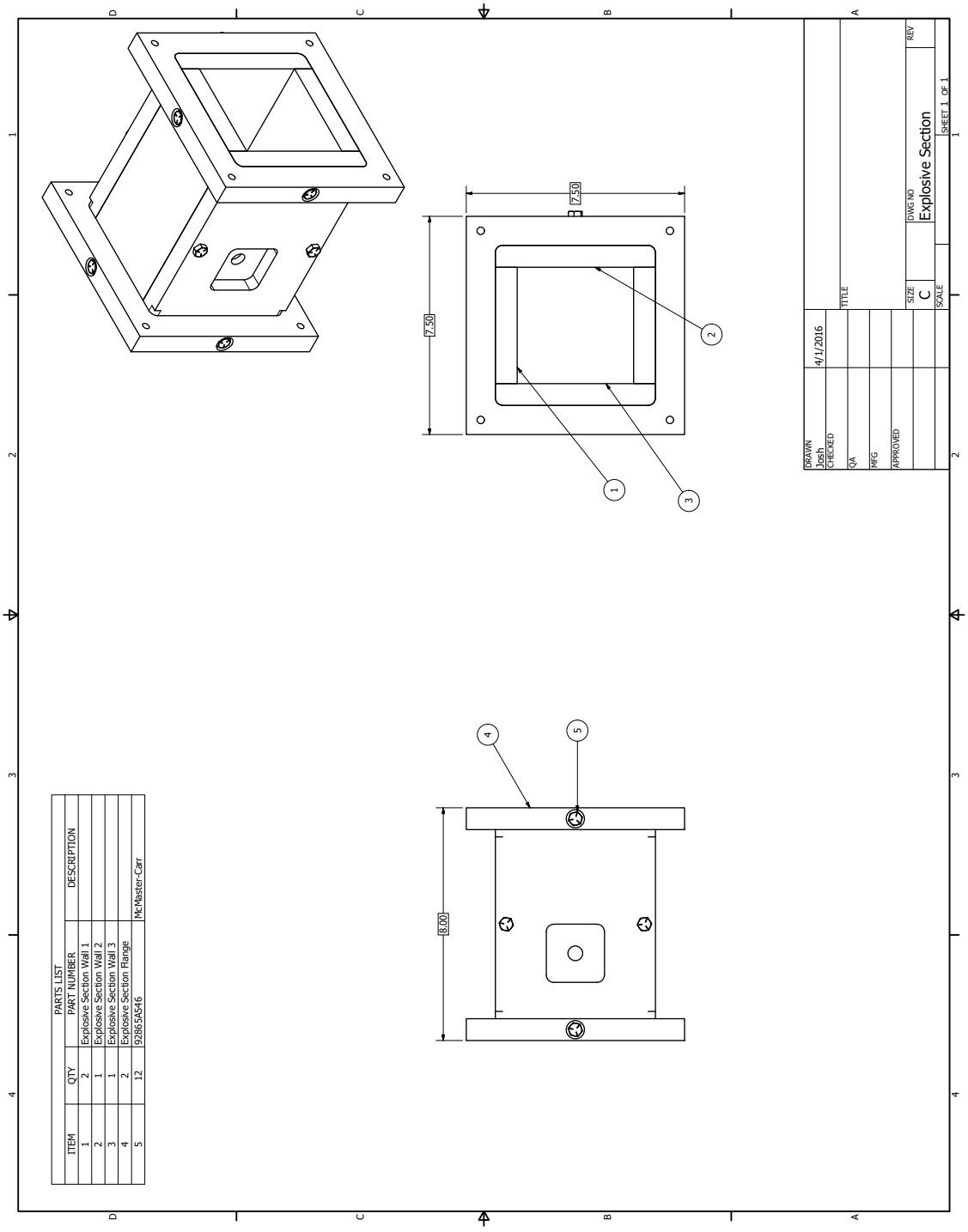

A.1.7 Diagnostic Section Wall 1

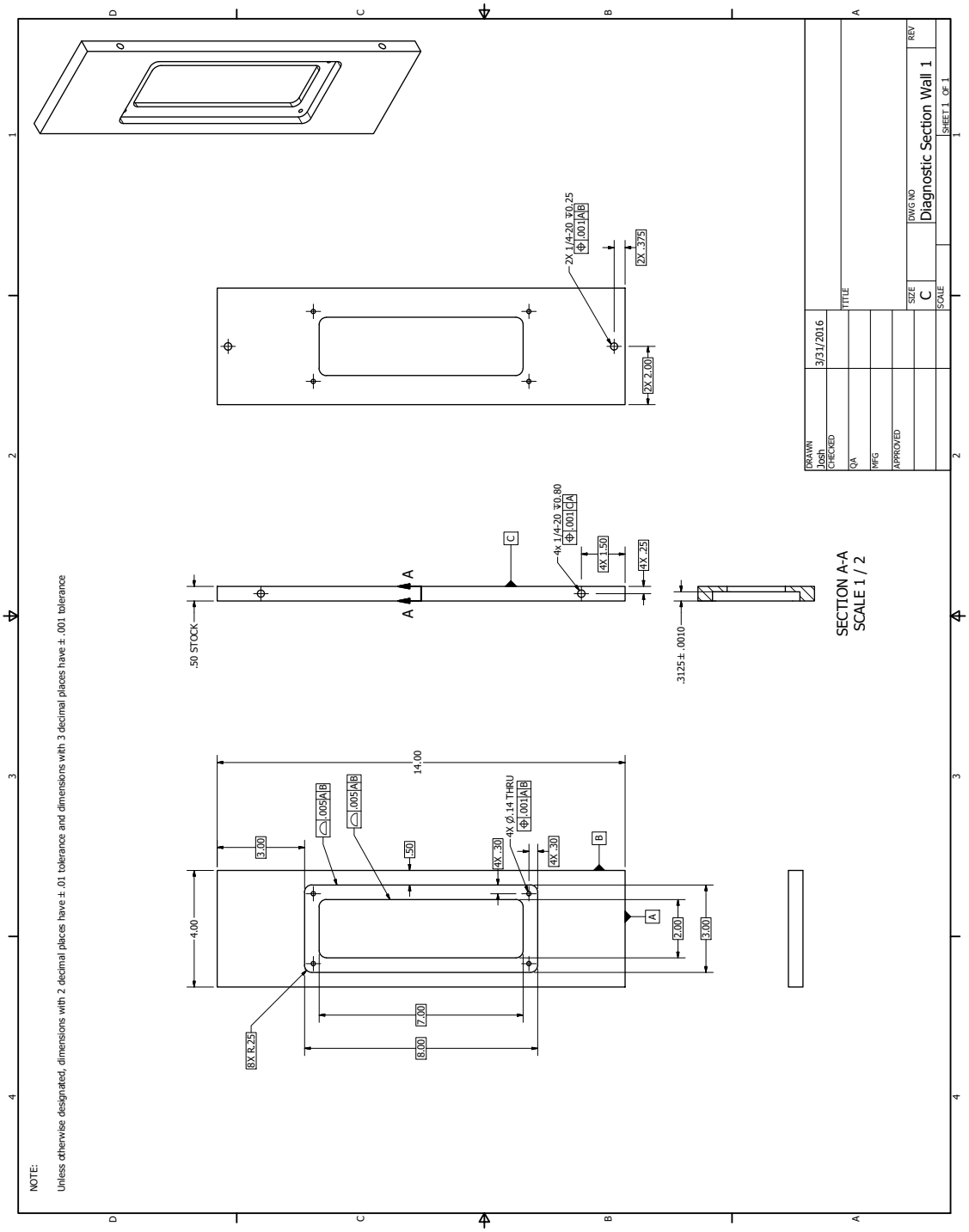

A.1.8 Diagnostic Section Wall 2

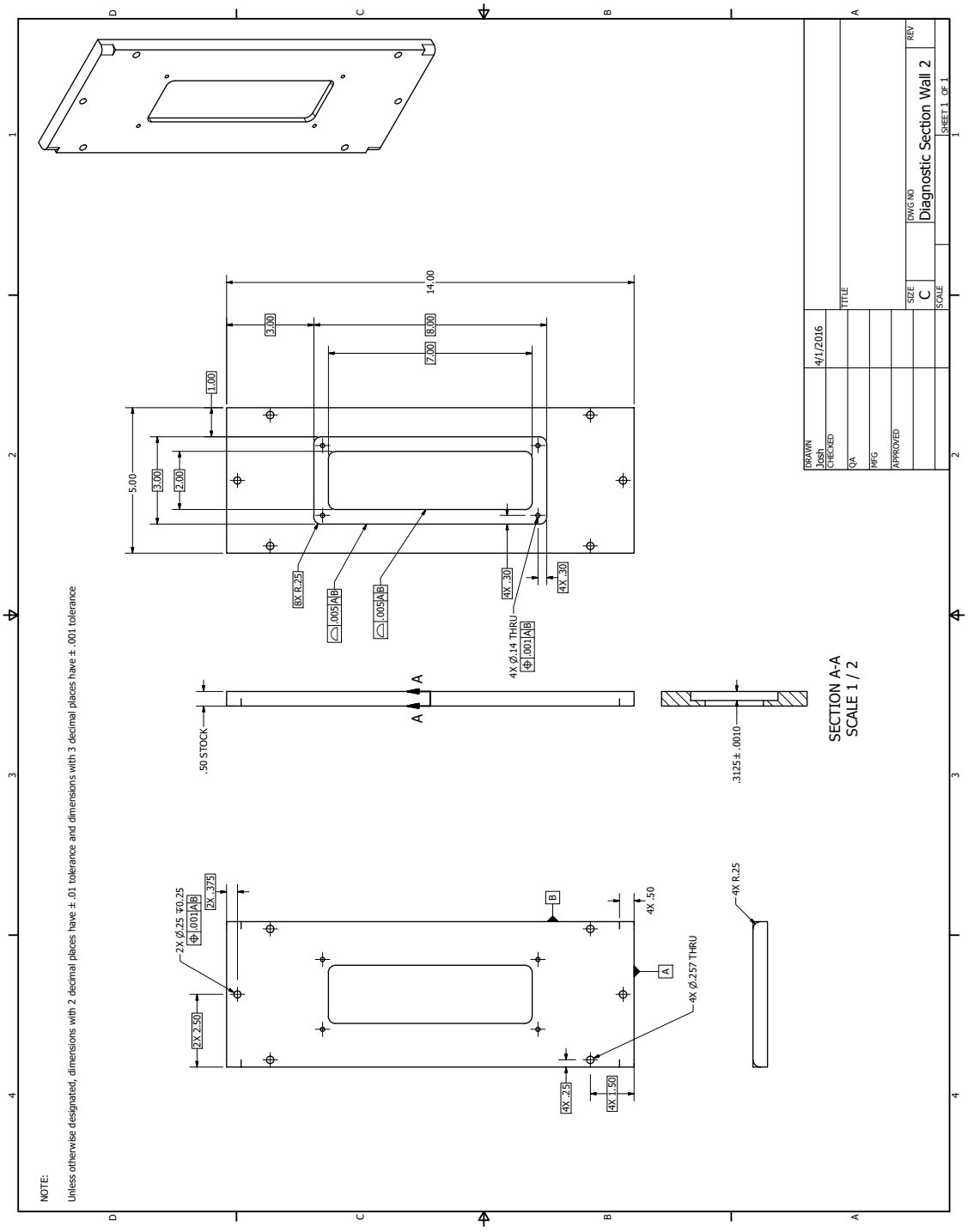

A.1.9 Diagnostic Section Wall 3

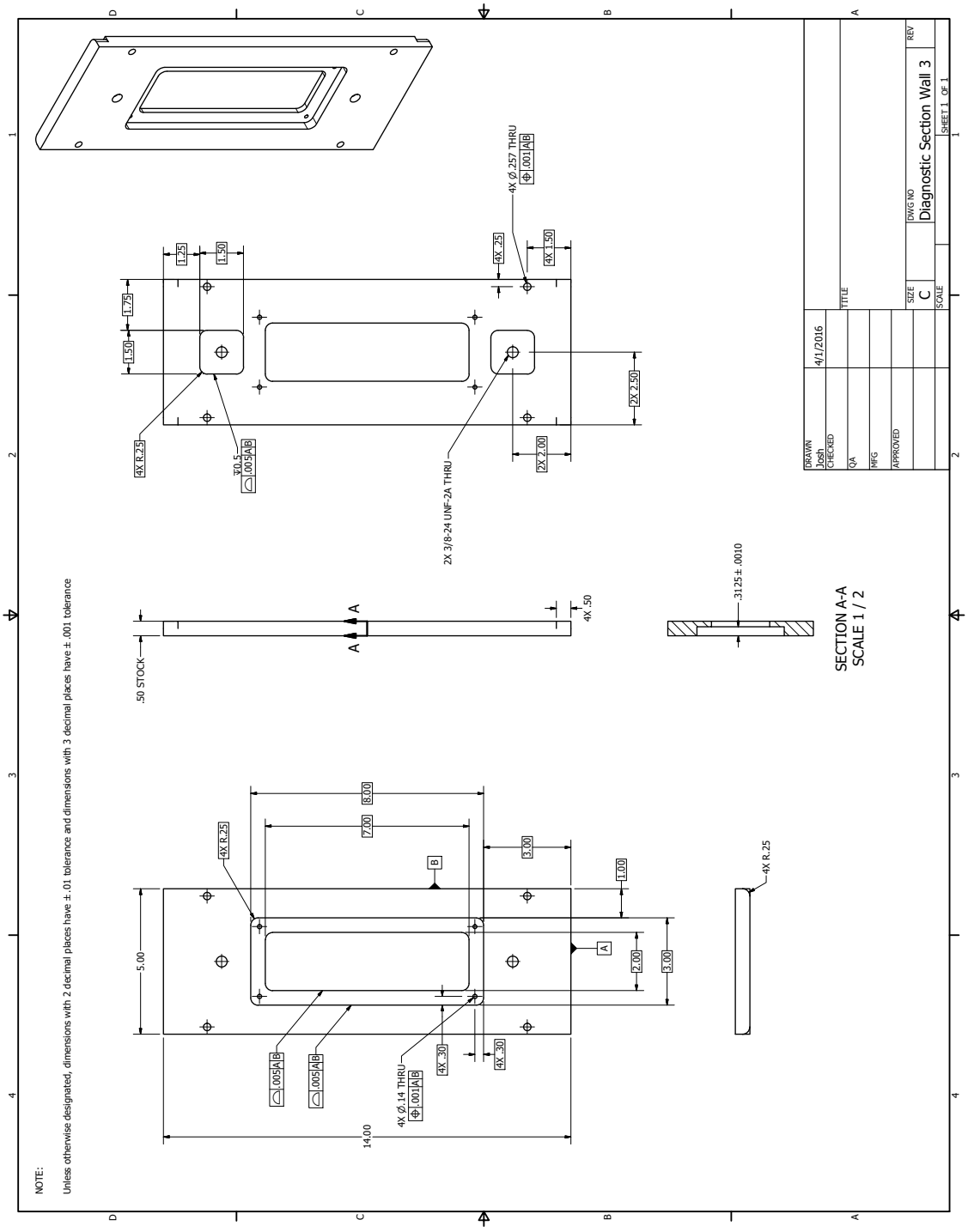

A.1.10 Diagnostic Section Flange

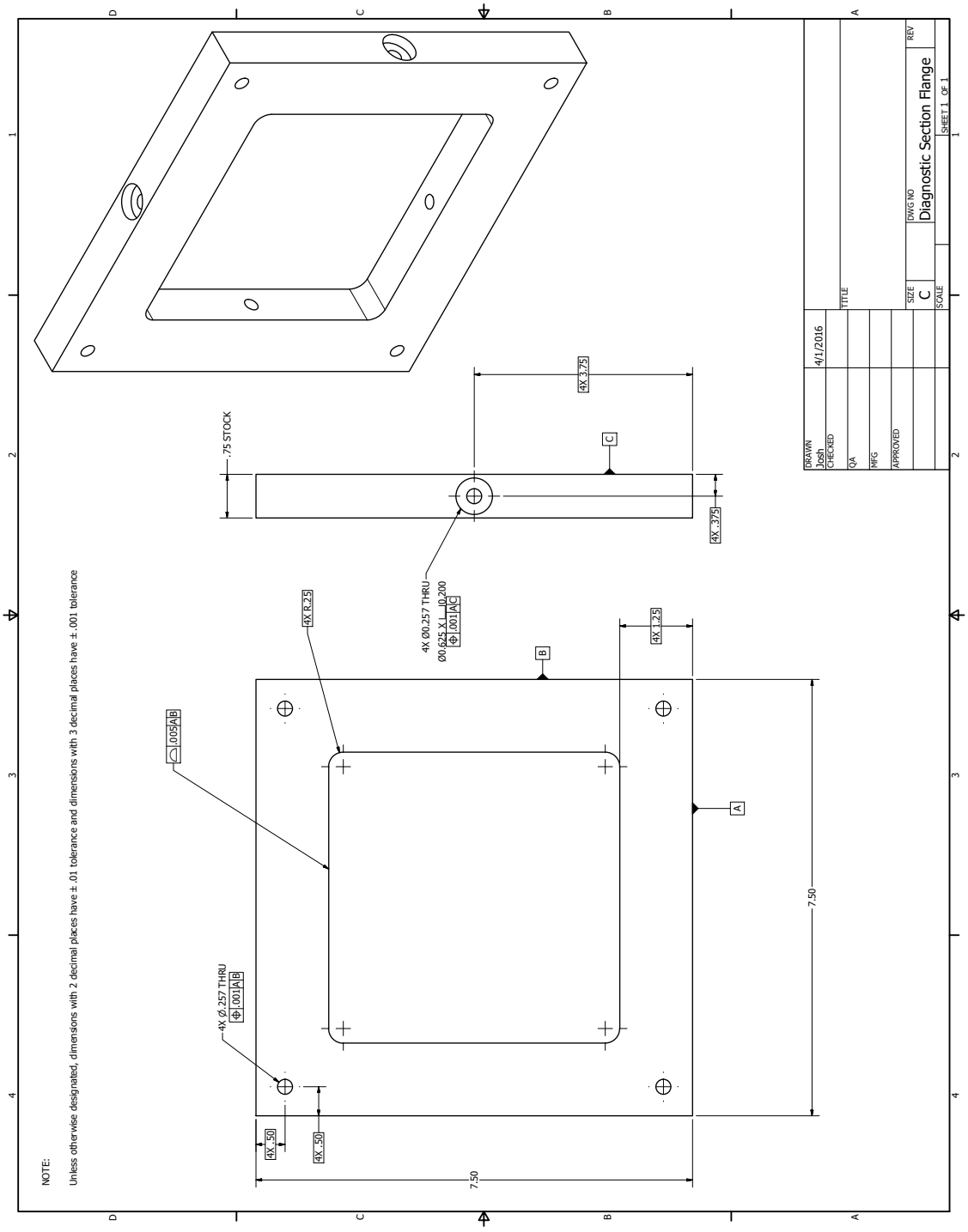

A.1.11 Window

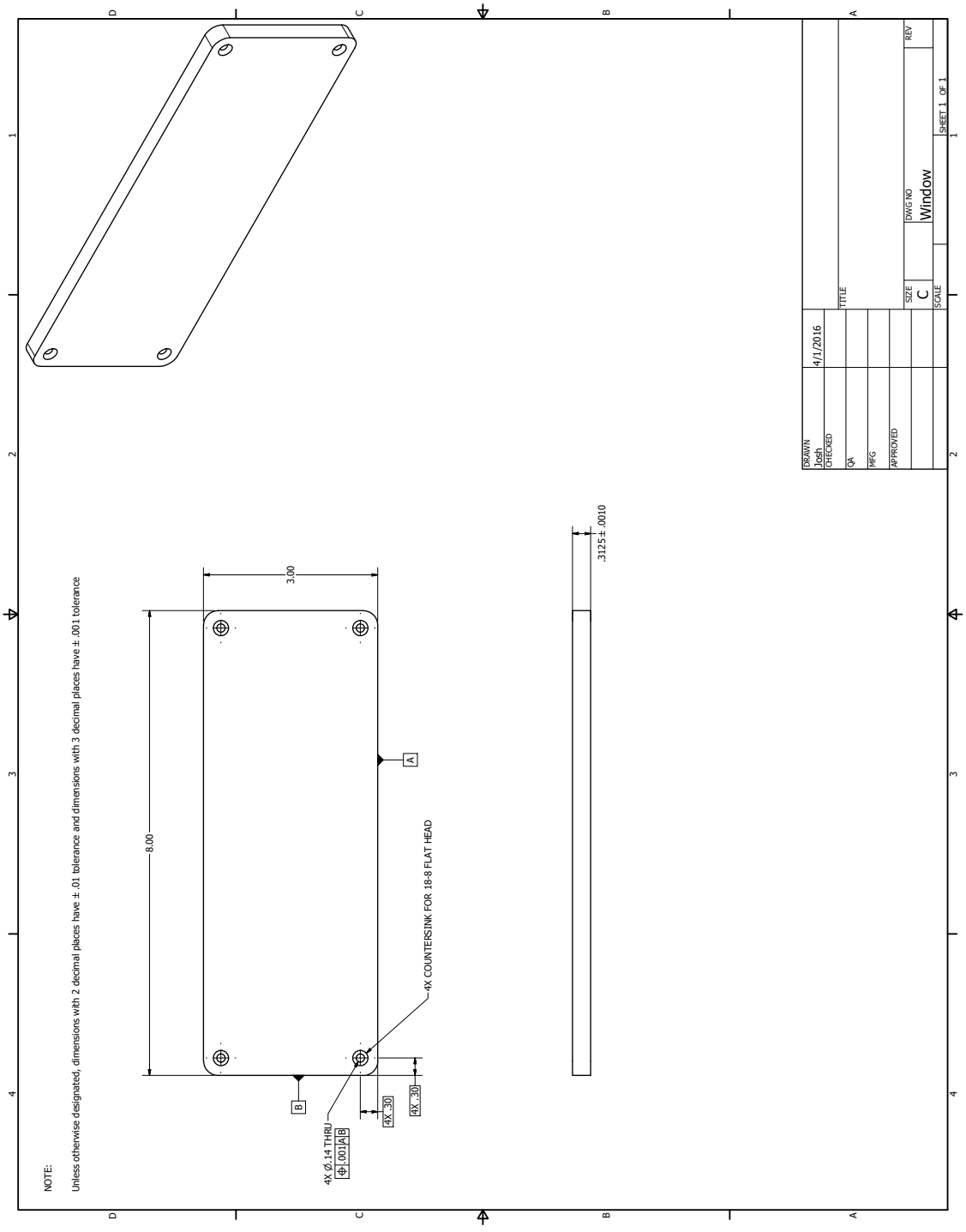
NOTE:
Unless otherwise designated, dimensions with 2 decimal places have ± .01 tolerance and dimensions with 3 decimal places have ± .001 tolerance
3.00
8.00
.3125±.0010
4X Ø.14 THRU
⌖ .001|A|B
4X .30
4X .30
4X COUNTERSINK FOR 18-8 FLAT HEAD
A
B
DRAWN
Josh
4/1/2016
CHECKED
QA
MFG
APPROVED
TITLE
SIZE
C
DWG NO
Window
REV
SCALE
SHEET 1 OF 1

A.1.12 Diagnostic Section

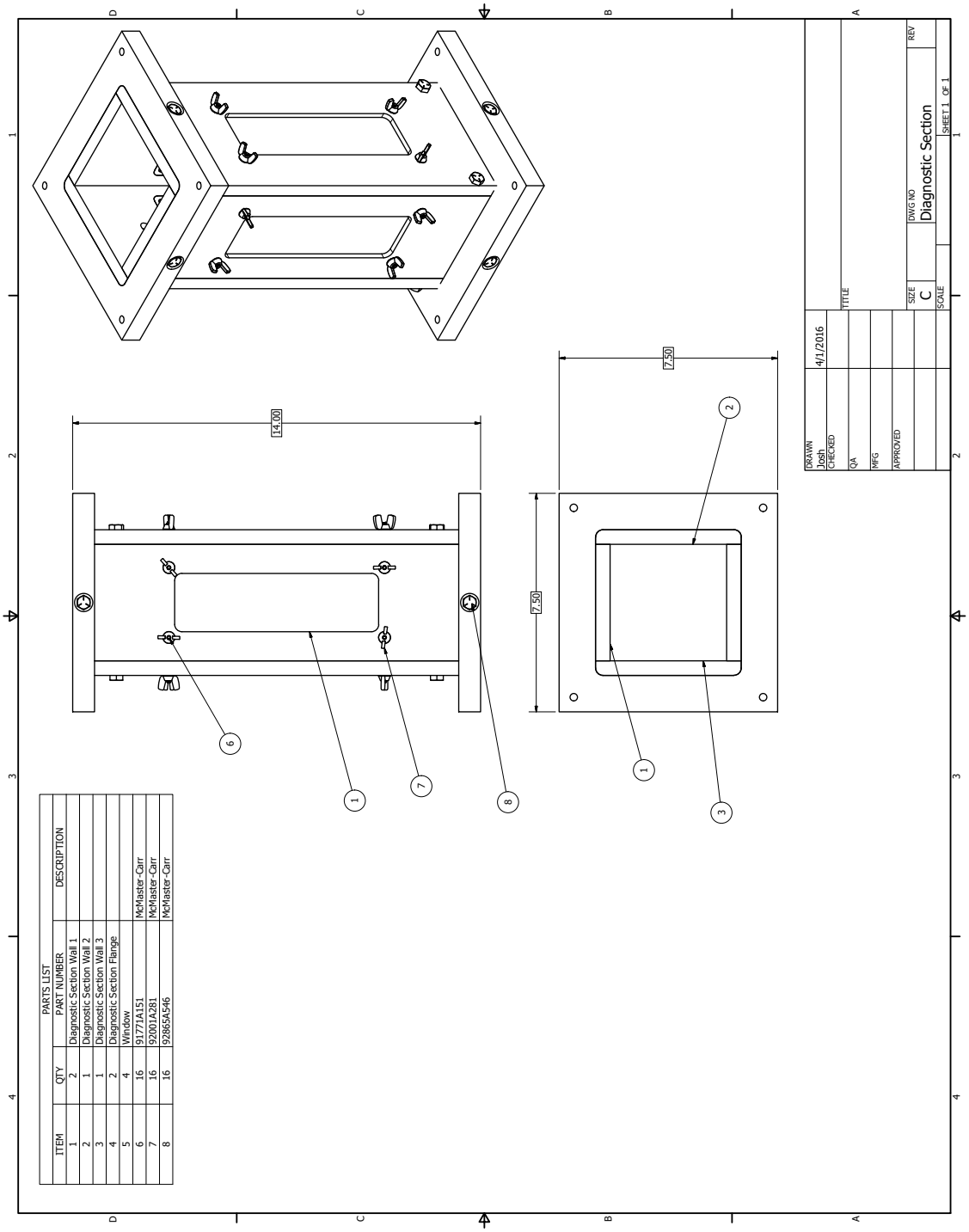

A.1.13 Exit Section Flange 8 Feet

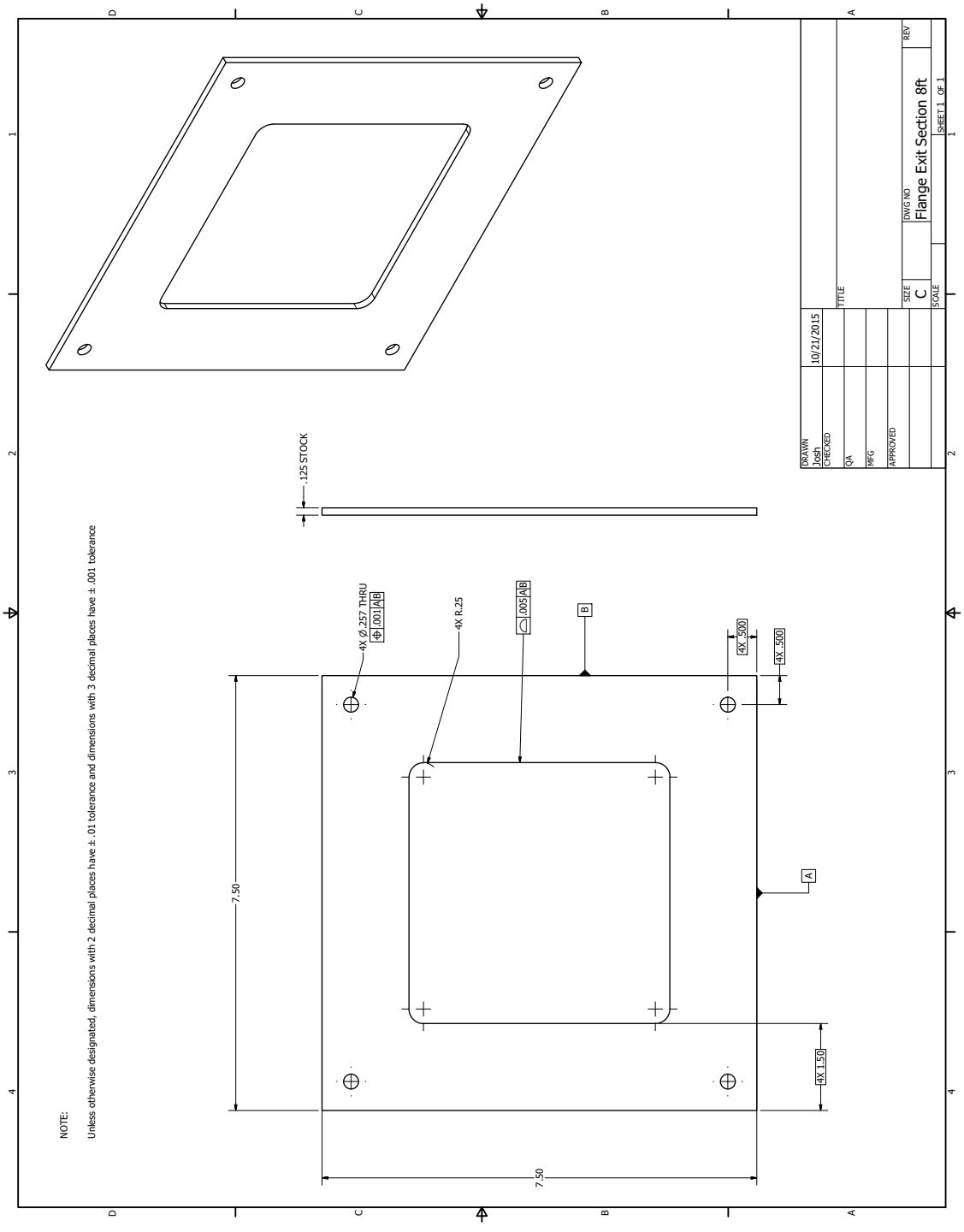

A.1.14 Exit Section 8 Feet

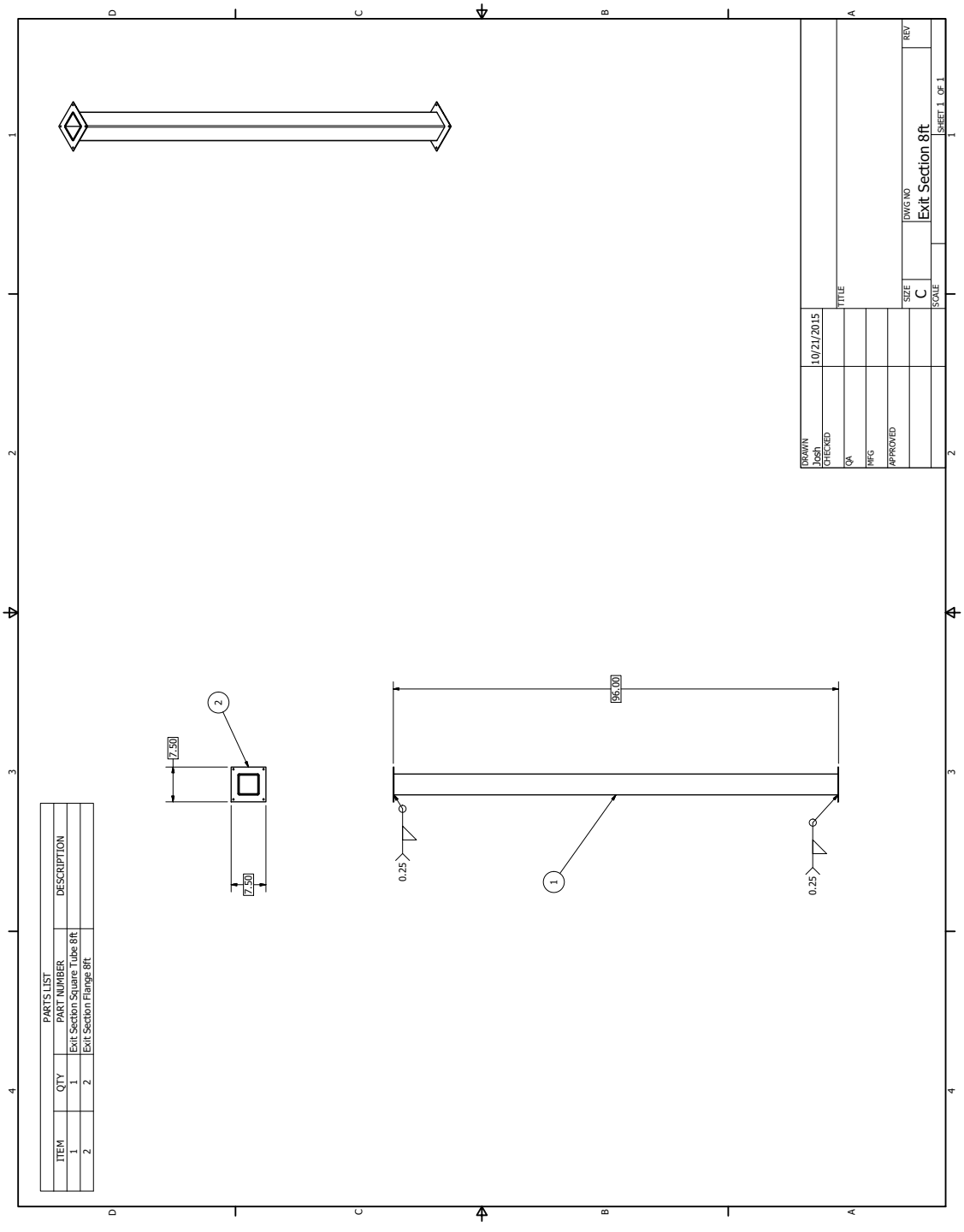

A.1.15 THOR

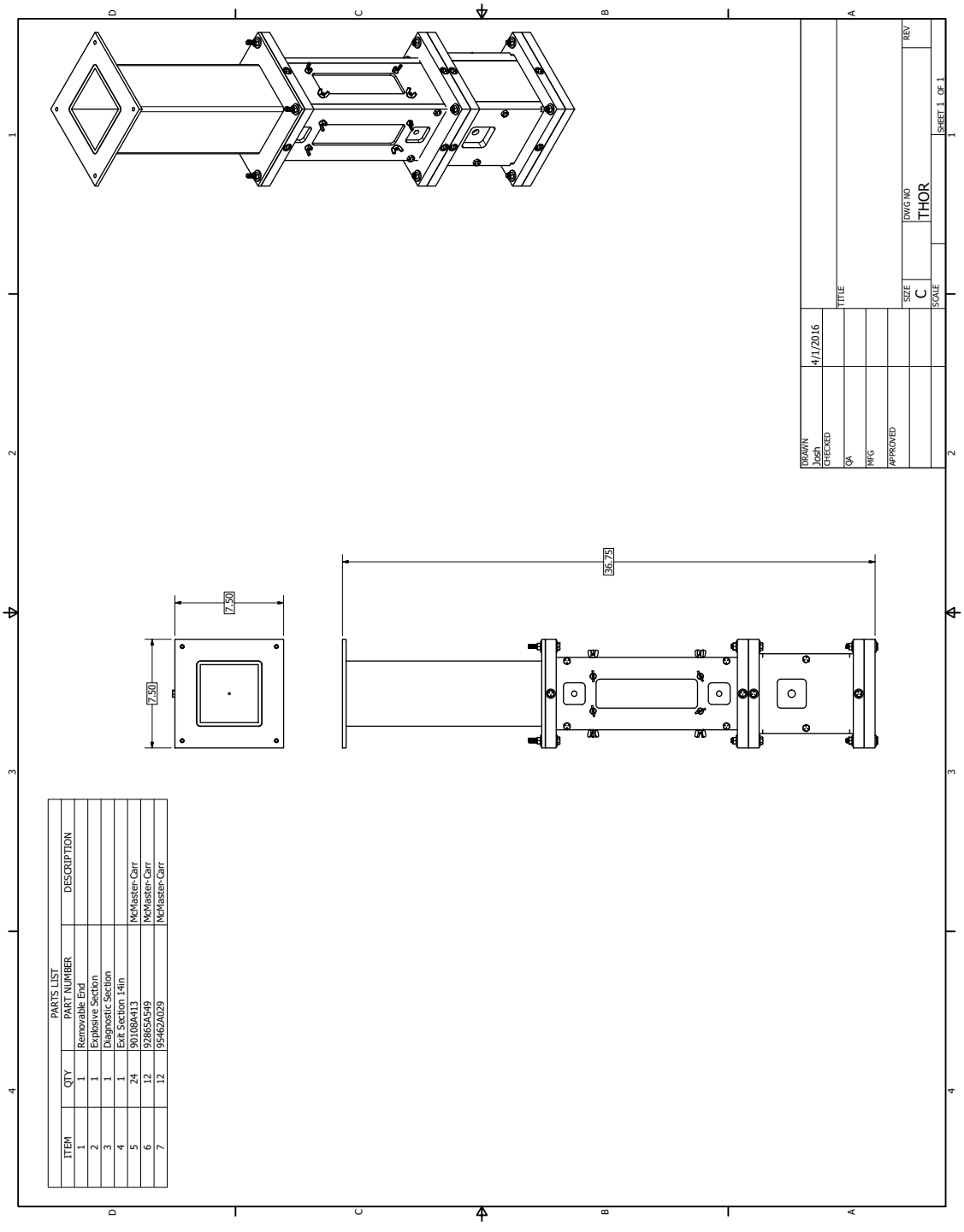
PARTS LIST
ITEM | QTY | PART NUMBER | DESCRIPTION
1 | 1 | Removable End |
2 | 1 | Explosive Section |
3 | 1 | Diagnostic Section |
4 | 1 | Exit Section 14in |
5 | 24 | 90108A413 | McMaster-Carr
6 | 12 | 92865A549 | McMaster-Carr
7 | 12 | 95462A029 | McMaster-Carr
7.50
7.50
36.75
DRAWN Josh
4/1/2016
CHECKED
QA
MFG
APPROVED
TITLE
SIZE C
DWG NO THOR
REV
SCALE
SHEET 1 OF 1

A.2 Powder Containment Fixture

A.2.1 Plate

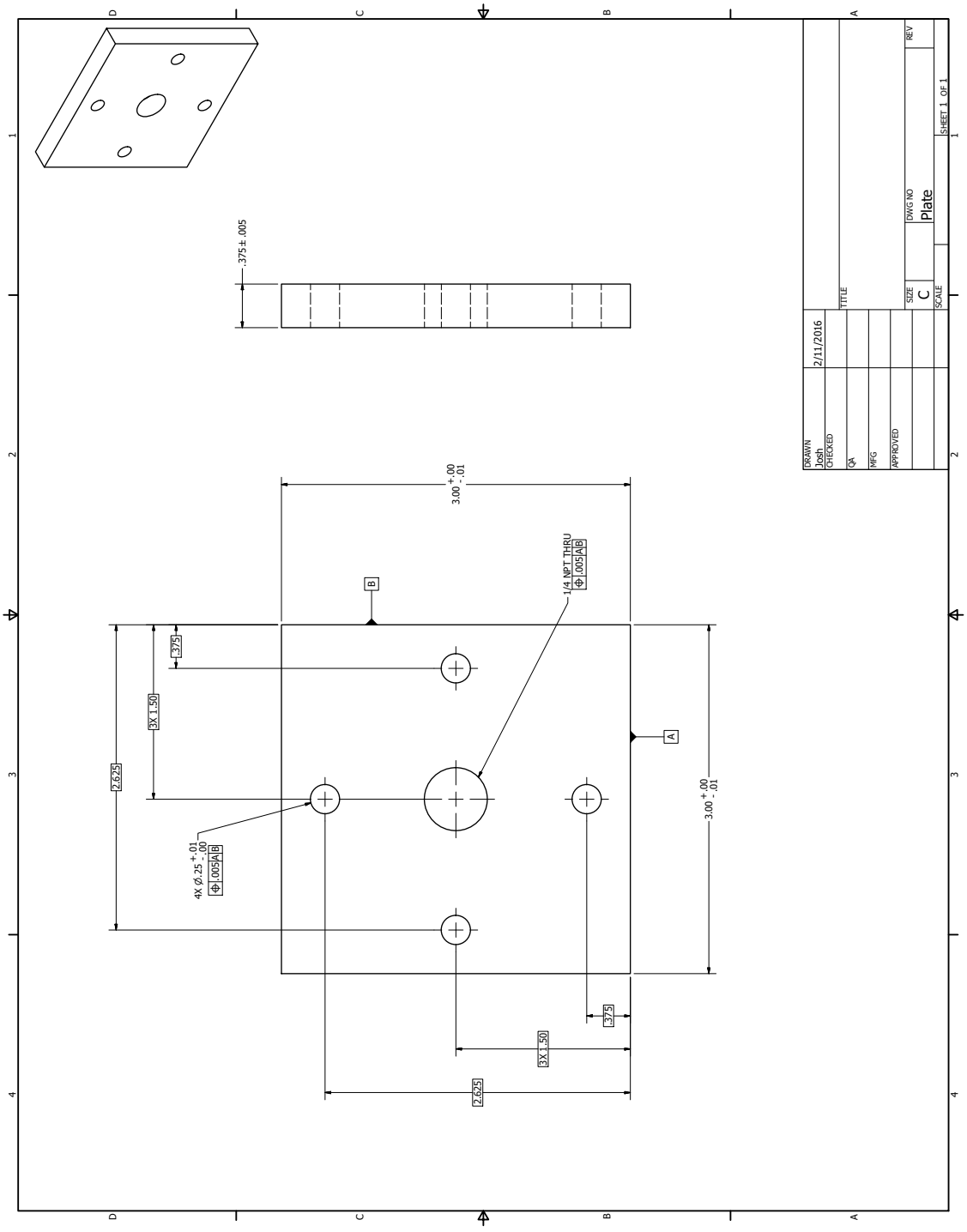

A.2.2 3g Volume

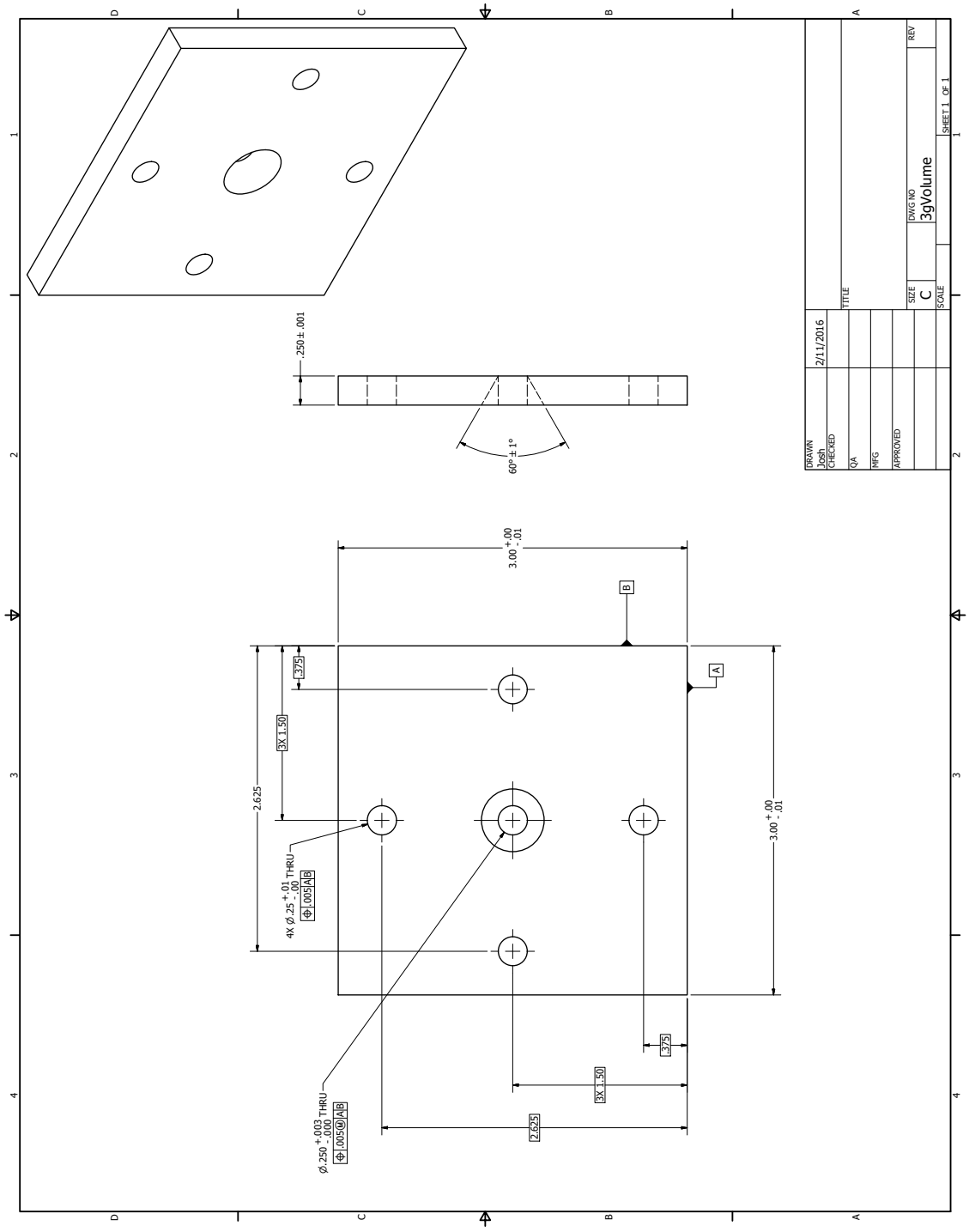

A.2.3 4g Volume

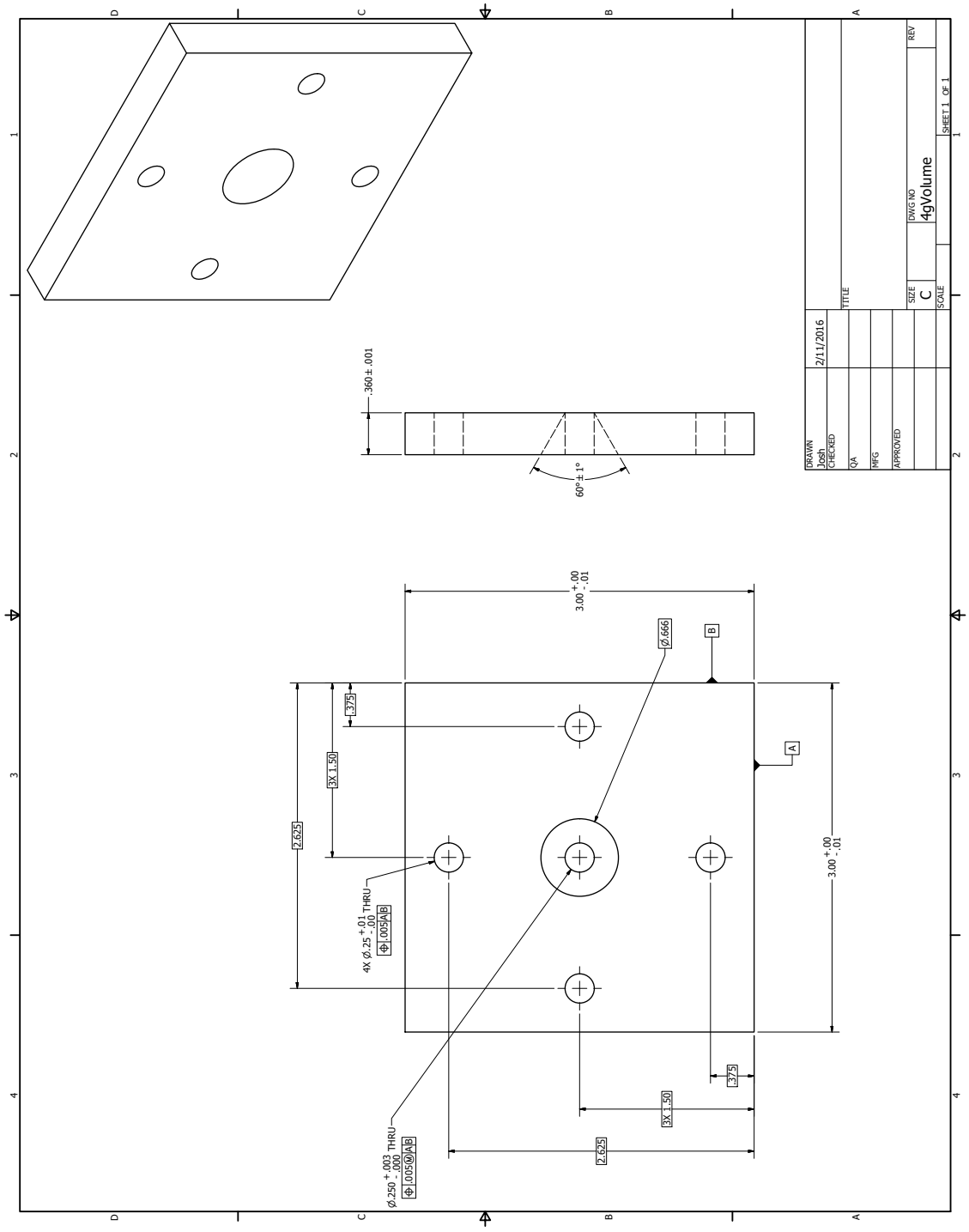

A.2.4 5g Volume

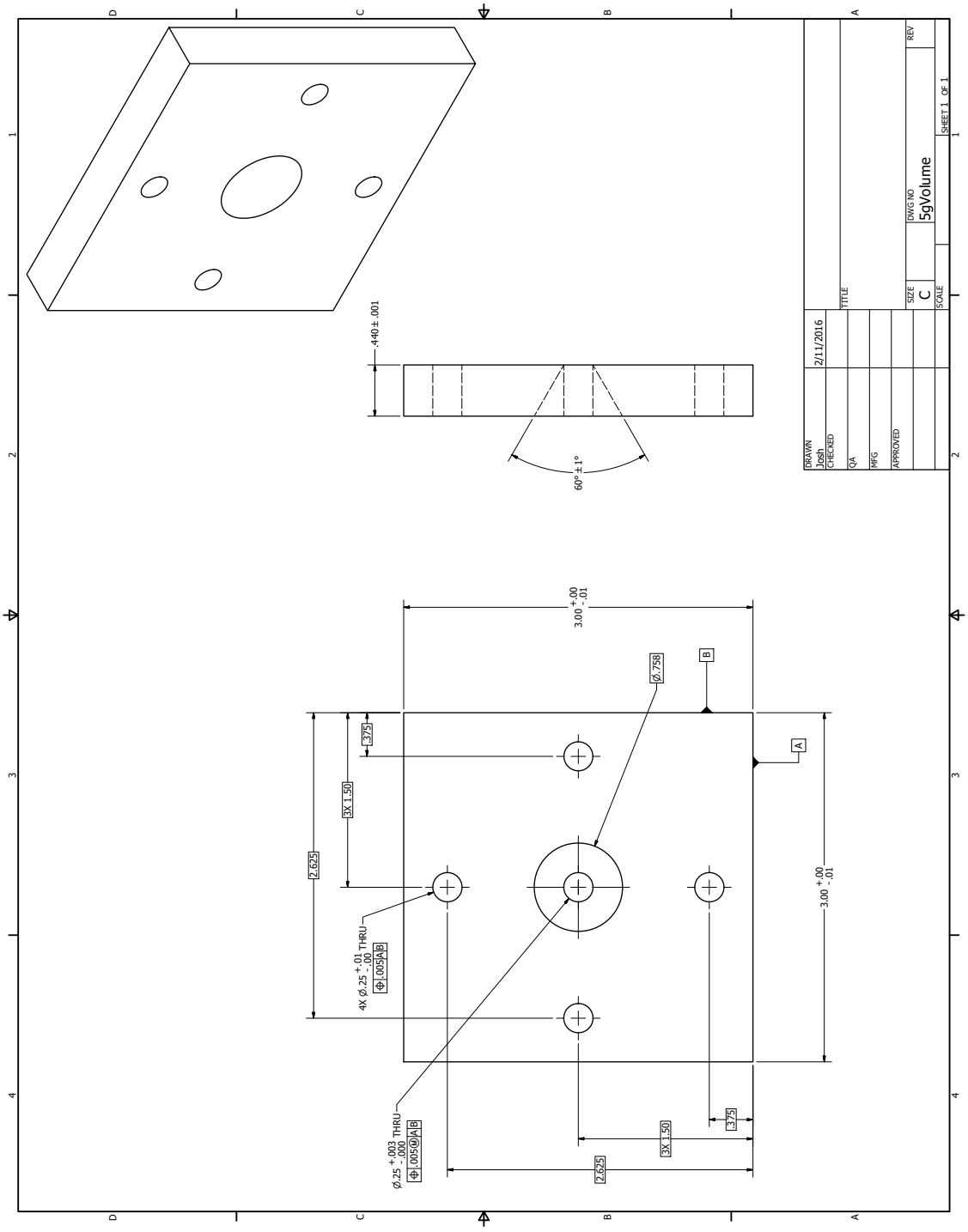

A.2.5 5g Assembly

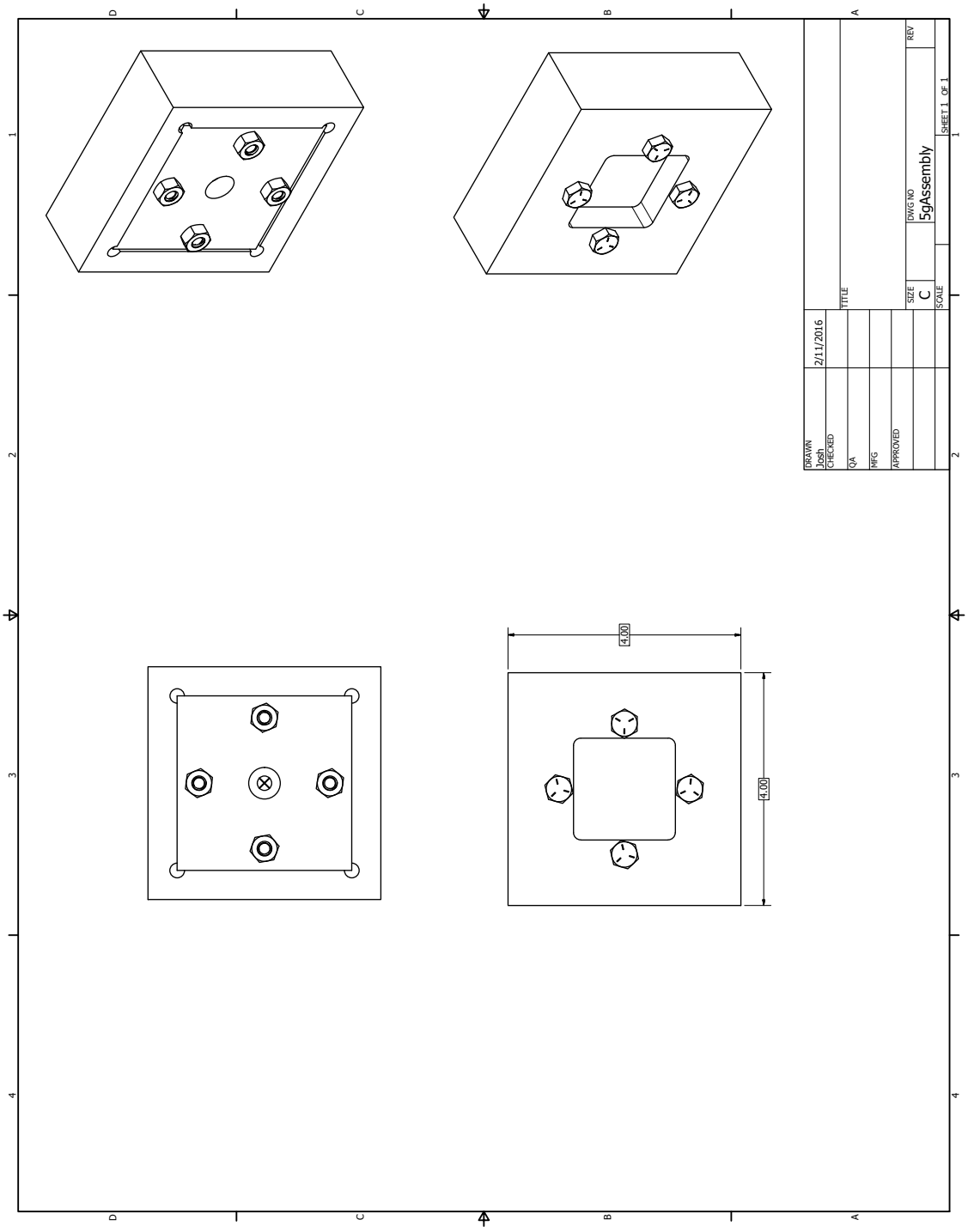

A.2.6 Block

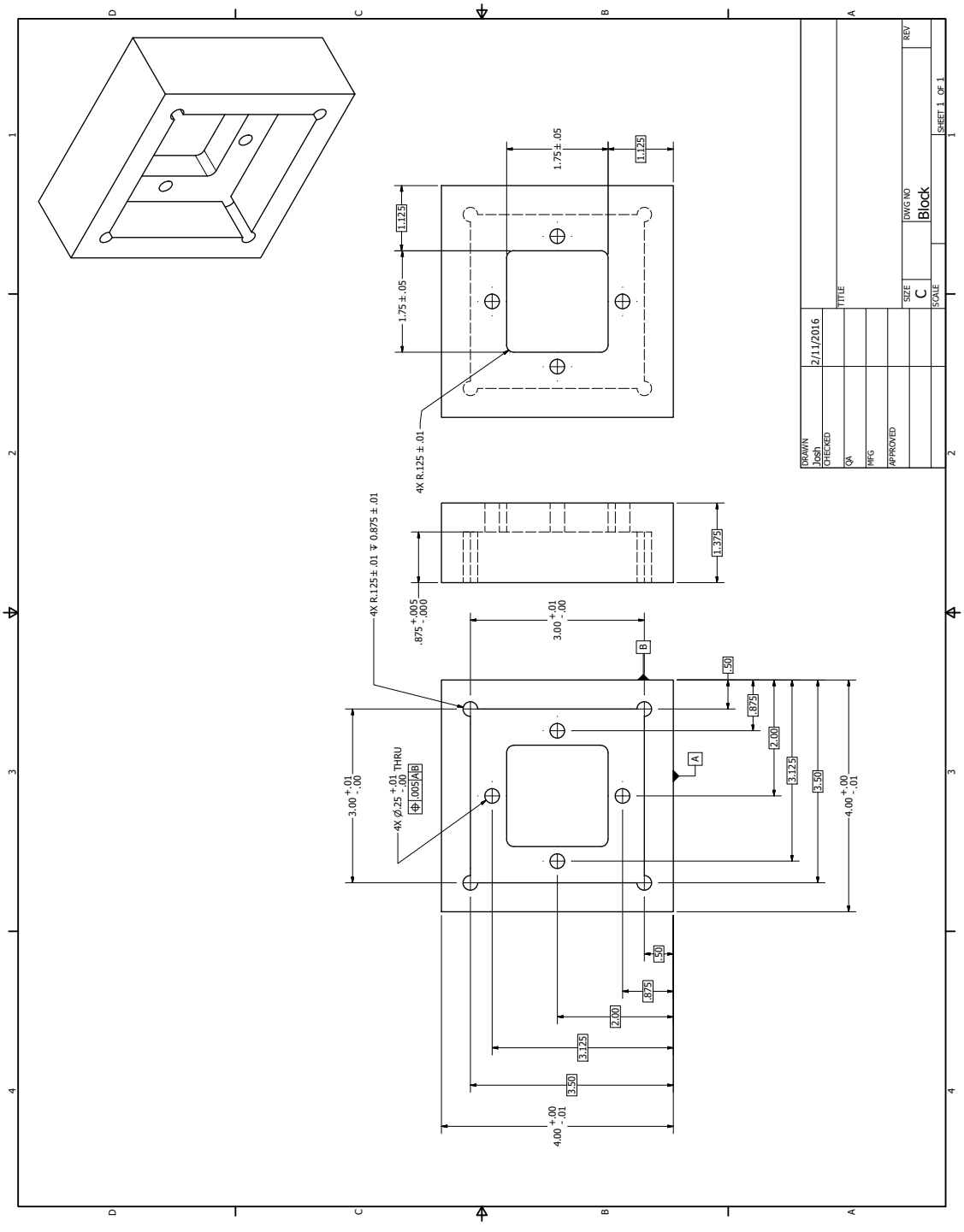
1.75 ± .05
1.125
1.125
1.75 ± .05
4X R.125 ± .01
4X R.125 ± .01 ▼ 0.875 ± .01
.875 +.005 -.000
1.375
3.00 +.01 -.00
B
.50
.875
2.00
3.125
3.50
4.00 +.00 -.01
A
4X Ø.25 +.01 -.00 THRU
⌖ .005 AB
3.00 +.01 -.00
DRAWN
Josh
CHECKED
QA
MFG
APPROVED
2/11/2016
TITLE
SIZE
C
DWG NO
Block
REV
SCALE
SHEET 1 OF 1

REFERENCES

[1] United Nations. *Protocol for the Prohibition of the Use in War of Asphyxiating, Poisonous or Other Gases, and of Bacteriological Methods of Warfare*, 1925.

[2] G. F. Webb. A silent bomb: The risk of anthrax as a weapon of mass destruction. *Proceedings of the National Academy of Sciences of the United States of America*, 100:4355–4356, 2003.

[3] Defense Threat Reduction Agency. Who we are. *http://www.dtra.mil*, 2016.

[4] R. Saurel, G. Huber, G. Jourdan, E. Lapebie, and L. Munier. Modelling spherical explosions with turbulent mixing and post-detonation. *Physics of Fluids*, 24:1–42, 2012.

[5] A. L. Kuhl, J. B. Bell, V. E. Beckner, and H. Reichenbach. Gas dynamic model of turbulent combustion in TNT explosions. *Proceedings of the Combustion Institute*, 33:2177–2185, 2011.

[6] K. Balakrishnan and S. Menon. Characterization of the mixing layer resulting from the detonation of heterogeneous explosive charges. *Flow Turbulence and Combustion*, 87:639–671, 2011.

[7] M. Brouillette. The Richtmyer-Meshkov instability. *Annual Review of Fluid Mechanics*, 34:445–468, 2002.

[8] L. Schwaederle, C. Mariani, G. Jourdan, L. Houas, and J. F. Haas. Shock-induced mixing zone characterization: an attempt by hot-wire diagnostic. *Shock Waves*, 17:203–207, 2007.

[9] D. L. Frost, C. Ornthanalai, Z. Zarei, V. Tanguay, and F. Zhang. Particle momentum effects from the detonation of heterogeneous explosives. *Journal of Applied Physics*, 101:1–14, 2007.

[10] F. Zhang, D. L. Frost, P. A. Thibault, and S. B. Murray. Explosive dispersal of solid particles. *Shock Waves*, 10:431–443, 2001.

[11] S. Hank, R. Saurel, O. Le Metayer, and E. Lapebie. Modeling blast waves, gas and particle dispersion in urban and hilly ground areas. *Journal of Hazardous Materials*, 280:436–449, 2014.

[12] K. G. Pennell, A. Naunovic, and E. R. Blatchley III. Sequential inactivation of bacillus subtilis spores with ultraviolet radiation and iodine. *Journal of Environmental Engineering*, 134:513–520, 2008.

[13] J. R. Morones, J. L. Elechiguerra, A. Camacho, K. Holt, J. B. Kouri, J. T. Ramirez, and M. J. Yacaman. The bactericidal effect of silver nanoparticles. *Nanotechnology*, 16:2346–2353, 2005.

[14] K. T. Sullivan, C. Wu, N. W. Piekiel, K. Gaskell, and M. R. Zachariah. Synthesis and reactivity of nano-Ag2O as an oxidizer for energetic systems yielding antimicrobial products. *Combustion and Flame*, 160:438–446, 2013.

[15] K. T. Sullivan, N. W. Piekiel, S. Chowdhury, C. Wu, M. R. Zachariah, and C. E. Johnson. Ignition and combustion characteristics of nanoscale Al/AgIO3: A potential energetic biocidal system. *Combustion Science and Technology*, 183:285–302, 2010.

[16] R. Russell, S. Bless, A. Blinkova, and T. Chen. Sporicidal effects of iodine-oxide thermite reaction products. *American Institute of Physics*, 1426:157–160, 2012.

[17] B. R. Clark and M. L. Pantoya. The aluminium and iodine pentoxide reaction for the destruction of spore forming bacteria. *Physical Chemistry Chemical Physics*, 12:12653–12657, 2010.

[18] J Feng, G. Jian, Q. Liu, and M. R. Zachariah. Passivated iodine pentoxide oxidizer for potential biocidal nanoenergetic applications. *ACS Applied Materials & Interfaces*, 5:8875–8880, 2013.

[19] L. L. Wang, Z. A. Munir, and Y. M. Maximov. Thermite reactions: their utilization in the synthesis and processing of materials. *Journal of Materials Science*, 28:3693–3708, 1993.

[20] Z. A. Munir and U. Anselmi-Tamburini. Self-propagating exothermic reactions: The synthesis of high-temperature materials by combustion. *Materials Science Reports*, 3:277–365, 1989.

[21] G. Jian, S. Chowdury, J. Feng, and M. R. Zachariah. The ignition and combustion study of nano-Al and iodine pentoxide thermite. In *8th U.S. National Combustion Meeting*, 2013.

[22] V. G. Ivanov, V. G. Ivanov, P. V. Lapin, and V. P. Kuznetsov. Role of iodation in the combustion of metal oxide with iodine pentoxide. *Combustion, Explosion, and Shock Waves*, 81:607–614, 1980.

[23] M. R. Weismiller, J. Y. Malchi, J. G. Lee, R. A. Yetter, and T. J. Foley. Effects of fuel and oxidizer particle dimensions on the propagation of aluminum containing thermites. *Proceedings of the Combustion Institute*, 33:1989–1996, 2011.

[24] K. S. Martirosyan, M. Zyskin, C. M. Jenkins, and Y. Horie. Fluid dynamic modeling nano-thermite reactions. *Journal of Applied Physics*, 115:1–5, 2014.

[25] K. S. Martirosyan, M. Zyskin, C. M. Jenkins, and Y. Horie. Modeling and simulation of pressure waves generated by nano-thermite reactions. *Journal of Applied Physics*, 112:1–9, 2012.

[26] B. K. Little, S. B. Emery, J. C. nittinger, R. C. Fantasia, and C. M. Lindsay. Physiochemical characterization of iodine oxide, part 1: Hydration rates. *Propellants, Explosives, Pyrotechnics*, 35:1–10, 2010.

[27] Thorlabs. Iodine material safety data sheet.

[28] UN. *Transport of Dangerous Goods*, 2009.

[29] Department of Defense. *Safety and Performance Test for the Qualification of Explosives (High Explosives, Propellants, and Pyrotechnics)*, December 2001.

[30] L. R. Simpson and M. F. Foltz. LLNL small-scale drop-hammer impact sensitivity test. Technical report, Lawrence Livermore National Laboratory, January 1995.

[31] L. R. Simpson and M. F. Foltz. LLNL small-scale friction sensitivity (bam) test. Technical report, Lawrence Livermore National Laboratory, June 1996.

[32] L. R. Simpson and M. F. Foltz. LLNL small-scale static spark machine: Static spark sensitivty test. Technical report, Lawrence Livermore National Laboratory, August 1999.

[33] R. A. Williams, J. V. Patel, and E. L. Dreizin. Ignition of fully dense nanocomposite thermite powders by an electric spark. *Journal of Propulsion and Power*, 30:765–774, 2014.

[34] R. Russell, S. Bless, and M. Pantoya. Impact-driven thermite reactions with iodine pentoxide and silver oxide. *Journal of Energetic Materials*, 29:175–192, 2011.

[35] G. S. Settles. *Schlieren and Shadowgraph Techniques: Visualizing Phenomena in Transparent Media*. Springer, 1st edition, corrected 2nd printing edition, 2001.

[36] C. R. Becker, G. J. Gillen, M. E. Staymates, and C. R. Stoldt. Nanoporous silicon combustion: Observation of shock wave and flame sunthesis of nanoparticle silica. *Applied Materials & Interfaces*, 7:25539–25545, 2015.

[37] L. Houas, E. E. Meshkov, and G. Jourdan. Overview of diagnostic methods used in shock-tube investigations of mixing induced by Richtmyer-Meshkov instability. *Shock Waves*, 9:249–257, 1999.

[38] J. L. Wagner, S. J. Beresh, S. P. Kearney, W. M. Trott, Castaneda J. N., B. O. Pruett, and M. R. Baer. A multiphase shock tube for shock wave interactions with dense particle fields. *Experiments in Fluids*, 52:1507–1517, 2012.

[39] M. J. Hargather, M. J. Lawson, and G. S. Settles. Focusing-schlieren PIV measurements of a supersonic turbulent boundary layer. *American Institute of Aeronautics and Astronautics*, 69:1–13, 2009.

[40] M. J. Hargather and G. S. Settles. Optical measurement and scaling of blasts from gram-range explosive charges. *Shock Waves*, 17:215–223, 2007.

[41] Gerhard Herzberg. *Molecular Spectra and Molecular Structure*. D. Van Nostrand Company, Inc., 1950.

[42] J. Joens. Gaussian approximation for the temperature dependence of a continuous electronic spectrum. *Chemical Physics Letters*, 138:512–515, 1987.

[43] A. Saiz-Lopez, R. W. Saunders, D. M. Joesph, S. H. Ashworth, and J. M. C. Plane. Absolute absorption cross-section and photolysis rate of I2. *Atmospheric Che*, 4:1443–1450, 2004.

[44] Mainuddin, M. T. Beg, Moinuddin, R. K. Tyagi, R. Rajesh, G. Singhal, and A. L. Dawar. optical spectroscopic based in-line iodine flow measurement system - an application to COIL. *Sensors and Accuators*, 109:375–380, 2005.

[45] S. V. Kireev and S. L. Shnyrev. Study of molecular iodine, iodate ions, iodide ions, and triiodide ions solutions absorption in the uv and visible light spectral bands. *Laser Physics*, 25:1–11, 2015.

[46] J. M. Peuker, P. Lynch, H. Krier, and N. Glumac. On alo emission spectroscopy as a diagnostic in energetic materials testing. *Propellants,*, 38:577–585, 2013.

[47] N. Glumac. Absorption spectroscopy measurements in optically dense explosive fireballs using a modeless broadband dye laser. *Applied Spectroscopy*, 63:1075–1080, 2009.

[48] N. Glumac. Early time spectroscopic measurements during high-explosive detonation breakout into air. *Shock Waves*, 23:131–138, 2013.

[49] S.H. Fischer and M. C. Grubelich. Theoretical energy release of thermites, intermetallics, and combustible metals. *International Pyrotechnics Seminar*, 1998.

[50] C. Farley and M. Pantoya. Reaction kinetics of nanometric aluminum and iodine pentoxide. *J Therm Anal Calorim*, 102:609–613, 2010.

[51] M. Stojanovska, V. M. Petrusevski, and B. Soptrajanov. The concept of sublimation - iodine as an example. *Emergent Topics on Chemistry Education*, 23:171–174, 2012.

[52] M. J. Hargather and G. S. Gary. A comparison of three quantitative schlieren techniques. *Optics and Lasers in Engineering*, 50:8–17, 2012.

[53] Horiba. microhr. *http://www.horiba.com*, 2016.

[54] N. Glumac. Personal communication. Absorption Spectroscopy.

[55] J. M. Hollas. *Modern Spectroscopy*. Wiley, 2004.

[56] J. M. Lerner. Imaging spectrometer fundamentals for researchers in the biosciences a tutorial. *International Society for Analytical Cytology*, 69A:712–734, 2005.

[57] J. Tellinghuisen. Resolution of the visibleinfrared absorption spectrum of i2 into three contributing transitions. *The Journal of Chemical Physics*, 58:2821–2834, 1973.

[58] W. E. Baker, P. A. Cox, P. S. Westine, J. J. Kulesz, and R. A. Strehlow. *Explosion Hazards and Evaluation*. Elsevier Scientific, 1983.

[59] P. W. Cooper. *Explosives Engineering*. Wiley-VCH, 1996.

[60] G. F. Kinney and Graham K. J. *Explosive Shocks in Air*. Springer-Verlag, 2 edition, 1985.

[61] Wunderground. Socorro, nm weather. *https://www.wunderground.com*, 2015.

[62] McMaster-Carr. 4140/4142 alloy steel. *http://www.mcmaster.com*, 2015.

[63] R. Roark and W. Young. *Roarks Formulas for Stress and Strain*. McGraw-Hill, 1989.

[64] G. Young, H. Wang, and M. R. Zachariah. Application of nano-aluminum/nitrocellulose mesoparticles in composite solid rocket propellants. *Propellants, Explosives, Pyrotechnics*, 40:413–418, 2015.

DESIGN AND CONSTRUCTION OF A FIXTURE TO EXAMINE THE EXPLOSIVE EFFECTS OF Al/I_2O_5

by

Joshua L. Smith